UCRL-16108

University of California

Ernest O. Lawrence Radiation Laboratory

LIQUID METAL EXTRACTION OF FISSION PRODUCTS
FROM URANIUM REACTOR FUELS

Berkeley, California

DISCLAIMER

UCRL-16108

UNIVERSITY OF CALIFORNIA

Lawrence Radiation Laboratory
Berkeley, California

AEC Contract W-7405-eng-48

LIQUID METAL EXTRACTION OF FISSION PRODUCTS FROM URANIUM REACTOR FUELS

Alan David Pasternak

January 1966

(Ph.D. Thesis)

LIQUID METAL EXTRACTION OF FISSION PRODUCTS FROM URANIUM REACTOR FUELS

Alan David Pasternak

Inorganic Materials Research Division,
Lawrence Radiation Laboratory
Department of Chemical Engineering,
University of California, Berkeley, California

ABSTRACT

January 1966

The rate of extraction of a rare earth fission product, lanthanum-140, and its precursor and Ba^{140} from the uranium - 5 w-% chromium eutectic by molten magnesium at 1000°C has been measured by the falling liquid drop technique. Use of the low melting U-Cr eutectic (MP 859°C) instead of pure uranium (MP 1132°C) permits operation at temperatures well below the boiling point of magnesium. Magnesium and the U-Cr alloy form an essentially immiscible two phase liquid-liquid system. Fission products were introduced in the U-Cr alloy by light neutron irradiation. The relative abundance of La^{140} was determined by scintillation counting of its 1.6 Mev gamma photopeak. The relative abundance of Ba^{140} was determined by following the decay of La^{140} activity after extraction.

Measurements were made on U-Cr drops of 2-4 mm diameter. The overall mass transfer coefficient for La, based on the U-Cr phase was determined to be .00417±30% cm/sec. Drop velocity was determined by measuring the time interval between the output of collimated scintillation counters placed along the extraction column. The measured velocity was about 70 cm/sec, 13% higher than predicted by the correlation of Hu and Kintner.

Equilibrium experiments showed the distribution coefficient for La (on a concentration basis) between U-Cr and Mg to be 0.14 at 1000°C,

and that for Ba to be about .0035.

The results of the kinetic and equilibrium measurements indicated that the mechanism of solute lanthanum transfer is molecular diffusion through a stagnant drop with external resistance.

Diffusion coefficients in liquid metal systems have been correlated by absolute rate and corresponding states theories.

TABLE OF CONTENTS

I. INTRODUCTION

A. The Role of Liquid Metal Extraction in Nuclear Technology

Nuclear power reactors generate heat by fissioning U^{235} or Pu^{239}. Fission or splitting of one of these isotopes is triggered by a collision with a neutron and results in the formation of two nuclear fragments called "fission products" or "fission product elements". Fission products have mass numbers from 72 to 158. Almost all of the heat released in a nuclear reactor is due to the recoil kinetic energy of fission products. They are almost always radioactive. For several reasons, which will be outlined below, it is necessary to withdraw a fuel element from the core of a reactor at some point in time before all the U^{235} has been consumed and to reprocess that fuel element. The most important step in reprocessing is the separation and recovery of U^{235} from the fission products. New fuel elements may then be fabricated from the recovered U^{235}.

There are three reasons why reactor fuel must be reprocessed:

1) Radiation damage must be repaired. When an atom of U^{235} fissions, the fission product fragments recoil with great velocity. By colliding with atoms in the metallic lattice they are slowed-down and their kinetic energy converted to heat. In this process the metallic lattice itself suffers damage which may adversely affect its thermal conductivity and strength. Even the shape of a solid fuel element may be altered.

2) The presence of fission-products in the metal lattice may adversely affect its strength or other metallic properties. This is because many fission products are non-metals and some, such as cesium, have larger atoms than uranium.

3) Many fission products absorb neutrons (have a high capture cross-section for neutrons) and compete with U^{235} for neutrons thus adversely affecting the reactor's neutron economy. This effect is called "poisoning" and is particularly serious in thermal reactors because many fission products have large resonances in their absorption cross-sections for thermal neutrons. Aside from resonance effects, most absorption cross-sections follow a 1/v relationship to neutron energy. For a fast reactor, (one whose fuel is fissioned by fast neutrons) poisoning is a much less serious problem.

Reprocessing of reactor fuels is conventionally accomplished by aqueous chemistry. In the usual aqueous reprocessing schemes the metal is first dissolved in nitric acid then an organic extractant such as tri-n-butylphosphate (TBP) is used to separate uranium from fission products. Separation of uranium from other fissionable material (e.g., Pu^{239} which is formed when U^{238} captures a fast neutron) is achieved by careful adjustment of the valence states of the two metals. Aqueous techniques are capable of achieving a high degree of removal of radioactive fission products. The degree of removal is quantitatively described by the term "decontamination factor", which is the ratio of fission products present per unit weight of fuel before processing to that after processing. Decontamination factors of 10^6 - 10^8 are common in aqueous processes and are high enough to permit direct handling of the reprocessed fuel during refabrication.

During the past fifteen years, a number of laboratories have investigated reprocessing techniques in which the fuel element is not dissolved but is maintained in metallic form. These processes make use of chemical reactions which occur at high temperatures and are designated "pyrometallurgical

processes". Some of the laboratories in the United States where pyrometallurgical processing has been studied are Hanford, Los Alamos, Argonne National Laboratory, the Ames Laboratory at Iowa State College, Oak Ridge National Laboratory and Brookhaven National Laboratory.

There are a number of techniques[61] which fall under the heading of pyrometallurgical processing.

1) Direct distillation: Pu and some fission products can be distilled from uranium at 1600°C.

2) Fused salt extraction: Because the chlorides and fluorides of many fission products are very stable, these fission products can be removed from molten uranium by extraction with a molten salt phase containing UF_4 or $MgCl_2$.

3) Oxide slagging: If uranium is melted in crucibles made of certain refractory oxides those fission products whose oxides are stable will be removed. Levenson[100] has described a pilot scale processing plant for the remote refabrication of fuel elements which operates in conjunction with Experimental Breeder Reactor-II (EBR-II) as a closed fuel cycle. Molten uranium at 1300°C is processed in zirconium oxide crucibles under a dry argon atmosphere. The EBR-II Fuel Recycle Facility is located at the USAEC reactor testing station in Idaho.

4) Liquid metal extraction: Some molten metals such as silver and magnesium are immiscible with molten uranium and can extract fission products by solvent action.

The remainder of this section will be devoted to a consideration of the advantages, disadvantages and applications of liquid metal extraction.

It is not expected that pyrometallurgical processes will achieve decontamination factors as high as in aqueous processes. The objective in a liquid metal reprocessing scheme is to remove a sufficient portion of the fission products to prevent "poisoning". Baker and Leary[63] estimate that decontamination factors of 10 to 100 will be adequate, but remote refabrication of fuel elements will be necessary. The melting and recasting steps will repair radiation damage to the lattice structure of solid metal fuels. Of course in a liquid metal fueled reactor this latter problem does not arise.

Besides the achievement of high decontamination factors, aqueous processes have other advantages. Most important is their proven reliability. Aqueous processes are ideally suited for use in centrally located reprocessing plants to which spent fuel elements can be shipped for treatment. Baker and Leary[63] have compared some of the relative merits of aqueous and pyrometallurgical processing. One big drawback in the aqueous processes is that organic extractants undergo radiation damage by highly burnt-up fuels. Long cooling times are therefore required before such fuels can be processed. This means that more fuel must be kept in the "fuel cycle" increasing fuel inventory charges. Liquid metal extractants are not subject to radiation damage from intensely radioactive fuel. Pyroprocessing plants are compact, do not involve the large capital expenses of aqueous plants and are therefore well suited to on-site processing. Pyrometallurgical processing is of course especially suited to use with liquid-metal fueled reactors.

Howe[64] has outlined some of the advantages and disadvantages of liquid fuels. Among the advantages are freedom from radiation damage to

the crystal lattice typical of a solid fuel, better heat transfer, simple preparation, and the possibility of less complicated cheaper reprocessing. Some problems associated with liquid fuels are those of corrosion, pumping radioactive fluids, and the necessity for compact heat exchanger design. One liquid metal fuel which has received considerable attention is a solution of U^{235} in bismuth. Bismuth's low absorption cross-section for thermal neutrons and low melting point make it ideal for this application.

Hammond and Humphreys[74] of the Los Alamos Scientific Laboratory have proposed a direct-contact core system having a molten plutonium alloy fast reactor core. The core would be circulated, cooled, and processed by direct contact with liquid sodium. The blanket would consist of U^{238}. The proposed core alloy is 67.5 a-% Ce, 25 a-% Co, and 7.5 a-% Pu and has a MP of 420°C. (The alloy melts at approximately 420°C at 25 a-% Co and over a wide range of Pu-Ce composition).

A sodium jet pump provides the energy for circulating the fuel. After very short contact times (local heat fluxes of several million Btu/hr-ft^2 are expected) the immiscible liquids are centrifugally separated, the fuel returns to the core, and the hot sodium goes to a heat exchanger where it is cooled by a secondary sodium loop before returning to the jet pump.

Many experimental problems remain to be solved before such a system can operate economically. Some of them are fuel carry-over, coolant carry-back as well as experimental determination of the limits of fuel pumping (which may limit the entire system to relatively small core sizes). Some experiments already performed indicate that tantalum will be required for the core container.

Hammond expects that the proposed system can overcome high initial cost by offering a low operating cost. A fluid core system also offers

some inherent safety features. There are no problems of fuel element melt-down or of void formation in the coolant.

Bidwell,[75] also working at Los Alamos, has considered the chemical behavior of fission products which might be expected in the "dynamic core" fast reactor. He predicts that the rare gases and the alkali and alkaline-earth metals will be sodium extractable, as well as the halogens which form sodium soluble sodium halides. The fission products would be separated from the sodium coolant by cold trapping or distillation. Rare earths, the transition metals and the refractory metals are assumed to remain in the fuel. Bidwell calculates that 5% to 35% of the extractable fission products are removed during each pass through a dynamic core.

It is expected that such a system can operate to a very high burn-up, i.e., until an amount of plutonium equal to the original inventory has been consumed. During this time it would be necessary to add 110% of the original amount of which 3% would compensate for poisoning. The ultimate limiting factor may be the precipitation of insoluble metals in the fuel or an upset of the neutron economy due to loss of delayed-neutron precursors to the sodium extractant. Bidwell[101] considers the latter problem in a separate article.

B. Object of Present Work

This thesis is an experimental study of the kinetics of liquid metal extraction of fission products from uranium reactor fuels. The liquid-liquid contacting procedure that was used is commonly called "drop extraction". Molten drops of a neutron-irradiated alloy of uranium and chromium were allowed to fall through a column of molten magnesium which is essentially immiscible with molten uranium. Both the amount of a rare earth fission product, La^{140}, and Ba^{140}, which were extracted from the

drop by the magnesium solvent and the velocity of the falling drop were measured in order to determine the rate of extraction.

The purpose of the experiment is to determine mass transfer coefficients for the system. The equilibrium distributions of La^{140} and Ba^{140} between the molten uranium-chromium alloy and magnesium phases were also measured.

The mass transfer coefficients determined in this study have application to the design of equipment and procedures for reprocessing metallic fuels for nuclear reactors.

Because this thesis deals with mass transfer in molten metal systems, and because diffusion is important in mass transfer, a survey of the available molten metal diffusion data was undertaken. The results of this survey and a discussion of two techniques for predicting diffusion in molten metals are presented.

The remainder of this chapter is devoted to a discussion of the U-Cr, Mg solvent pair and the La^{140}, Ba^{140} solutes, and to a brief summary of the problem of containment of these corrosive liquids at high temperatures.

In succeeding chapters the drop extraction experiments will be described and the results of the experiments will be discussed.

C. The Immiscible U-Cr Eutectic —— Mg System

One of the mutually immiscible systems which has been investigated as a result of interest in pyrometallurgical processing is the uranium-magnesium system. Some of the equilibrium data for this system will be reviewed in the next chapter. Barney and Keneshea[67] equilibrated uranium and magnesium in tantalum crucibles at 1150°C. (Uranium melts at 1132°C.) Because this temperature is well above the boiling point of magnesium, it was necessary to carry out the equilibrations in mild steel bombs.

In order to avoid the necessity of operating the experiment under pressure, the uranium-20 a-% chromium eutectic (MP 859°C) was used instead of pure uranium. In this way a liquid uranium rich phase can be contacted with a molten magnesium phase at temperatures well below the boiling point of magnesium. Magnesium vapor pressure is about 300 mm of Hg at 1000°C, the experimental temperature.

The uranium-chromium system has been studied by Daane and Wilson[76] using x-ray, thermal and metallographic techniques. (See also "Constitution of Uranium and Thorium Alloys", BMI-1300 by F. A. Rough and A. A. Bauer.)[102] The system forms a eutectic with a melting point of 859°C and a eutectic composition of 20 a-% (5 w-%) chromium.

The phase diagram for the magnesium-uranium system at 3 atmospheres has been established by Chiotti, Tracy, and Wilhelm.[77] They found limited mutual solubility at temperatures up to 1255°C. At 1135°C the magnesium-rich phase contains 0.14±0.05 w-% uranium and the uranium-rich phase contains 0.004 w-% magnesium.

The magnesium — U-Cr eutectic system has not been as thoroughly studied as has the Mg-U system. Some measurements have been reported by Argonne National Laboratory.[78] When the uranium-chromium eutectic was equilibrated with magnesium at 940°C, the magnesium phase contained 0.05 w-% U and 0.06 w-% Cr.

Figure 1 is a section showing the interface between the U-Cr phase (bottom) and the magnesium phase (top) obtained in the present study. The sample illustrated was heated to 1000°C under argon in a graphite crucible. Magnesium has a silver color; the U-Cr surface has a slight yellow tint.

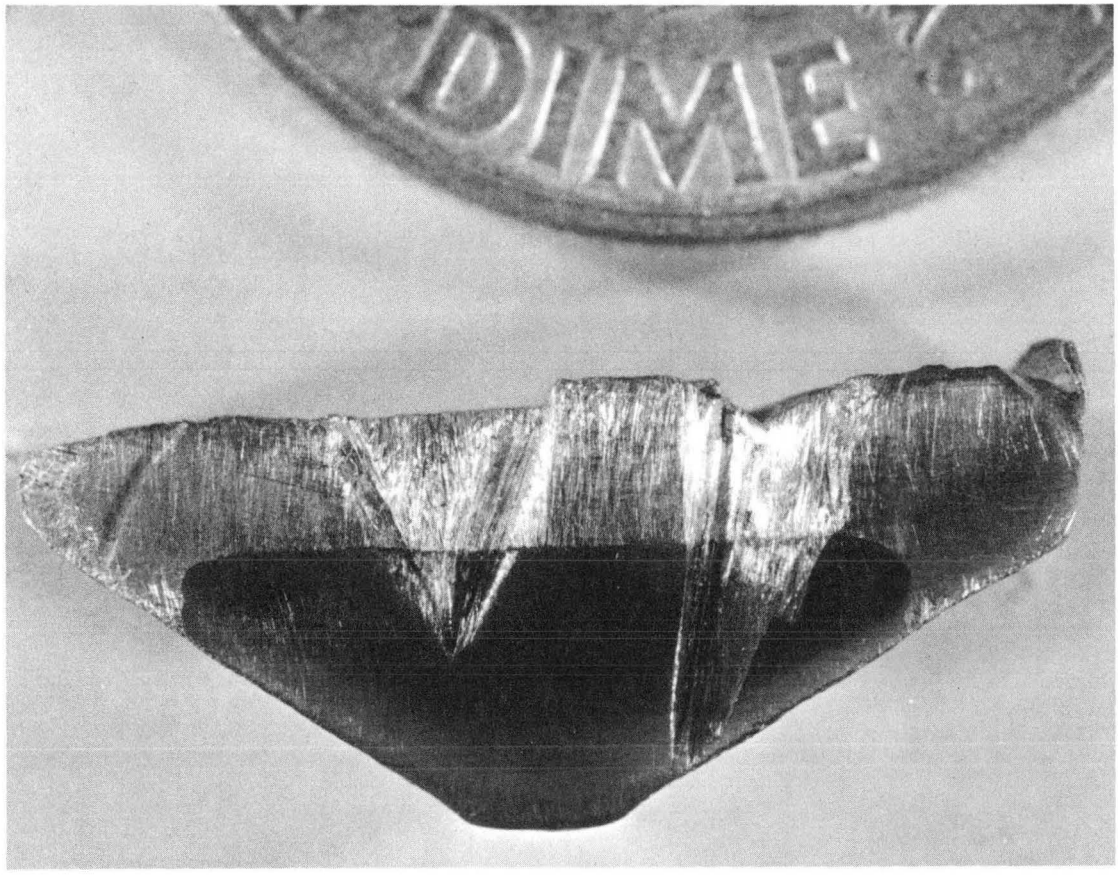

ZN-5472

Fig. 1

D. The Transferring Solutes: La^{140} and Ba^{140}

The transferring solute directly measured in the experiment is the rare-earth, lanthanum-140. La^{140} is not produced directly in the fission of U^{235}; it is a daughter of Ba^{140} which is formed with a direct fission yield of 6.4% and subsequently undergoes β-decay with a 12.8 day half-life to La^{140}. La^{140} in turn emits a β-particle and decays with a half-life of 40.2 hours to Ce^{140}. The decay of La^{140} to Ce^{140} is accompanied by the emission of a 1.6 Mev gamma-ray. (More accurately, 99% of the La^{140} to Ce^{140} decays are accompanied by a 1.6 Mev photon, 1% of the decays are accompanied by a 2.5 Mev photon.) The decay scheme is symbolically represented by Eq. (1).

$$_{56}Ba^{140} \xrightarrow[12.8\ d]{\beta^-} {}_{57}La^{140} \xrightarrow[40.2\ h]{\beta^-} {}_{58}Ce^{140} \qquad (1)$$

When U^{235} fissions, a wide range of fission-product nuclides is formed. Most of these nuclides are radioactive. Those nuclides which emit "hard" or high-energy gamma rays tend to have short half-lifes. Because the precursor to La^{140} has a relatively long half-life, the 1.6 Mev γ-ray from La^{140} will dominate the γ-ray spectrum of a sample of irradiated uranium which has been allowed to cool for several days. Figure 2 shows the γ-ray spectrum of a sample of the U-Cr eutectic which was irradiated in the Livermore Pool Type Reactor (LPTR) for 2 days and allowed to cool for 24 days.

The peak due to the 1.6 Mev γ-ray from La^{140} is unmistakable. Two other peaks are also apparent. One, at .5 Mev is due to the photon from Ru^{103}. Another peak at about .75 Mev is due to the .72 and .76 Mev

photons from Zr^{95} and the .77 Mev photon from Nb^{95}. The spectrum of irradiated uranium taken with a multichannel analyzer is shown in Fig. 2. The count rate for any energy interval (0.1 Mev per channel) is an arbitrary number depending not only on source strength but on the counting geometry. The shape of the spectrum, however, depends only on the irradiation and cooling times and reflects the relative abundance of various nuclides. Details of the statistical treatment of the counting data, corrections for self-absorption of γ-rays in the U-Cr pellet, and the geometrical corrections required when measuring line sources (e.g., the Mg ingot) are described in Appendices A, B, and C.

Since La^{140} abundance (and therefore measured La^{140} activity) is in part controlled by the 12.8 day half-life decay of its precursor Ba^{140}, the fraction of Ba^{140} extracted can also be determined by following the decay of La^{140} in the Mg phase. This can be qualitatively illustrated by considering the two extreme cases. If the Mg contains only La^{140} and no Ba^{140}, La^{140} activity will decay logarithmically with a half-life of 40.2 hours. On the other hand, if the Mg contains only Ba^{140} and no La^{140}, then La^{140} activity will initially increase from zero to some maximum value and then decrease, the apparent rate of decay approaching the 12.8 day half-life of the precursor Ba^{140}.

As derived in Appendix D, the La^{140} activity as a function of time after extraction is given by:

$$\frac{a_{La}}{a^{0}_{La}} = \frac{e^{-\lambda_{Ba} t}}{F} + \left(1 - \frac{1}{F}\right) e^{-\lambda_{La} t} \qquad (2)$$

where F represents the departure of the La to Ba abundance ratio in either phase immediately after extraction to the ratio which would exist at secular equilibrium.

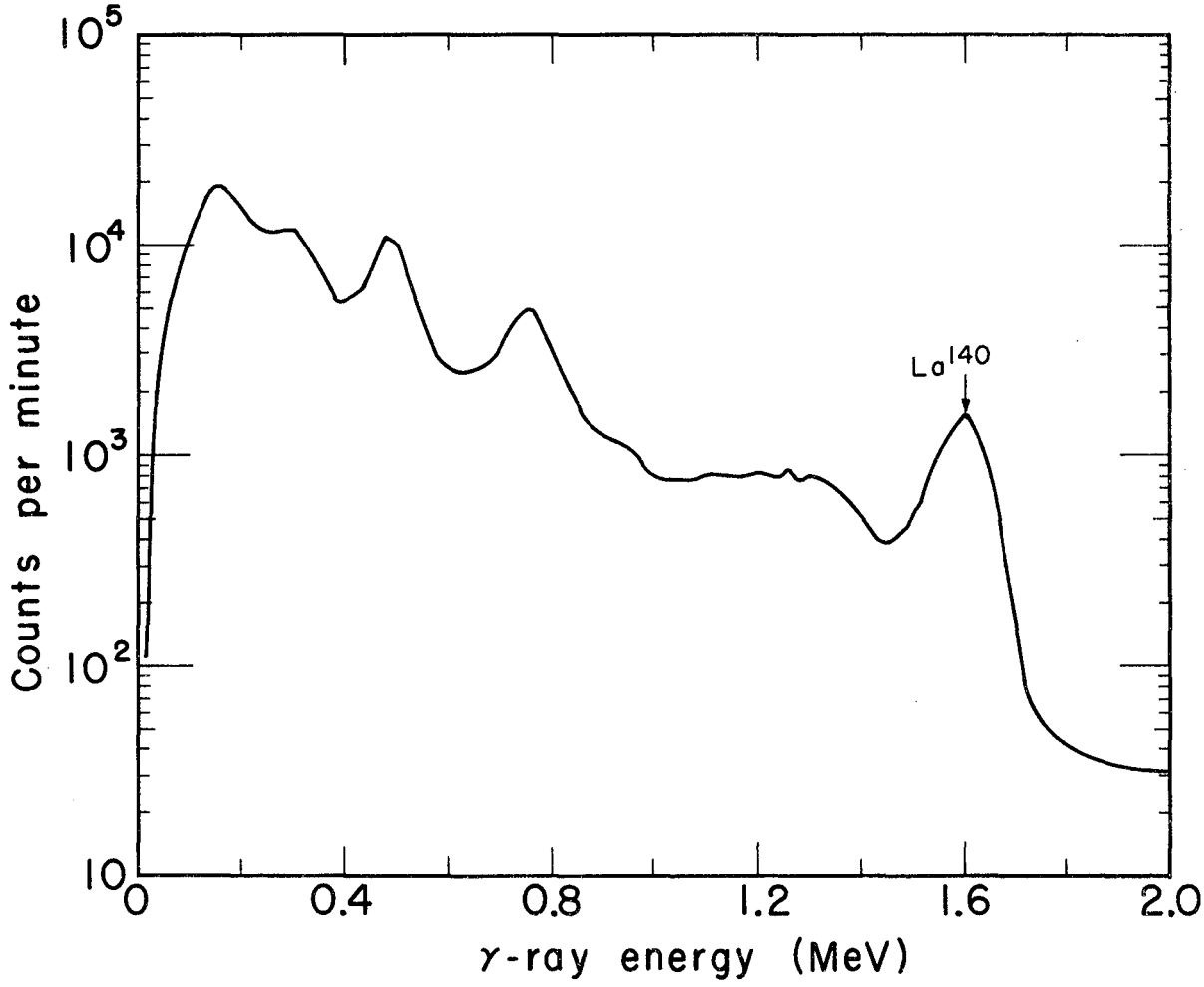
10^5
10^4
10^3
10^2
10
Counts per minute
La^{140}
0
0.4
0.8
1.2
1.6
2.0
γ-ray energy (MeV)
MUB-6388

Fig. 2

$$F = \frac{N^0_{La}}{N^0_{Ba}} \frac{\lambda_{La} - \lambda_{Ba}}{\lambda_{Ba}} \qquad (3)$$

Since all irradiated U-Cr samples were cooled sufficiently long enough to reach secular equilibrium, F for the magnesium phase in the kinetic experiments is the ratio of the extracted fractions of lanthanum to barium.

$$F = \frac{f_{La}}{f_{Ba}} \qquad (4)$$

The notation is as follows: λ is the decay constant $= \frac{.693}{t_{1/2}}$, a_{La} is measured lanthanum activity at time t after extraction, a^0_{La} is the measured lanthanum activity immediately after extraction, and f is the fraction extracted.

Examination of Eq. (2) shows that a plot of $\left(a_{La}/a^0_{La}\right) e^{\lambda_{Ba} t}$ vs $e^{-(\lambda_{La}-\lambda_{Ba})t}$ will yield a straight line with an intercept of 1/F. Since f_{La} in the kinetic experiments is obtained by comparing the La^{140} activity of the Mg phase immediately after extraction to the original pellet activity, knowledge of the ratio F permits f_{Ba} to be computed by Eq. (4). As far as is known, this is the first time that precursor abundance has been determined by following the decay of daughter activity in pyrometallurgical processing experiments. In a similar manner, the time dependence of the La^{140} activity of the U-Cr sample after extraction permits calculation of an F value for the U-Cr phase by a plot of Eq. (2). In this way, the lanthanum to barium abundance ratio in the U-Cr phase was determined in the equilibrium experiments.

E. Container Materials

Fisher and Fullhart[65] have studied some of the corrosion problems

associated with U-Bi alloys and the U-Cr eutectic (possible molten fuels) and the Mg-Th eutectic (a possible molten breeder blanket). Both static tests and dynamic isothermal tests in a rocking furnace were performed with the following results: Tantalum is a satisfactory container for the Mg-Th alloy up to 800°C and for the Bi-U solution (5-10 w-% U) up to 1100°C. Because tantalum surfaces oxidize above 300°C, a protective sheath is necessary. Inconel was satisfactory as a sheathing material for tantalum up to 1100°C. Tantalum was not satisfactory as a container material for U-Cr, U-Fe, or U-Ni alloys. Yttrium, with a sheath of 446 stainless steel (high chromium content and less than .2% Ni) was found to be satisfactory for containing the U-Cr eutectic up to 1000°C. Yttrium is not a good container material for bismuth or Bi-U alloys or for Al-Th-U alloys. Fisher and Fullhart[65] outline techniques for inert gas welding and fabrication of tantalum and yttrium crucibles. They emphasize the importance of using high purity tantalum.

Several materials were considered for holding molten magnesium. Some of them were stainless steel (type 446), quartz, ceramic, and graphite. A small piece (about 3 grams) of magnesium was melted in a quartz test tube over a Fisher burner. As soon as any part of the magnesium melted, a black substance was seen to form at the molten magnesium-quartz interface. On cooling, the quartz test tube shattered, and the magnesium was left with a hard shiny black coating. Molten magnesium quickly burned through a crucible made of mullite.

Graphite had been used by Culpin[24] to determine the viscosity of liquid magnesium by the oscillating hollow sphere method. When small crucibles of test tube size made of graphite were used to melt magnesium, no reaction between magnesium and graphite was observed; after cooling,

it was possible to pull the solid magnesium plug out of the crucible. The outer surfaces of graphite crucibles heated in a small resistance "clam-shell" heater exposed to the atmosphere became powdery. However, when the crucible was heated in the reducing atmosphere of a gas flame or was completely protected by an argon stream, no damage to the crucible surfaces was noted. Since it was found possible either to drill crucibles of the required length (about 30", 9/16" diameter hole) or to purchase graphite tubing, graphite was selected as the container material for the magnesium column in the kinetic experiments. Small graphite crucibles were used in the equilibrium experiments.

II. EQUILIBRIA: DISTRIBUTION COEFFICIENTS IN LIQUID METAL SYSTEMS

A. Previous Studies

Most previous studies of pyrometallurgical processing have concentrated on the determination of distribution coefficients and decontamination factors. The decontamination factor is the ratio of solute concentration in the original unprocessed metal to its concentration in the final metal. It is a measure of solute removal by all methods: extraction, volatilization, crucible and surface reactions. The decontamination factor for a particular fissionable metal-extractant metal-fission product solute system will depend on temperature, heating time, relative volumes of the two phases and geometry. Distribution, or equilibrium, coefficients are fundamental thermodynamic properties of the systems studied and depend, for any given metal-metal-solute system, on temperature and solute concentration. The distribution coefficient is defined as the ratio of solute concentration in the extractant phase to its concentration in the final metal phase at equilibrium on either a mole fraction or a concentration basis. It is a measure of solute removal by extraction only.

Voigt[66] has reported the results of liquid metal extraction experiments in which silver, cerium, and lanthanum were used to extract fission products and plutonium from uranium and the uranium-5 w-% chromium eutectic (MP 860°C). Voigt used three different materials as the working fuel: irradiated natural uranium, the irradiated uranium-chromium eutectic and artificial mixtures. The natural uranium samples were irradiated for various lengths of time and contained plutonium concentrations from 2 to 250 ppm. Some of the U-Cr used was irradiated for several months and then cooled for several months producing plutonium at a level of 11 ppm.

Another portion of the U-Cr alloy was irradiated for seven days and cooled for seven days. In order to simulate a reactor fuel which has been irradiated to a 2% "burn-up" (i.e., 2% of the U^{235} fissioned), Voigt prepared an artificial mixture of fission product elements and uranium. Per kilogram of uranium, the artificial mixture called "fissium" contained 1.18 g of zirconium, 0.69 g of ruthenium, 0.76 g of molybdenum, and 3.40 g of rare earths.

The extractions were carried out in an induction furnace to promote stirring and used 150 g of uranium and an equal volume of extractant in each experiment. Graphite and tantalum crucibles were used. After heating, the samples were cooled slowly so that the two phases which had been mixed by induction stirring might be completely separated by gravity. After solidification, the phases were sectioned in such a way as to avoid the interface in either metal sample. Radiochemical methods were used to analyze samples of both phases. From analyses of samples of the uranium phase before and after extraction, decontamination factors were calculated. Distribution coefficients are reported on a weight basis, i.e., counting rate per gram of extractant divided by counting rate per gram of final metal.

Table I lists the results of extraction of irradiated uranium with silver. These experiments were done in graphite crucibles at 1200°C for 20 minutes. Samples listed as having "medium" or "high" fission product content had been irradiated to a level of Pu concentration of 18 and 230 ppm respectively.

Table II lists the results of extraction of irradiated uranium with the rare earth metals cerium and lanthanum. These equilibrations were also done at 1200°C for 20 minutes, but tantalum crucibles were used

Table I Solute Distribution Between Uranium and Silver
(Voigt, Reference 66)

Solute	Decontamination factor fission product content		Distribution coefficient fission product content	
	Medium	High	Medium	High
Cs	29	1000		~10
Sr	14	420		400
La	9		6.3	
Ce	11	55	18	270
Zr	3.0		1.4	
Te	2.6		2.1	
Ru	~1	1.04	0.02	0.03
Pu	3.7	5.1	4.6	7.0

Table II Solute Distribution Between Uranium and Rare Earths
(Voigt, Reference 66)

Solute	Decontamination factor fission product level		Distribution coefficient fission product level	
	Medium	High	Medium	High
		Cerium		
Cs	85	2420	0.16	0.43
Sr	28	260	0.39	0.85
Ce	6.9	9.8	11	23
Ru		1.17	0.18	0.17
Pu	1.50	1.58	0.95	1.02
		Lanthanum		
Cs	56	280	0.26	0.20
Sr	37	17	4.4	0.09
Ce	15.7	16.4	44	41
Ru	1.15	1.19	0.42	0.28
Pu	1.28	1.22	0.65	0.56

Table III Extraction of U-Cr Alloy
(Voigt , Reference 66)

Fission Product	Decontamination factors extractant				Distribution coefficients extractant			
	Ag	Ag*	Ce	La	Ag	Ag*	Ce	La
Cs	3.8	14.6	15	3.0	2.3	1.08	1	1.7
Sr	9.4	10.1	15	5.2	8.8	9.5	.5	1.1
Ba	9.7		50	5.2	7.9		6	1.0
Y	7.1	8.1	34	3.5	8.1	9.2	63	4.6
La	8.6		210	4.9	9.7		475	6.5
Ce	12	8.4	43	3.0	18	12	94	4.5
Zr	7.8	10.6	37	1.7	1.5	2.2	6.7	0.26
Nb			1.2	1.2			0.2	0.01
Mo	1.25		2.5		0.06		0.03	
Ru	1.2		1.6	1.4	0.04		1.2	0.23
Te	1.5		75	5.3	3.2		98	2.0
Pu	13.5	6.8	1.4	1.13	21	8.3	0.64	0.52

*Higher content of fission products and plutonium

Table IV Extraction of Fissium
(Voigt , Ref. 66)

	Decontamination factors extractant		Distribution coefficients extractant	
	Ag	Ce	Ag	Ce
Zr	2.7	2.5	0.6±0.3	0.8±0.2
Mo	1	1	0.02±0.015	0.04±0.01
Ru	1	1.9	0.02±0.015	1.0±0.2
Nd	9	20	3.7±2	30±20

because graphite reacts with the rare earths to form carbides.

Table III summarizes the results of extractions of the uranium-chromium eutectic with silver, cerium and lanthanum. These extractions were at 1050-1150°C for 20 to 40 minutes in tantalum crucibles.

Table IV summarizes Voigt's results for extraction of "fissium".

Voigt blames the lack of reproducibility in the results on the low concentrations of fission products. It is believed that traces of oxide, carbide, or fluoride impurities in the uranium might affect the measured distribution coefficients. For this reason, further experiments were conducted on "fissium" in which the concentration levels correspond to 2% burn-up as compared with a burn-up of only 0.03% in the irradiated samples of "high" fission product concentration.

Because the reproducibility of these experiments was also poor by the standards of aqueous solution chemistry, results are reported in Tables V and VI as ranges of values rather than actual values. The experiments were performed in tantalum crucibles in vacuum at 1200 to 1220°C on 150 g samples of uranium using an equal volume of extractant.

Table V Distribution Coefficients for Extraction of Fissium (Voigt, Reference 62)

Fission Products	Extractants			Legend	
	Ag	Ce	La	Letter	Range
Mo	B	C	B	B	0.003-0.03
Ru	B	D	D	C	0.03 -0.3
Zr	D	D	D	D	0.3 -3
Nd	E	E		E	3 -30
Ce	D		E		

Table VI Decontamination Factors for Extraction of Fissium (Voigt, Reference 62)

Fission Products	Extractants			Legend		
	Ag	Ce	La	Letter	Dec. Fac.	% Removed
Mo	P	P	P	P	1-1.3	0-23
Ru	P	Q	Q	Q	1.3-1.8	23-45
Zr	S	Q	S	S	2.5-5	60-80
Nd	T	U		T	5-10	80-90
Ce	S		S	U	10-50	90-98

Voigt performed several experiments, reextracting fission products with inactive uranium to determine whether or not equilibrium conditions had been attained in the original extractions. The agreement was good for some fission products, but note the results in Table VII for forward and reverse extraction of the rare earths neodymium and cerium with silver.

Table VII Forward and Reverse Extractions (Voigt, Ref. 62)

Fission Products	Ag		Ce		La		Legend	
	For.	Rev.	For.	Rev.	For.	Rev.	Letter	Dist. Coeff.
Mo	B	D	C	C	B	D	B	0.003-0.03
Ru			D	D	D	D	C	0.03-0.3
Zr	D	D	D	E	D	E	D	0.03-3
Nd	E	G	E	G			E	3-30
Ce	D	G			E	F	F	30-100
							G	100

Voigt also reports attempts to extract molybdenum from uranium with magnesium and magnesium alloys of tin, zinc and aluminum. The measured distribution coefficient was 0.2 in all cases.

Voigt measured mutual solubilities for the silver — uranium, silver — U-Cr eutectic, cerium — uranium, and cerium — U-Cr eutectic systems.

Table VIII Mutual Solubility Data

Solvent	Solute	T(°C)	Solubility
U	Ag	1135	0.03%
Ag	U	1135	~4%
U-Cr eutectic	Ag	960	0.02%
Ag	U-Cr eutectic	960 960	U: 2.8% Cr: 0.03%
U	Ce	1150	1.2%
Ce	U	1150	3.6%
U-Cr eutectic	Ce	970	1.5%
Ce	U-Cr eutectic	970 970	U: 2.5% Cr: 0.4%

Voigt draws the following conclusions from his experiments. The volatile fission products cesium, strontium, and barium are easily removed. The rare-earth metals are readily extracted with silver showing decontamination factors and distribution coefficients of about 10. Crucible reactions particularly with graphite crucibles remove significant amounts of the rare-earths. Cerium and silver remove zirconium and tellurium. Ruthenium and molybdenum are the most difficult fission products to remove; removal is poor with silver, fair with cerium.

Silver is a promising extractant for plutonium and it appears that the plutonium distribution coefficient is concentration dependent.

Chiotti and Voigt[68] prepared uranium-cerium samples by induction melting in tantalum crucibles. A considerable accumulation of the radioactive tracer at the crucible interface was detected by autoradiograph. The outer layer of metal was machined off to obtain a surface free of "hot spots" before running extraction experiments with silver. Autoradiographs made after the silver extraction also showed considerable accumulation of cerium radioactivity at the uranium-crucible interface and also at the U-Ag interface.

Magnesium has received attention as a possible liquid metal extractant because of its low mutual solubility with molten uranium. Barney and Keneshea[67] have studied the distribution of plutonium and fission products between uranium and magnesium at 1150°C in tantalum crucibles. Their experiments were done inside a mild steel bomb because of the high vapor pressure of magnesium. (Magnesium boils at 1107°C.) The weight of uranium samples used ranged from about 1 to 50 grams and contained from 0.03 to 97 ppm of Pu. U/Mg weight ratios varied from about 0.1 to 6. Heating times varied from 5 minutes to 1 hour. Distribution coefficients are reported on a mole fraction basis. Distribution coefficients for Pu have the value 0.23±.03. This value was constant over the range of Pu concentrations from 0.03 to 97 ppm. The results for fission products are summarized in Table IX.

Pyrometallurgical techniques have been considered for processing breeder blankets. By an appropriate choice of liquid metal extractant, it is possible to separate fissile U^{233} from a blanket of fertile Th^{232}, or fissile Pu^{239} from a blanket of U^{238}.

Table IX Distribution of Fission Products Between Uranium and Magnesium at 1150°C (Barney and Keneshea, Reference 67)

Fission Product	Distribution Coefficient (mole fraction basis)
Ce	1.9±0.4
*R.E.	1.0±0.6
Te	1.7±0.7
Ru	0.007±0.003
Ba	~ .03
Zr	~ .016

* Rare earth activity mainly long-lived Pm^{147}. Distribution coefficients for the "rare-earths" were lower in experiments performed on diluted samples than on samples with 97 ppm Pu. No such effect was observed with Ce.

Chiotti and Voigt[68] and Chiotti and Shoemaker[69] have measured mutual solubility in the uranium-magnesium-thorium system. Molten uranium and magnesium are essentially immiscible and so are molten thorium and uranium. Thorium and magnesium, however, form a eutectic at 42 w-% Th (M.P. 582°C). Therefore magnesium is a possible extractant for processing uranium blankets. Thorium can be precipitated from the eutectic as ThH_2.

Liquid metal extraction of plutonium from uranium has been studied by McKenzie[70] using silver as the extractant. When equal weights of silver and uranium containing 0.1% plutonium were equilibrated at 1350°C, 88% of the total plutonium was found in the silver phase. Each phase weighed about 4 grams. The equilibrations were carried out in beryllia crucibles under argon. Equilibrium was attained in 20 minutes. The

reproducibility of McKenzie's experiments is remarkably good: as good as that typical of aqueous solution chemistry. The variation of distribution coefficient (K_{Pu}) with temperature and also with initial plutonium concentration was measured. Distribution coefficients were measured at five temperatures between 1160 and 1350°C using an initial plutonium concentration of 0.1 w-%. A plot of log K_{Pu} vs: 1/T gave a straight line with almost no scatter in this temperature range. A value of ΔH (the sum of a total or integral heat of solution of Pu in Ag and a heat of dilution of Pu in U) of 12.5 kcal is obtained from the slope of this line. Values of K_{Pu} (on a mole fraction basis) are 2.01 at 1160°C and 3.45 at 1350°C. Distribution coefficients were found to increase with decreasing plutonium concentration. Measurements at 1325°C gave a value of 3.16 for K_{Pu} at 1.0×10^{-1} w-% Pu and 7.48 at 3.63×10^{-4} w-% Pu. McKenzie found that small additions of gold affected the plutonium distribution coefficient. K_{Pu} passed through a maximum of 13.5 at a total gold concentration of 3.5 w-% of uranium.

The data reported above show that silver and magnesium not only extract fission products from uranium but that some plutonium is also extracted. Since Pu^{239} is fissionable, it would be advantageous in core processing to use a liquid metal extractant which does not remove plutonium from uranium. Such an extractant would of course be required for reprocessing plutonium cores. Molten calcium has been found to have the required properties. Martin, Jenkins, and Keen[71] report the results of equilibrations between 10 ml samples of U-Pu-Ce and U-Ce alloys and equal volumes of calcium under argon at temperatures ranging from 1120-1235°C. Tables X and XI give the measured distribution coefficients on a weight fraction basis.

Table X The Distribution of Plutonium, Uranium and Cerium Between Calcium and Various Alloy Phases at 1120°-1235°C (Martin, et al. Reference 71)

Alloy	Constituent	Distribution Coefficient
U/Pu/Ce	U	0.0043±.0015
U/Pu/Ce	Pu	0.0073±.0006
U/Pu/Ce	Ce	11.1 ±1.1
U/Ce	Ce	9.5 ±0.7

Table XI The Distribution of Fission Products Between Molten Calcium and Uranium or Uranium-Plutonium Alloy (Martin, et al. Reference 71)

Element	Distribution Coefficient	% Volatilized (1 hr. at 1200°C)
Cs^{137}	0.05-0.11	60-95
Sr^{90}	3.2 -12	6-29
Y^{90} (Sr^{90} daughter)	2.5	
Ba^{140}	v. high	2
Mo	< 0.005	nil
Ru	$< 1 \times 10^{-4}$	nil
La^{140}	50-100	nil
Ce	9	nil

Crucibles of both tantalum and tantalum coated with Ta_2B or TaB were used. Martin reports that tantalum was not a satisfactory container at 1200°C. The boride coated crucibles proved better, increasing crucible life from 5 to 24 hours.

Leary et al.[72] have removed fission products from the liquid Pu-9.5 a-% Fe eutectic (MP 406°C) by extraction with the 18 a-% calcium - 32 a-% magnesium eutectic which has a very low mutual solubility with the Pu-Fe alloy. Equal volumes of the two alloys were equilibrated under helium for 24 hours at 600°C. The following distribution coefficients (defined as w-% element in the extractant Ca-Mg phase divided by w-% in the Fe-Pu phase) were reported.

Table XII Solute Distribution Between the Pu-Fe Eutectic and the Ca-Mg Eutectic (Leary et al. Reference 72)

Element	Distribution Coefficient
Zr	0.35
Nb	< 0.7
Mo	0.16
Ru	< 0.06
La	61
Ce	1.02
Fe	.011
Pu	.015

B. Measurement of the Distribution of La and Ba Between U-Cr and Mg

Equilibrium experiments to measure the distribution of La^{140} and Ba^{140} between the molten U-Cr eutectic and Mg were undertaken primarily to resolve an order of magnitude discrepancy in the literature. The coefficients reported by Barney and Keneshea[67] for the distribution of Ce and Ba between U and Mg at 1150°C are more than two orders of magnitude lower than values for the distribution of the same two solutes between the U-Cr eutectic and Mg reported by the laboratory at Ames.[103] It seems unlikely that this large difference could be a real effect due to the presence of 20 a-% chromium in the uranium-rich phase. Haefling and Daane[95] measured mutual solubility in uranium-rare earth systems. They found the solubility of Ce in U to be 1.16 w-% at 1150°C. Voigt[66] measured the solubility of Ce in U and also in the U-Cr eutectic. His value for the solubility of Ce in U is 1.2% at 1150°C, very close to that measured by Haefling and Daane. Voigt's value for the solubility of Ce in the U-Cr eutectic is 1.5% at 970°C, not very different from its solubility in U. Since the solubility of Ce is about the same in the U-Cr eutectic as in U, one would expect its distribution between the U-Cr eutectic and Mg to be about the same as it is between U and Mg.

The equilibrium experiments were performed on ~5 g samples of lightly irradiated (11 hours at a flux of 2×10^{13} n/cm^2-sec) samples of the depleted U-Cr eutectic using an equal volume of Mg extractant. Equilibration was in graphite crucibles. Graphite was used because it simplified handling problems. After equilibration and cooling, the graphite crucible could be broken easily with a hammer and the uranium-magnesium slug removed. From a chemical point of view, graphite is a poor choice of container

material for this system since both La and Ba, the solutes of interest, form carbides. (Voigt[66] used tantalum crucibles when doing extractions with the rare earths. Culpin[96] used graphite to measure the viscosity of liquid magnesium and calcium but found that barium attacked graphite vigorously above the melting point.) Tantalum would have been a better choice of container material, but its use would have required remote handling facilities to saw open the crucible and separate the U-Cr and Mg phases after equilibration. As it was, γ-ray exposure to the experimenter reached the maximum allowable weekly dosage during the course of the equilibrium experiments.

Small graphite crucibles 3/4-in. O.D. with a 1-1/2-in. deep 1/4-in. hole were used. Each crucible was baked out at 1000°C for 45 minutes under argon to remove traces of oxygen and water. The weighed irradiated U-Cr slug was placed in the crucible first with an equal volume of magnesium on top of it. The crucible was then closed with a tightly fitting graphite plug. (This charging operation was done under an argon stream.) The crucible was then placed in a tantalum basket and suspended inside a stainless steel sheath in a resistance furnace by means of a steel chain. By jerking the chain at intervals during the heating period the molten metal phases were agitated. A stream of argon was kept flowing in the sheath. Runs were made at 900, 1000, and 1100°C for 30 minutes. (The temperature inside the crucible was calibrated against the "furnace temperature" at the position where the tantalum basket was suspended by a probe thermocouple.) Agitation was stopped about 5 minutes before the end of the heating period to prevent inclusion of uranium in magnesium. At the end of the heating period, the tantalum basket was pulled up out of the furnace and into a stainless steel "cooling can". The purpose of

the cooling device was to freeze the two metal phases as quickly as possible so that the measured "equilibrium" distribution would be characteristic of the elevated temperature of the heating period. A slow cooling period might have permitted the equilibrium distribution to shift to that existing at 860°C, the melting point of the eutectic. An argon stream was kept flowing vigorously through the cooling device to prevent oxidation of the tantalum or entry of oxygen into the crucible while the metals cooled. Figure 3 is a photograph of the cooling arrangement. The device located just above the top of the furnace sheath and just below the "cooling can" is an exhaust designed to trap any fission product gases which might escape from the crucible. After a 10-15 minute cooling period, the graphite crucible was smashed (inside a polyethelene bag to trap radioactive particles) and the metal ingot recovered and weighed. Mg loss during heating was about 4%. The ingot was placed inside a glove box where the two phases were sawed apart. The cut was made in the magnesium phase about 1/16-in. from the interface. The 1/16-in. of Mg remaining on the U-Cr slug was dissolved in HCl. Also dissolved was some of the U-Cr nearest the interface. The recovered Mg was placed in dilute HCl for a few seconds until the surface was bright in order to remove any rare earth carbides which might be present on the surface. This procedure is designed to avoid measurements of radioactivity present at the metal-crucible and metal-metal interfaces.

In the first chapter, it was pointed out that Chiotti and Voigt,[68] who studied the extraction of Ce from U using Ag as the extractant, reported accumulation of cerium radioactivity at the U-Ag interface and at the metal-tantalum crucible interface. Voigt,[66] in his equilibrium studies, also avoided measurements of radioactivity at the interface.

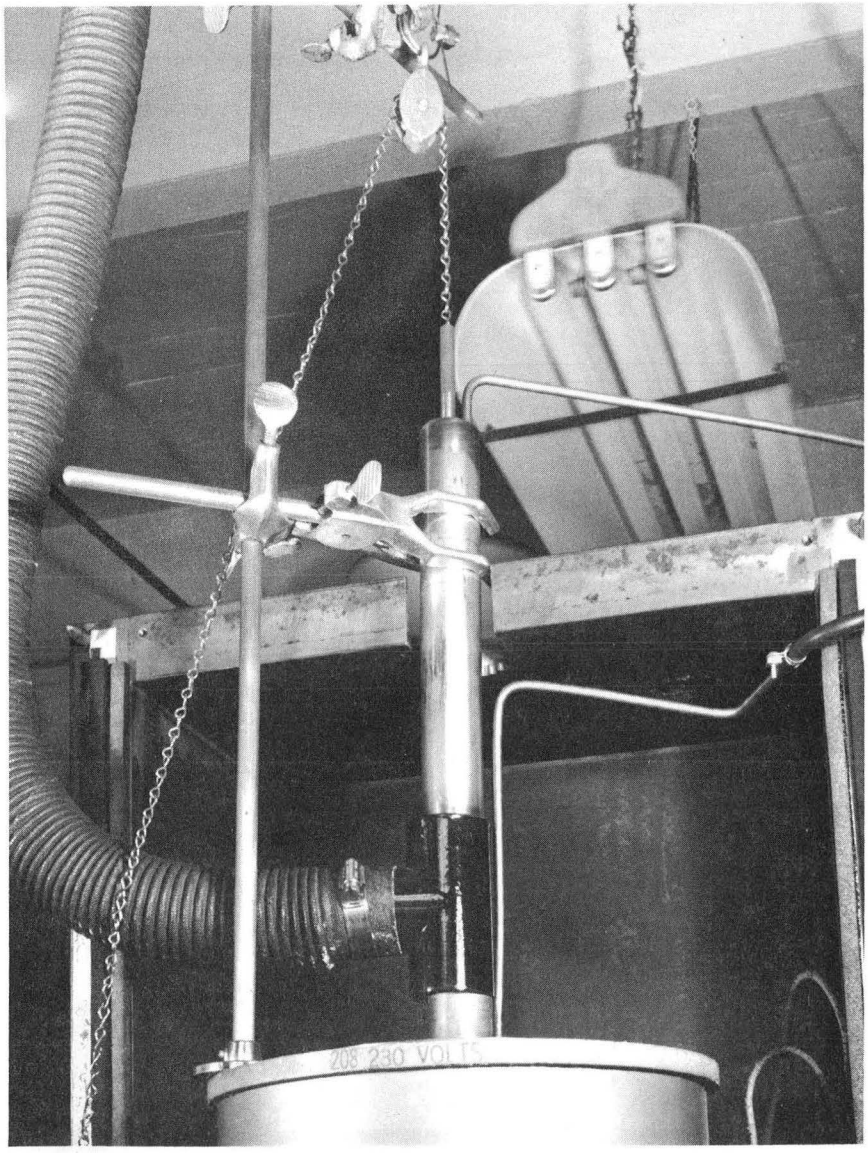

ZN-5471

Fig. 3

Therefore, in determining the distribution coefficients, only the radioactivity in the bulk U-Cr and Mg phases was counted. In this way it was hoped to avoid LaC_2 and La_2O_3 which would be expected to accumulate at the interface.

After washing in HCl, the U-Cr and Mg phases were weighed and the activity of La^{140} in each phase was then measured by the techniques described in Appendix A.. The decay of La^{140} activity in each phase was followed in order to determine the La to Ba abundance ratio immediately after extraction. It was found in all cases except Run. no. 23 that La^{140} activity in the bulk Mg phase decayed with a half-life of 40.2 hours. In other words there was no measurable Ba^{140} in the bulk Mg phase. It is supposed that what little Ba^{140} might have been extracted by Mg was absorbed by the graphite crucible during the short cooling period. Decay of the U-Cr phase showed Ba^{140} to be present in greater proportion than the 6.64:1 barium to lanthanum ratio of secular equilibrium. In fact, in some cases, La^{140} activity increased to a maximum and then decreased. This is to be expected when a larger fraction of La^{140} than Ba^{140} is extracted. Figure 4 is the decay plot for both the U-Cr and the Mg phases for Run no. 21.

The La^{140} distribution coefficients on a concentration basis, m_{La}, have been calculated from the La^{140} activities, a^0_{La}, of the two phases immediately after extraction by Eq. (5).

$$m_{La} = \frac{a^{Mg}_{La}}{a^{U\text{-}Cr}_{La}} \times \frac{\text{wt. U-Cr}}{\text{wt. Mg}} \times \frac{\rho_{Mg}}{\rho_{U\text{-}Cr}} \qquad (5)$$

The measured distribution coefficients are probably low, due to the tendency of the graphite crucibles to pick up fission products.

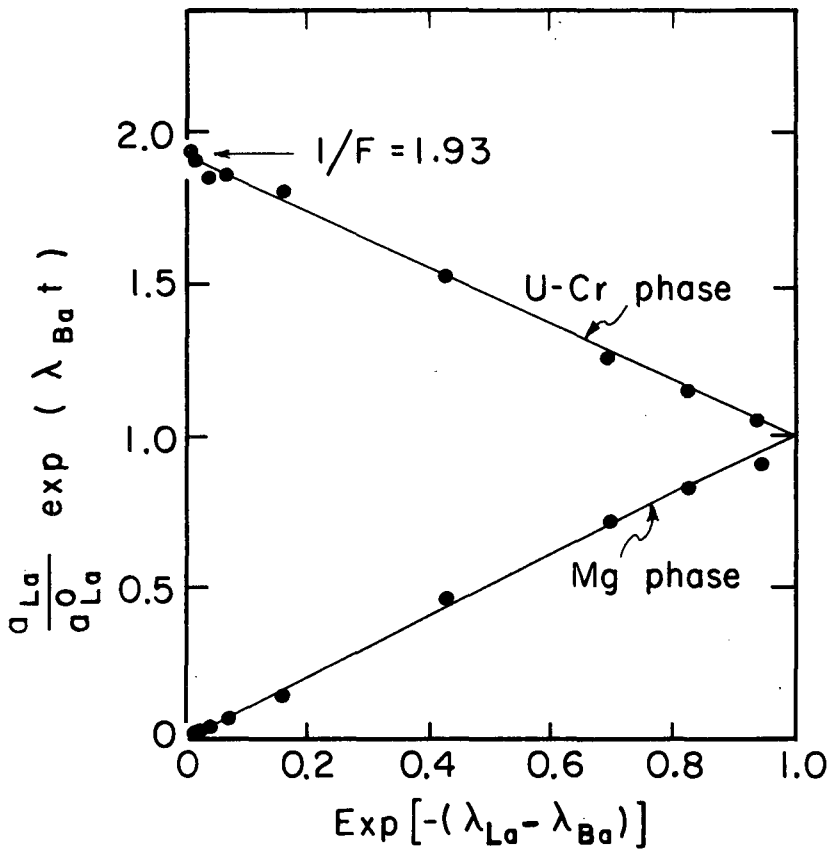

MU-37032

Fig. 4

The decay of La^{140} activity in the Mg phase for Run no. 23 showed the presence of a small amount of Ba^{140}. The distribution coefficient, in this case, can be calculated from the La to Ba abundance ratios in each phase (determined by F) and the distribution coefficient for La, m_{La}.

$$m_{Ba} = m_{La} \frac{F^{U\text{-}Cr}}{F^{Mg}} \quad . \tag{6}$$

Distribution coefficients on a concentration basis, m, may be converted to distribution coefficients on a mole function basis, K^x, as follows:

$$K^x = m \frac{\rho_{U\text{-}Cr}}{\rho_{Mg}} \times \frac{\text{Mol. wt. Mg}}{\text{Mol. wt. U-Cr}} \tag{7}$$

At 1000°C,

$$K^x = m\ (1.33) \tag{8}$$

Decontamination factors for La, $D.F._{La}$, are calculated from the ratio of activity per unit weight before extraction to activity per unit weight after extraction

$$D.F._{La} = \frac{a_{La}(\text{Before})}{a_{La}(\text{After})} \times \frac{\text{wt. U-Cr (After)}}{\text{wt. U-Cr (Before)}} \tag{9}$$

Decontamination factors for Ba, $D.F._{Ba}$, are calculated from the La decontamination factor and the change in the La to Ba abundance ratio in the U-Cr phase, $F^{U\text{-}Cr}$ (all U-Cr samples were at secular equilibrium before extraction):

$$D.F._{Ba} = D.F._{La} \times F^{U\text{-}Cr} \tag{10}$$

The data for runs 20-23 are given below.

RUN NO. 20 1000°C

	weight, g.	a_{La}*	fe	a_{La}	F
U-Cr before extraction	5.2458	12,900	.8	16,100	1
U-Cr after extraction	5.2124	6,300	.8	7,880	.525
Mg after extraction	.5963	1,900	1	1,900	infinity

$$D.F._{La} = \frac{a_{La}(\text{before})}{a_{La}(\text{after})} \times \frac{\text{wt. U-Cr (after)}}{\text{wt. U-Cr (before)}} = \frac{16,100}{7880} \times \frac{5.212}{5.246} = 2.03$$

$$D.F._{Ba} = D.F._{La} \times F^{U\text{-}Cr} = 2.03\ (.525) = 1.06$$

$$m_{La} = \frac{a_{La}^{Mg}}{a_{La}^{U\text{-}Cr}} \times \frac{\text{wt. U-Cr}}{\text{wt. Mg}} \times \frac{\rho_{Mg}}{\rho_{U\text{-}Cr}} = \frac{1900}{7800} \times \frac{5.212}{.596} \times .0909 = .192$$

$$K_{La}^{x} = m_{La}(1.33) = (.192)(1.33) = .256$$

* activity measured in counts per minute, detector 75-in. from sample, uncorrected for self-absorption.

RUN NO. 21 1000°C

	weight, g	a^{*}_{La}	fe	a_{La}	F
U-Cr before extraction	4.5544	51,075	.8	63,800	1
U-Cr after extraction	4.4862	11,000	.8	13,750	.518
Mg after extraction	.6100	1,870	1	1,870	infinity

$$D.F._{La} = \frac{63,800}{13,750} \times \frac{4.486}{4.554} = 4.58$$

$$D.F._{Ba} = 4.58\ (.518) = 2.37$$

$$m_{La} = \frac{1,870}{13,750} \times \frac{4.4862}{.6100} \times .0909 = .0906$$

$$K^{x}_{La} = (.0906)(1.33) = .120$$

* activity measured in counts per minute, detector 75-in. from sample, uncorrected for self-absorption

RUN NO. 22 900°C

	weight, g	a^{*}_{La}	fe	a_{La}	F
U-Cr before extraction	4.6955	48,900	.8	61,000	1
U-Cr after extraction	4.6518	18,300	.8	22,900	.732
Mg after extraction	.6183	2,630	1	2,630	infinity

$$D.F._{La} = \frac{61,000}{22,900} \times \frac{4.6518}{4.6955} = 2.65$$

$$D.F._{Ba} = 2.65\ (.732) = 1.94$$

$$m_{La} = \frac{2,630}{22,900} \times \frac{4.6518}{.6183} \times .0909 = .0785$$

$$K^{x}_{La} = (.0785)\ (1.33) = .104$$

* activity measured in counts per minute, detector 75-in. from sample, uncorrected for self-absorption.

RUN NO. 23 1100°C

	weight, g	a^{*}_{La}	fe	a_{La}	F
U-Cr before extraction	4.961	24,265	.8	30,400	1
U-Cr after extraction	4.837	7,750	.8	9,700	.337
Mg after extraction	.4875	4,300	1	4,300	18.2

$$D.F._{La} = \frac{30,400}{9,700} \times \frac{4.837}{4.961} = 3.06$$

$$D.F._{Ba} = 3.06\ (.337) = 1.03$$

$$m_{La} = \frac{4300}{9700} \times \frac{4.837}{.4875} \times .0909 = .400$$

$$K^{x}_{La} = .400\ (1.33) = .532$$

$$m_{Ba} = \frac{F^{U\text{-}Cr}}{F^{Mg}}\ m_{La} = \frac{.337}{18.2}\ (.400) = .0074$$

* activity measured in counts per minute, detector 75-in. from sample, uncorrected for self-absorption.

Table XIII summarizes the decontamination factors and distribution coefficients for runs 20-23.

Table XIII Summary of Equilibrium Runs

Run No.	T(°C)	$D.F._{La}$	$D.F._{Ba}$	m_{La}	K^x_{La}	m_{Ba}	K^x_{Ba}
20	1000	2.03	1.06	.192	.256		
21	1000	4.58	2.37	.091	.120		
22	900	2.65	1.94	.078	.104		
23	1100	3.06	1.03	.400	.532	.0074	.0098

The values measured in this work and reported in Table XIII may be compared with data reported by Barney and Keneshea[67] and by the Ames Laboratory.[103]

Barney and Keneshea have measured distribution coefficients of various fission products between uranium and magnesium at 1150°C. On a mole fraction basis values of K^x_{Ce} range from 1.3 to 2.8. Values of $K^x_{R.E.}$ range from 0.23 to 2.4. Two measurements were made for the distribution coefficient of barium: $K^x_{Ba} = 0.023$ and $K^x_{Ba} = 0.039$ for cerium and the rare earths. The average values are

$$K^x_{Ce} = 1.9 \pm 0.4$$

$$K^x_{R.E.} = 1.0 \pm 0.6$$

The average of the two values for barium is

$$K^x_{Ba} = .031$$

All of the above values are on a mole fraction basis.

The values on a concentration basis are,

$$m_{Ce} = 1.5$$

$$m_{R.E.} = .81$$

$$m_{Ba} = .025$$

Measurements at Ames give much higher values for the distribution coefficients of cerium and barium between Mg and the U-Cr eutectic. The reported values are $m_{Ce} \approx 500$ and $m_{Ba} \approx 5$. (The temperature was not reported but is presumed to be 860°C, the melting point of the eutectic.)

The measured distribution coefficients have been plotted in Fig. 5 and compared with the data of Barney and Keneshea, and with distribution coefficients estimated by regular solution theory. The details of this estimation are given in Appendix F. The four data points have been treated by the least squares method to give the equation $\log K^x_{La} = 3.73 - 5.6 \times 10^3/T$. A value for ΔH of 25.6 kcal is computed from the slope of this line. (McKenzie's value for ΔH for the distribution of Pu between U and Ag is 12.5 kcal.)

The best value of the distribution coefficient for La, K^x_{La}, at 1000°C as determined by these experiments is 0.215. On a concentration basis the coefficient m_{La} is .161.

C. Estimation of the Distribution of Ba Between U-Cr and Mg at 1000°C

The run made at 1100°C (Run no. 23) was the only one which showed a measurable amount of Ba^{140} in the extractant Mg phase. The distribution coefficient for Ba, m_{Ba}, was determined to be .0074. The value of m_{Ba} at 1000°C can be estimated from the value measured at 1100°C by assuming the same temperature coefficient for Ba as that measured for La in the same solvent pair.

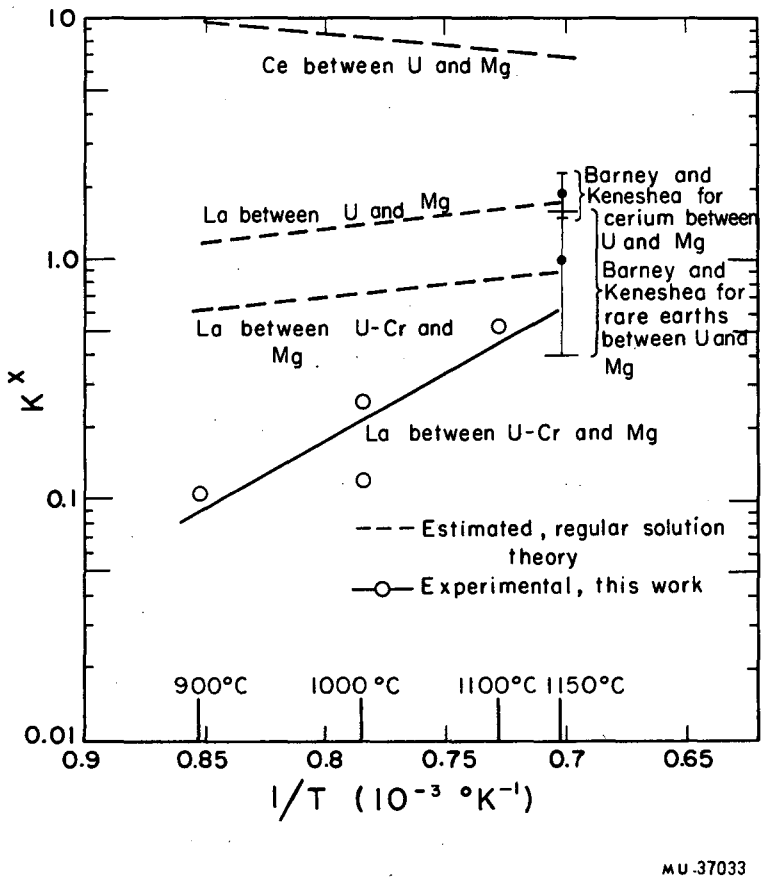
10
1.0
0.1
0.01
Kx
Ce between U and Mg
La between U and Mg
Barney and Keneshea for cerium between U and Mg
Barney and Keneshea for rare earths between U and Mg
La between U-Cr and Mg
La between U-Cr and Mg
Estimated, regular solution theory
Experimental, this work
900°C
1000°C
1100°C
1150°C
0.9
0.85
0.8
0.75
0.7
0.65
1/T (10⁻³ °K⁻¹)
MU-37033

Fig. 5

$$\frac{K^x_{La}(1000°C)}{K^x_{La}(1100°C)} \approx \frac{0.215}{0.45} = .478$$

$$m_{Ba}(1100°C) = 0.0074 \quad \text{(Run no. 23)}$$

Therefore $$m_{Ba}(1000°C) = (0.478)(0.0074) = 0.0035$$

This value may be compared with the data of Barney and Keneshea who measured K^x_{Ba} at 1150°C in the U-Mg solvent pair.

$$K^x_{Ba} = .031 \text{ at } 1150°C$$

$$m_{Ba}(1150°C \text{ between U and Mg}) = \frac{.031}{1.23} = .025$$

Assuming the same temperature coefficient for Ba in the Mg-U solvent pair as that measured for La in the U-Cr-Mg pair:

$$\frac{K^x_{La}(1000°C)}{K^x_{La}(1150°C)} \approx \frac{.215}{.64} = 0.336$$

Assume that the effect of changing the solvent from U to U-Cr is the same on Ba as on Ce. (See discussion of activity coefficients in U and U-Cr in Appendix F.)

$$\frac{m_{Ba}(\text{between U-Cr and Mg})}{m_{Ba}(\text{between U and Mg})} = 0.516$$

Therefore $$m_{Ba}(1000°C \text{ between U-Cr and Mg}) = (0.516)(0.336)(.025) = 0.0043$$

The value for m_{Ba} between U-Cr and Mg at 1000°C has been estimated on the basis of

1) a measured value at 1100°C in the U-Cr — Mg solvent pair:

$m_{Ba}(1000°C) = 0.0035$

2) a measured value of Barney and Keneshea at 1150°C in the U-Mg

solvent pair: $m_{Ba}(1000°C) = .0043$.

The two values are in good agreement.

Using a value of .0035 for m_{Ba} at 1000°C it is possible to calculate values of F^{Mg} for runs 20 and 21 (1000°C) from Eq. (6) and the measured values of m_{La} and F^{U-Cr}. The calculated values of F^{Mg} are 28.8 and 13.4 for runs 20 and 21 respectively. The corresponding 1/F values are 0.035 and 0.0745 which represent detectable amounts of Ba. It is concluded that the fact that Ba was not detected in the Mg extractant phase for these runs is due to Ba pick-up by the graphite crucibles.

While the measured distribution coefficients for La and Ba may be in error because of the tendency of the graphite crucibles to pick-up fission products, the results of the experiments indicate that the low values given by Barney and Keneshea are probably more accurate than the high values reported by the Ames Laboratory.

III DIFFUSION IN LIQUID METAL SYSTEMS

Introduction

Since Roberts-Austen's[1] measurements in the 1890's of the diffusion of noble metals in lead, bismuth, and tin, a number of workers have studied mutual diffusion in dilute molten metal systems. Most of the data have been obtained by studying diffusion in capillaries; diffusion coefficients in mercury have sometimes been obtained by electrochemical methods.[2-4]

The purpose of this study is to discuss two techniques for correlating the available data. The first, due to Olander,[5] has been used successfully to correlate mutual diffusion data in dilute binary systems where both solute and solvent are organic liquids. Olander's technique is a modification of Eyring's absolute rate theory[6,7] and includes a means for estimating the difference between the free energy of activation for diffusion and that for viscosity in dilute binary systems. (This difference may be assumed equal to zero for self-diffusion but not for mutual diffusion.)

The second correlation to be discussed is an application of the principle of corresponding states, which has been applied to liquified rare gases and some organics by Thomaes and Itterbeek,[8] to diffusion in liquid metals.

A. Some Older Correlations

Self-diffusion and mutual diffusion in both organic liquids and molten metals has often been correlated by means of the Stokes-Einstein equation

$$\frac{D\mu}{kT} = \frac{1}{4\pi a}$$

or

$$\frac{D\mu}{kT} = \frac{1}{6\pi a} \qquad (11)$$

where D is the diffusion coefficient of the solute, μ the viscosity of the solvent, k the Boltzmann constant, T the absolute temperature, and a the radius of the diffusing molecule. The choice of the constant 4 or 6 in Eq. (11) depends on taking this hydrodynamic model so seriously as to imagine that either a "slip" or "no-slip" situation prevails as the solute moves through a "continuous" fluid. The Stokes-Einstein equation gives the correct order of magnitude ($D = 10^{-5}$ cm^2/sec) if a reasonable choice is made for the radius of the diffusing atom. For liquid metals it has been found that measured values of D suggest values of a closer to the ionic radius than to the atomic radius of the diffusing atom. On the basis of viscosity and heat of vaporization data, Eyring[6] has concluded that the "unit of flow" in metals is the metal ion stripped of its conductance electrons.

Li and Chang[9] have attempted to explain the constant in the Stokes-Einstein equation on the basis of a lattice structure picture of the liquid state. First, with 2a as $(V/N_{Av})^{1/3}$, the first form of Eq.(11) can be written:

$$\frac{D\mu}{kT} = \frac{1}{2\pi}\left(\frac{N_{Av}}{V}\right)^{1/3} \qquad (12)$$

for self-diffusion. Then they develop the equation,

$$\frac{D\mu}{kT} = \frac{\sigma-\tau}{2\sigma}\left(\frac{N_{Av}}{V}\right)^{1/3} \qquad (13)$$

where the lattice parameters σ and τ are the number of all the closest neighbors in all directions and the number of closest neighbors in one layer, respectively. N_{Av} is Avogadro's number and V is the molar volume of the liquid. If the liquid structure is simple cubic packing, $\sigma = 6$, $\tau = 4$, $2\sigma/(\sigma-\tau)$ is 6, and Eq. (13) is close to the first form of Eq. (11).

The experimental data examined by Li and Chang give values of about 6 for $\frac{kT}{D\mu}\left(\frac{N_{Av}}{V}\right)^{1/3}$. They therefore conclude that most liquids have approximately a cubical packing structure. One datum point for the self-diffusion of lead gives a value of 3.8 for $\frac{kT}{D\mu}\left(\frac{N_{Av}}{V}\right)^{1/3}$, leading to the conclusion that liquid metals have a closely packed structure of spheres with $\sigma = 12$, $\tau \doteq 6$, and

$$2\sigma/(\sigma-\tau) = 4.$$

Substitution of this numerical value of $2\sigma/(\sigma-\tau)$ in Eq. (13) gives

$$\left(\frac{D\mu}{T}\right)\left(\frac{4}{k}\right)\left(\frac{V}{N_{Av}}\right)^{1/3} = 1 \qquad (14)$$

B. Absolute Rate Theory

In his modification of Eyring's theory, Olander[5] correlated mutual diffusion data in dilue binary organic systems with the equation

$$Y = \left(\frac{D\mu}{T}\right)\left(\frac{\xi}{k}\right)\left(\frac{V}{N_{Av}}\right)^{1/3} = \exp\left\{\frac{\Delta F^*_\mu - \Delta F^*_D}{RT}\right\} \qquad (15)$$

The exponential in the R.H.S. of Eq. (15) represents the difference between the free energies of activation of the viscous and diffusive processes. The equation is due to Eyring; Olander's contribution is a technique for estimating this difference in dilute binary systems from pure component viscosity data.

Before attempting to apply this equation to mutual diffusion in molten metals, two questions should be answered. Does this equation work for self-diffusion in molten metals? What value of ξ should be used? (Olander used $\xi = 5.6$, determined empirically.[7] Li and Chang suggest a value of 4 as discussed previously.)

For self-diffusion, $\Delta F^*_\mu = \Delta F^*_D$ and Eq. (15) becomes

$$Y = \left(\frac{D\mu}{T}\right)\left(\frac{\xi}{k}\right)\left(\frac{V}{N_{Av}}\right)^{1/3} = 1 \qquad (16)$$

Walls and Upthegrove[10] have correlated self-diffusion data for ten metals by means of the equation

$$D = \frac{k\,T\gamma^{-1/3}}{2\pi hb(2b\ 1)}\left[\frac{V}{N_{Av}}\right]^{2/3} \exp\left[\frac{\Delta S^*}{R}\right] \exp\left[-\frac{\Delta H^*}{RT}\right] \qquad (17)$$

where h is Planck's constant, γ is a configuration constant = 4/3, b is the ratio of atomic diameter to interatomic distance, and ΔH^* and ΔS^* are the enthalpy and entropy of activation for viscosity. ΔS^* and ΔH^* are determined from viscosity data through Eyring's[11] defining equation

$$\mu = \frac{N_{Av}h}{V} \exp\left[-\frac{\Delta S^*}{R}\right] \exp\left[\frac{\Delta H^*}{RT}\right] \qquad (18)$$

By a proper choice of the constants ΔH^* and ΔS^* this equation represents viscosity data for molten metals very well. But nothing is gained by incorporating this representation of viscosity in Eq. (17). For the purposes of the following discussion Eq. (17) can be rewritten

$$D = \frac{kT\,\gamma^{-1/3}}{2\pi b(2b+1)\mu}\left[\frac{N_{Av}}{V}\right]^{1/3}$$

or

$$\left(\frac{D\mu}{T}\right)\left(\frac{2\pi b(2b+1)\gamma^{1/3}}{k}\right)\left(\frac{V}{N_{Av}}\right)^{1/3} = 1 \qquad (19)$$

By comparison of Eq. (19) with Eq. (16), it is readily seen that the real significance of Walls and Upthegrove's paper is a theoretical explanation for the constant ξ in Eq. (16). On the basis of geometrical considerations, they show that in evaluating the mobility of an atom,

one may imagine that a force acts on that atom over an area A and that the ratio of the area to the interatomic spacing d is

$$\frac{A}{d} = 2\pi r(2b+1) \tag{20}$$

where r is the atomic radius and b = r/d and is assumed to be the same for all molten metals. r is eliminated from Eq. (20) by Eqs. (21) and (22),

$$r = bd \tag{21}$$

$$\gamma = \frac{N_{Av}d^3}{V} \tag{22}$$

to obtain

$$\frac{A}{d} = 2\pi b(2b+1)\,\gamma^{1/3}\left(\frac{V}{N_{Av}}\right)^{1/3} \tag{23}$$

Walls and Upthegrove evaluate b empirically by comparing Eq. (17) with self-diffusivity data for mercury. By choosing b = .419, Eq. (17) fits the data for mercury. The same value of b is then used to reproduce other self-diffusivity data. (See Figs. 8-10.)

Comparing Eqs. (19) and (16) once again one can write

$$\xi = 2\pi b(2b+1)\,\gamma^{1/3} \tag{24}$$

using b = .419 and $\gamma = 4/3$, $\xi = 5.31$.

It is interesting to note that this value of ξ is close to 5.6, the value determined empirically[7] from mutual diffusion data.

Walls and Upthegrove also calculate b for mercury using Pauling's univalent radius,[12] r = 1.25Å and inter-atomic spacing data from Hendus,[13] d = 3.00Å. Calculated in this way, b = .416. Walls and Upthegrove admit that this agreement is fortuitous and that "in general, the b values calculated from ionic radii and x-ray diffraction data for most liquid

metals are closer to 0.3 than to 0.4." In fact, for the ten metals studied b values range from a low of .256 for sodium to a high of .437 for silver. These values of b correspond (through Eq. (24)) to values of ξ of 2.68 and 5.66. Yet a value of b = .419 (ξ = 5.31) works quite well for all ten metals.

From these observations, it is concluded that Eq. (16) with ξ = 5.31 correlates self-diffusivity data for molten metals, and that 5.31 is the right number to use regardless of the ratio of atomic diameter to interatomic spacing in the solid lattice. Whether or not the Walls and Upthegrove model is a good one, and whether or not their assumption is correct that the ratio of atomic radius to interatomic spacing is a constant for metals in the molten state, it appears that 5.31 is the correct constant to use. This conclusion will be extended to mutual diffusion and no importance will be attached to the atomic or ionic radius of the diffusing species as is done in the Stokes-Einstein equation.

To estimate the difference between free energies of activation of the viscous and diffusive processes, Olander[5] adopts the Eyring "hole" picture of the liquid state and imagines that the viscous process consists of two steps: 1) the formation of a hole, and 2) the "jump" of a neighboring molecule into the hole. Each step is characterized by a free energy of activation. If the jumping molecule is the same as the solvent molecule, the sum of these free energies of activation is ΔF^*_μ. If the jumping molecule is a diffusing solute the sum is ΔF^*_D. In dilute solution, step 1 is the same in both cases because the hole is always formed in the solvent.

Thus

$$\Delta F^*_\mu = \Delta F^h_{AA} + \Delta F^j_{AA} \tag{25}$$

$$\Delta F^*_D = \Delta F^h_{AA} + \Delta F^j_{AS} \tag{26}$$

where h and j represent the hole-making and jumping steps respectively and AA and AS represent solvent-solvent interactions and solvent-solute interactions respectively. Thus the desired difference in Eq. (15) equals the difference in the jumping steps for the viscous and diffusive processes. The free energy change for the jump step is related to the zero point energy difference and the ratio of the partition functions in the activated and equilibrium states. If it is assumed that all partition function ratios are close to unity and that zero point energy differences depend linearly on the force constants, then the geometric mean combination rule for force constants can be applied to the zero point energy differences and thus to a calculation of ΔF^j_{AS} from ΔF^j_{AA} and ΔF^j_{SS}. It is also assumed that the kinetic contribution is a constant fraction of the total free energy of activation:

$$f = \frac{\Delta F^j}{\Delta F^*} \quad . \tag{27}$$

It will be assumed here that f is the same for a given class of pure substances, e.g. molten metals.

Olander's final expression for the difference between the total free energies of activation for viscosity and mutual diffusion is

$$\Delta F^*_\mu - \Delta F^*_D = RTf\delta \tag{28}$$

where

$$\delta = \left(\frac{\Delta F_{AA}{}^*}{RT}\right)\left[1 - \left(\frac{\Delta F^*_{SS}}{\Delta F^*_{AA}}\right)^{1/2}\right] \tag{29}$$

Therefore

$$Y = \left(\frac{D\mu}{T}\right)\left(\frac{5.31}{k}\right)\left(\frac{V}{N_{Av}}\right)^{1/3} = e^{f\,\delta} \qquad (30)$$

The slope of a plot of $\ell n\ Y$ against δ should be equal to f.

Table XIV is a summary of the data for mutual diffusion in dilute molten metal systems for which viscosity data are available for both pure solute and solvent. Calculated values of Y and δ are also tabulated. Values of the free energy of activation for viscosity for the pure metals have been calculated from viscosity and density data by means of the defining Eq. (31).

$$\Delta F^* = RT\ \ell n \frac{V\mu}{N_{Av}h}\,. \qquad (31)$$

Plots of ΔF^* versus T determined in this way are linear with positive slopes. Since

$$\Delta F^* = \Delta H^* - T\Delta S^*, \qquad (32)$$

where ΔH^* and ΔS^* are the enthalpy and entropy of activation, ΔH^* and ΔS^* can be obtained from the intercept and slope of such a plot. Table XV gives values of ΔH^* and ΔS^* for the molten metals. ΔS^* is always negative for the molten metals.

Many diffusion measurements in molten metal systems have been made below the melting point of the solute. What value of ΔF^*_{SS} can be assigned to the solute in such cases? Cavalier[13] has measured the viscosity of molten and undercooled tin, copper, iron, cobalt, and nickel by means of an oscillating viscometer. He found that the energy of activation for viscosity was practically constant above and below the melting point. In other words, a plot of the logarithm of viscosity against reciprocal temperature can be extended below the melting point to represent the

viscosity of undercooled metals. It therefore seems reasonable that a plot of ΔF^* versus T can also be extended below the melting point to determine ΔF^*_{SS} for high melting solutes in low melting solvents. This procedure was used in the calculation of δ for such systems.

Figure 6 is a plot of the data listed in Table XIV. The best line through the points determined by the "method of averages",[48] has a slope of 0.5 and passes through the point $\delta = 0$, $Y = 1.1$. The dashed lines on either side of the best line represent 25% deviations. A slope of 0.5 indicates that one-half of the total free-energy of activation is due to the "jumping" step and one-half due to the "hole-making" step. (See Eq. (27)). This result is similar to Olander's. The fact that the best line passes through $\delta = 0$ at $Y = 1.1$ rather than at $Y = 1.0$ indicates that the constant 5.31 is slightly too high. A value of $\xi = 4.8$ would be better.

Despite the scatter in Fig. 6, it can be seen that consideration of the difference in free energies of activation for viscosity and diffusion according to Olander's method (Eq. (30)), produces a more reliable correlation than neglecting this difference (Eq. (16)). If the difference were of no importance, the values for Y would fall around the line $Y = 1$.

Table XIV Summary of mutual diffusion data in molten metals

System	T (°K)	$D \times 10^5$ (cm^2/sec)	μ (cp)	$\frac{D\mu}{T} \times 10^{10}$	V $\frac{cm^3}{mol}$	$V^{1/3}$ $\frac{cm}{mol^{1/3}}$	Y	ΔF_{AA}^* (cal/mol)	ΔF_{SS}^* (cal/mol)	δ	Refs.
Bi in Sn	723	3.6	1.21	6.03	17.40	2.59	.711	5750	6060	-.107	14
	773	4.6	1.15	6.85	17.50	2.59	.807	6060	6370	-.098	
	823	5.8	1.08	7.61	17.58	2.60	.900	6680	6680	-.094	
	873	6.6	1.04	7.86	17.69	2.61	.934	6990	6990	-.090	
Sb in Sn	723	5.0	1.21	8.36	17.40	2.59	.984	5750	6670	-.308	14
	773	5.7	1.15	8.48	17.50	2.59	.999	6060	6940	-.275	
	823	6.3	1.08	8.26	17.58	2.60	.976	6370	7200	-.245	
	873	6.9	1.04	8.22	17.69	2.61	.976	6680	7460	-.221	
Ag in Sn	828	4.8	1.08	6.26	17.58	2.60	.740	6400	9100	-.749	1
Au in Sn	828	5.37	1.08	7.01	17.58	2.60	.829	6400	9740	-.908	1
Pb in Sn	828	3.68	1.08	4.80	17.58	2.60	.567	6400	7270	-.258	1
Sn in Pb	723	2.6	1.97	7.09	19.60	2.70	.869	6550	5750	+.289	14
	783	3.9	1.78	8.86	19.80	2.70	1.089	6960	6120	+.279	
	823	4.3	1.68	8.77	19.90	2.71	1.081	7240	6370	+.275	
	873	5.5	1.56	9.82	20.05	2.71	1.210	7580	6680	+.269	
Bi in Pb	723	5.0	1.97	13.6	19.60	2.70	1.67	6550	6060	+.175	14
	773	6.2	1.81	14.5	19.80	2.70	1.78	6890	6370	+.172	
	823	7.3	1.68	14.9	19.90	2.71	1.84	7240	6680	+.174	
	873	8.3	1.56	14.8	20.05	2.71	1.82	7580	6990	+.174	

System	T (°K)	$D \times 10^5$ (cm^2/sec)	μ (cp)	$\frac{D\mu}{T} \times 10^{10}$	V $\frac{cm^3}{mol}$	$V^{1/3}$ $\frac{cm}{mol^{1/3}}$	Y	ΔF_{AA}^* (cal/mol)	ΔF_{SS}^* (cal/mol)	δ	Refs.
Sb in Pb	723	3.1	1.97	8.45	19.60	2.70	1.04	6550	6670	-.043	14
	773	4.1	1.81	9.60	19.80	2.70	1.18	6890	6940	-.018	
	823	5.5	1.68	11.22	19.90	2.71	1.38	7240	7200	+.011	
	873	6.4	1.56	11.44	20.05	2.71	1.41	7580	7460	+.035	
Cd in Pb	723	3.9	1.97	10.62	19.60	2.70	1.31	6550	6090	+.163	14
	773	5.0	1.81	11.70	19.80	2.70	1.44	6890	6400	+.163	
	823	6.0	1.81	12.25	19.90	2.71	1.51	7240	6710	+.163	
	873	6.8	1.56	12.15	20.05	2.71	1.50	7580	7020	+.164	
Au in Pb	823	3.7	1.68	7.55	19.90	2.71	.93	7240	9700	-.698	1
Sn in Bi	723	5.5	1.28	9.74	21.2	2.77	1.225	6050	5750	+.107	14
	773	6.5	1.18	9.92	21.3	2.77	1.25	6365	6060	+.099	
	823	7.3	1.10	9.76	21.5	2.78	1.23	6680	6370	+.093	
	873	8.2	1.02	9.59	21.6	2.78	1.21	6990	6680	+.091	
Au in Bi	828	5.22	1.08	6.81	21.5	2.78	.86	6710	9730	-.831	1
Sn in Ag	1250	3.87	3.78	11.7	11.60	2.26	1.21	11,630	9025	.607	22
	1350	4.66	3.30	11.4	11.72	2.27	1.18	12,240	9650	.561	
	1450	5.41	2.92	10.9	11.86	2.28	1.13	12,850	10,275	.471	
	1550	6.20	2.64	10.6	11.97	2.29	1.10	13,450	10,910	.435	
	1625	6.82	2.47	10.4	12.05	2.29	1.18	13,900	11,400	.407	

System	T (°K)	$D \times 10^5$ (cm^2/sec)	μ (cp)	$\frac{D\mu}{T} \times 10^{10}$	V $\frac{cm^3}{mol}$	$V^{1/3}$ $\frac{cm}{mol^{1/3}}$	Y	ΔF_{AA}^* (cal/mol)	ΔF_{SS}^* (cal/mol)	δ	Refs.
Sb in Ag	1250	4.09	3.78	12.4	11.60	2.61	1.28	11,630	9460	+.460	23
	1350	4.85	3.30	11.9	11.72	2.27	1.23	12,240	9990	+.444	
	1450	5.61	2.92	11.3	11.86	2.28	1.17	12,850	10,510	+.424	
	1550	6.38	2.64	10.9	11.97	2.29	1.14	13,450	11,040	+.411	
In in Ag	1250	3.78	3.78	11.4	11.60	2.26	1.18	11,630	8400	+.704	23
	1350	4.64	3.30	11.3	11.72	2.27	1.17	12,240	8950	+.663	
	1450	5.49	2.92	11.1	11.86	2.28	1.15	12,850	9520	+.622	
	1550	6.41	2.64	10.9	11.97	2.29	1.14	13,450	10,100	+.585	
Mg in Al	973	7.54	1.14	8.83	11.45	2.26	.906	6740	7140	-.103	25
Pb in In	661	3.85	.99	5.76	16.79	2.56	.671	5050	6130	-.431	28
	760	4.75	1.13	7.06	17.0	2.57	.828	5610	6800	-.372	
Co in Fe	1911	5.5	5.05	14.53	8.10	2.01	1.33	17,580	16,780	+.106	29
Au in Hg	284	0.83	1.61	4.70	14.78	2.45	.524	2300	5885	-2.45	1
	298	0.73	1.53	3.75	14.78	2.45	.418	2390	5980	-2.35	25
Bi in Hg	298	0.99	1.53	5.09	14.78	2.45	.566	2390	3390	-.780	3
	298	1.5	1.53	7.70	14.78	2.45	.858	2390	3390	-.780	31
Cu in Hg	298	1.06	1.53	5.45	14.78	2.45	.606	2390	6025	-2.37	2
Cd in Hg	298	1.52	1.53	7.80	14.78	2.45	.870	2390	3400	-.780	33

System	T (°K)	$D \times 10^5$ (cm^2/sec)	μ (cp)	$\frac{D\mu}{T} \times 10^{10}$	V $\frac{cm^3}{mol}$	$V^{1/3}$ $\frac{cm}{mol^{1/3}}$	Y	ΔF_{AA}^* (cal/mol)	ΔF_{SS}^* (cal/mol)	δ	Refs
Pb in Hg	298	1.16	1.53	5.95	14.78	2.45	.664	2390	3635	-.940	2
	298	1.28	1.53	6.56	14.78	2.45	.733	2390	3635	-.940	33
Sn in Hg	298	1.68	1.53	8.62	14.78	2.45	.961	2390	3000	-.489	3
Zn in Hg	293	1.67	1.55	8.82	14.78	2.45	.985	2390	3700	-.985	34
Tl in Hg	298	.99	1.53	5.09	14.78	2.45	.566	2390	4000	-1.182	2
Ag in Hg	298	1.1	1.53	5.65	14.78	2.45	.630	2390	5855	-2.28	31

Table XV Activation Enthalpy and Entropy for Various Liquid Metals

Element	Melting Temp. °K	$\Delta H^* \frac{cal}{mole}$	$\Delta S^* \frac{cal}{mole\,^\circ K}$	Refs.
Mercury	234	550	-6.16	30
Indium	429	1330	-5.67	24
Tin	505	1125	-6.31	15
Bismuth	544	1520	-6.27	16
Thallium	577	2440	-5.30	36
Cadmium	594	1610	-6.20	21
Lead	601	1590	-6.86	20
Zinc	693	2030	-5.70	35
Antimony	903	2850	-5.29	17,18
Magnesium	923	5320	-2.0	27
Aluminum	932	2640	-3.98	26
Silver	1234	4300	-5.89	19
Gold	1336	3870	-7.09	19
Copper	1356	4400	-5.45	32
Cobalt	1768	9060	-4.04	13
Iron	1812	8555	-4.72	13

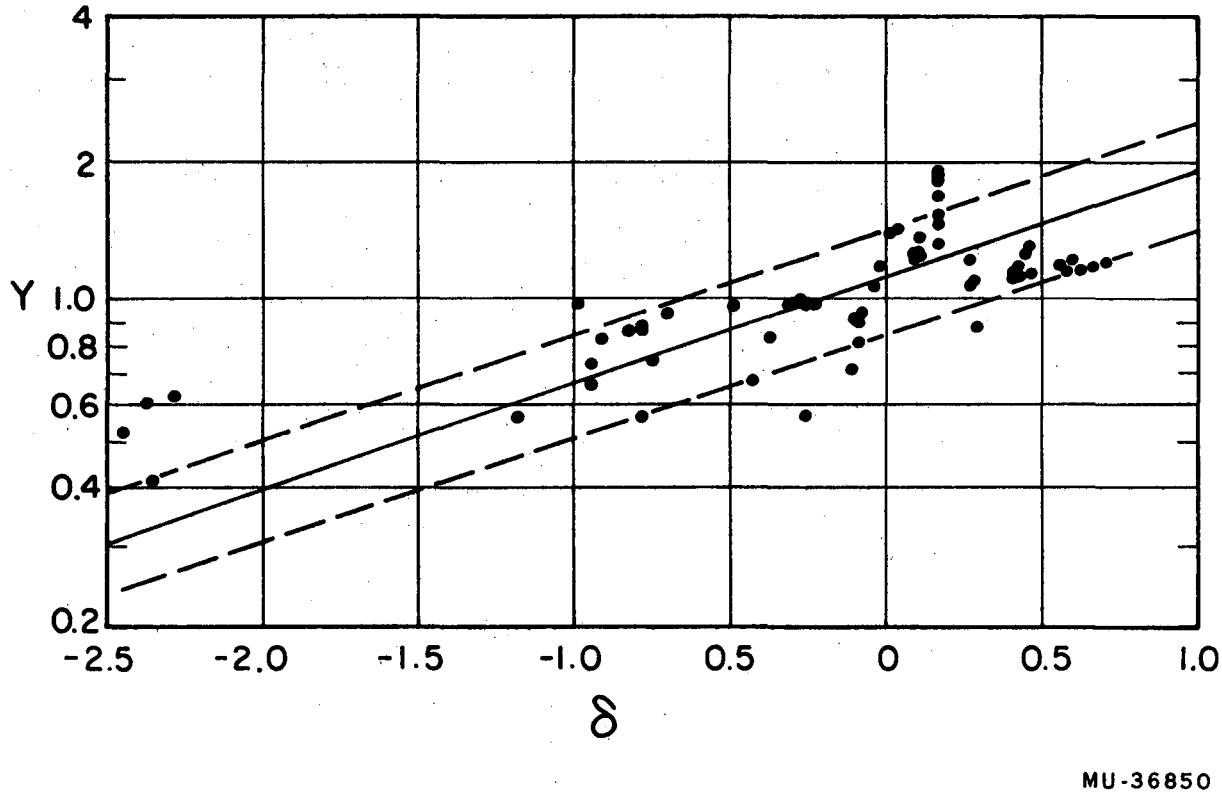

Fig. 6

C. Corresponding States Theory

1. Self-Diffusion

Thomaes and Itterbeek[49] have attempted to establish a theorem of corresponding states for the diffusion and viscosity of pure liquids and solutions. According to this theorem, reduced viscosity or diffusivity should be a universal function of reduced temperature, pressure, and volume for similar substances. Several assumptions are made:

a) The molecules are simple: monatomic or spherical

b) The potential energy of a pair of molecules can be represented by a universal two-parameter function Φ

$$\epsilon(r) = \epsilon^* \Phi\left(\frac{r}{r^*}\right) \tag{33}$$

where ϵ^* and r^* are the energy and distance coordinates of the function minimum,

c) the molecular species can be characterized by the three parameters ϵ^*, r^*, and the mass m.

For reducing factors, Thomaes and Itterbeek use

$$\text{for } \mu\text{:} \quad Z = (m\epsilon^*)^{1/2}\, r^{*-2} \tag{34}$$

$$\text{for D:} \quad \kappa = \epsilon^{*1/2}\, r^*\, m^{-1/2} \tag{35}$$

Thus reduced viscosity $\tilde{\mu}$ and reduced diffusivity $\tilde{D}$ are given by

$$\tilde{\mu} = \mu Z^{-1} \tag{36}$$

and

$$\tilde{D} = D\kappa^{-1} . \tag{37}$$

If a theorem of corresponding states is valid for those substances under consideration

$$\tilde{\mu} = \tilde{\mu}(\tilde{p}, \tilde{V}, \tilde{T})$$

and

$$\tilde{D} = \tilde{D}(\tilde{p}, \tilde{V}, \tilde{T}) \tag{38}$$

where

$$\tilde{p} = pr^{*3}/\epsilon^*$$

$$\tilde{V} = Vr^{*-3}$$

$$\tilde{T} = kT/\epsilon^* \qquad (39)$$

All reducing parameters given in Eqs. (34), (35), and (39) are the same as those given by Rice.[50,51]

By use of an equation of state, the three variables in Eq. (38) can be reduced to two, e.g. $\tilde{p}$ and $\tilde{T}$. Furthermore, one might expect that for liquid metals ϵ^* would be large and therefore $\tilde{p}$ very small. Thus the pressure effect on diffusivity would be small. Petit and Nachtrieb[46] found the self-diffusivity of gallium to be quite insensitive to pressure. (See Table XVI.)

Table XVI Self-Diffusivity of Liquid Gallium (Reference 46)

Temperature (°K)	Pressure (Atmos.)	$D(10^{-5}$ cm^2/sec)
303.7	1	1.65
303.7	1	1.70
303.7	1	1.65
303.7	1985	1.62
303.7	1985	1.57
303.7	3776	1.51
303.7	10008	1.34

Hence, it should be possible to consider the reduced self-diffusion coefficient as a function of reduced temperature only

$$\tilde{D} = \tilde{D}(\tilde{T}) \qquad (40)$$

In order to write reduced values for $\tilde{D}$ and $\tilde{T}$ to test Eq. (40), it is necessary to choose values for ϵ^* and r^* for the liquid metals.

Recently, Chapman[52] has correlated viscosity data for twenty-one liquid metals by a corresponding states approach. Chapman's correlation is based on the pair distribution function theory of the liquid state as developed by Kirkwood[53] and Born and Green.[54] The functional relationship developed is

$$\tilde{\mu}\tilde{V}^2 = f\left(\frac{1}{\tilde{T}}\right) \tag{41}$$

where viscosity temperature and volume are reduced as follows:

$$\tilde{\mu} = \frac{\mu\, r^{*2} N_{Av}}{(MRT)^{1/2}} = \mu\left[\frac{r^{*2}}{(m\epsilon^*)^{1/2}}\right]\frac{1}{\tilde{T}^{1/2}} = \frac{\mu}{Z\tilde{T}^{1/2}}$$

$$\tilde{T} = \frac{kT}{\epsilon^*}$$

$$\tilde{V} = \frac{V}{N_{Av} r^{*3}} \tag{42}$$

In order to establish the relationship given by Eq. (41), Chapman used for ϵ^* the effective Lennard-Jones parameters for liquid sodium and potassium determined from experimental x-ray scattering data by Ling.[55] Goldschmidt atomic diameters were used for the distance parameter r^*. Viscosity data for sodium and potassium were then reduced as indicated by Eq. (42) and plotted as indicated by Eq. (41). The resulting curve was then used to establish the energy parameters ϵ^* for the other nineteen metals. By properly choosing ϵ^*, the viscosity data for each of the liquid metals could be made to fit the same curve for Eq. (41) as that established by sodium and potassium. The energy parameters determined in this way were found to be a linear function of the melting point. The advantage of Chapman's approach is that the energy parameters thus assigned to the liquid metals are based on the values for sodium and

potassium determined by independent x-ray scattering data.

In order to test Eq. (40), the reduced self-diffusivity $\tilde{D}$ will be calculated by Eqs. (35) and (37) using Chapman's values of the energy parameters for ϵ^* and Goldschmidt atomic diameters for r^*.

Table XVI Reducing Factors for Self-Diffusivity for Nine Molten Metals

Metal	ϵ^*/k(°K)	r^*(Å)	$\kappa = \frac{\epsilon^{*1/2} r^*}{m^{1/2}}$	Diffusivity References
Mercury	1250	3.10	70.6×10^{-5}	38
Sodium	1970	3.84	322×10^{-5}	37
Indium	2500	3.14	134×10^{-5}	28
Tin	2650	3.16	132×10^{-5}	28
Silver	6400	2.88	203×10^{-5}	22
*Gallium	1575	3.06	133×10^{-5}	46
Lead	2800	3.50	174×10^{-5}	42
Copper	6600	2.50	238×10^{-5}	44
Zinc	4700	2.74	212×10^{-5}	47

* The procedure for calculating the parameters ϵ^* and r^* was reversed for Ga. Smithell's Metal Reference Book gives an approximate value of ~2.7 for the Goldschmidt atomic diameter. Therefore the energy parameter was calculated first using Chapman's rule $\frac{\epsilon}{K} = 5.20$ Tm where Tm is the melting point and a value of $r^* = 3.06$ was "backed-out" from Chapman's universal viscosity correlation.

Table XVI summarizes the reducing factors for diffusion, κ, given by Eq. (35). Figure 7 is a plot of reduced diffusivity versus reduced temperature (Eq. (40)) for the nine liquid metals listed in Table XVI.

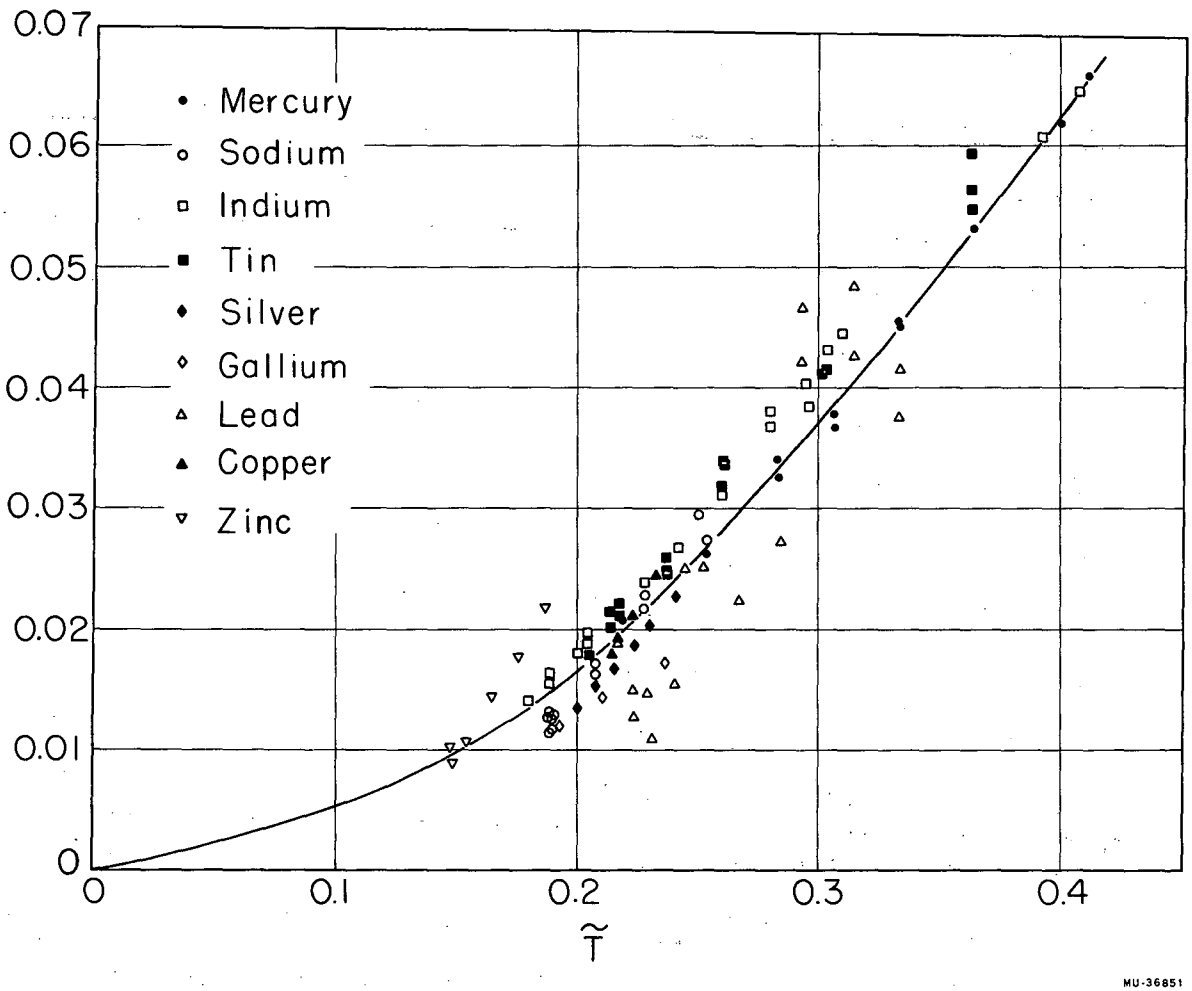
0.07
0.06
0.05
0.04
0.03
0.02
0.01
0
0
0.1
0.2
0.3
0.4
$\tilde{T}$
Mercury
Sodium
Indium
Tin
Silver
Gallium
Lead
Copper
Zinc
MU-36851

Fig. 7

The "best line" has been drawn through the points for mercury. One might use this line to predict the self-diffusivity as a function of temperature for a metal "B", provided the molecular weight, energy parameter ϵ^* and distance parameter r^* for B were available:

1) Calculate $\tilde{T}$

$$\tilde{T} = \frac{Tk}{\epsilon^*_{BB}}$$

2) Determine $\tilde{D}$

$\tilde{D}$ is read from Fig. 7 as a function of $\tilde{T}$

3) $D = \tilde{D}\,\kappa$

where $\kappa = \dfrac{\epsilon^{*\,1/2}_{BB}\, r^*_{BB}}{m_B^{1/2}}$

Figures 8, 9, and 10 compare this procedure for calculating self-diffusivity with the data and also with the theory of Walls and Upthegrove.

While the Walls and Upthegrove calculations are slightly better (except for silver and copper) the agreement shown in Figs. 7-10 indicates that self-diffusion in liquid metals can be adequately described in terms of only three fixed parameters: an energy parameter ϵ^*, a distance parameter r^* and a mass parameter m.

The theory will now be extended to mutual diffusion in dilute binary systems.

2. Mutual Diffusion

The extension of the corresponding states theory to mutual diffusion follows the ideas of Thomaes and Itterbeek up to a point.

Consider two systems. One is a solution of B in solvent A. The second is a solution of C in solvent A.

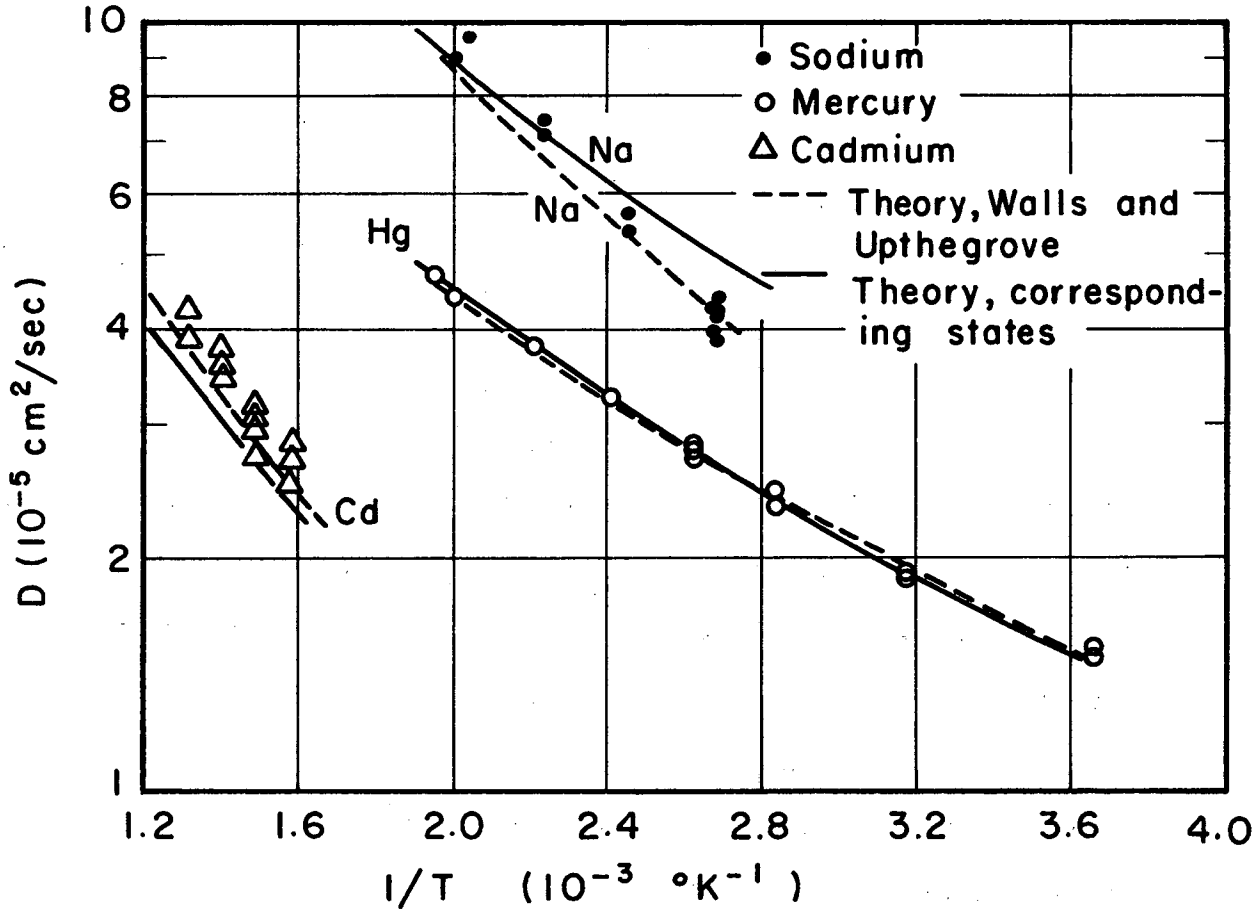

MU-36853

Fig. 8

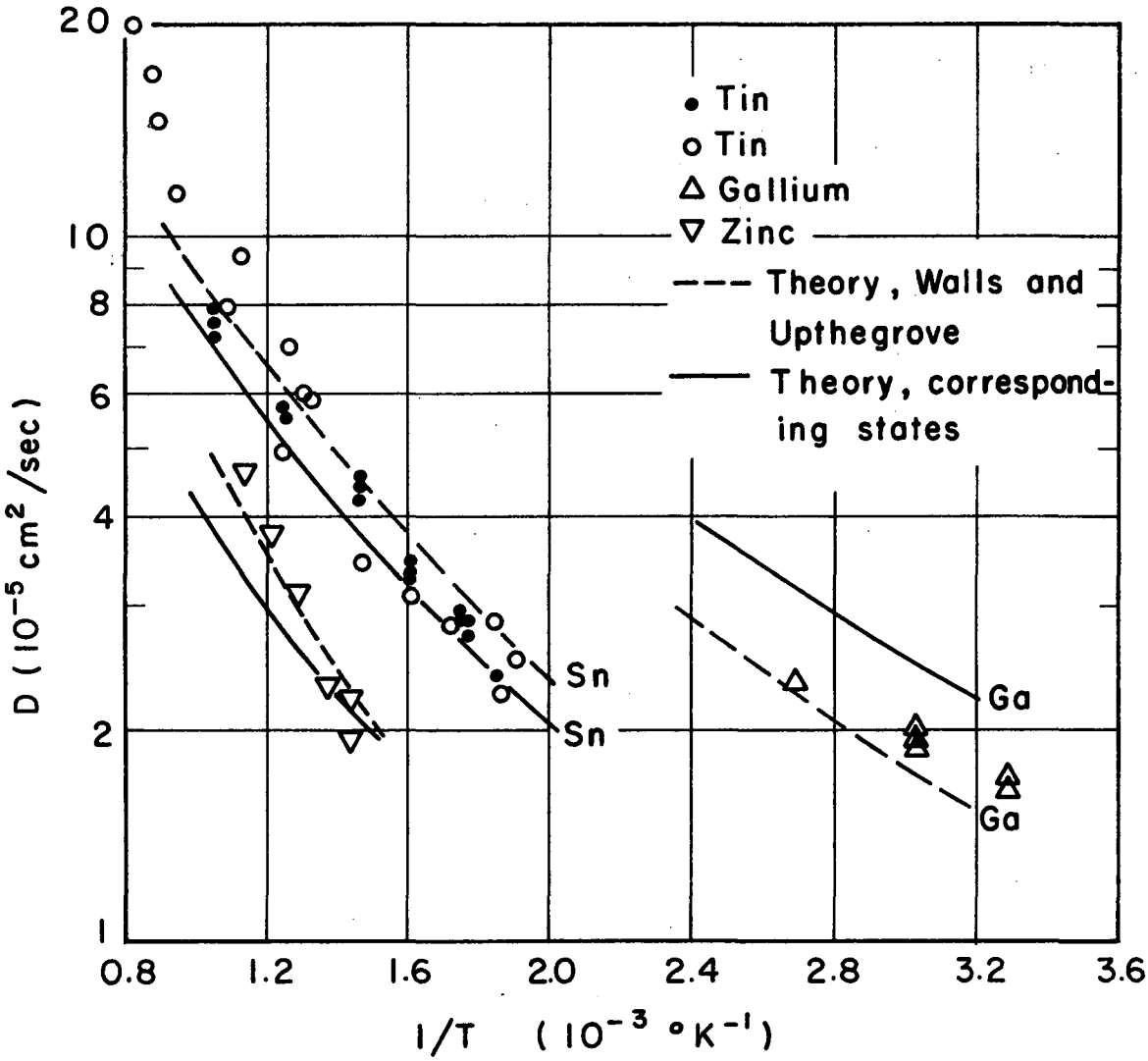
20
10
8
6
4
2
1
D (10^{-5} cm^2 /sec)
0.8
1.2
1.6
2.0
2.4
2.8
3.2
3.6
1/T (10^{-3} °K^{-1})
• Tin
o Tin
Δ Gallium
∇ Zinc
--- Theory, Walls and Upthegrove
—— Theory, corresponding states
Sn
Sn
Ga
Ga
MU-36852

Fig. 9

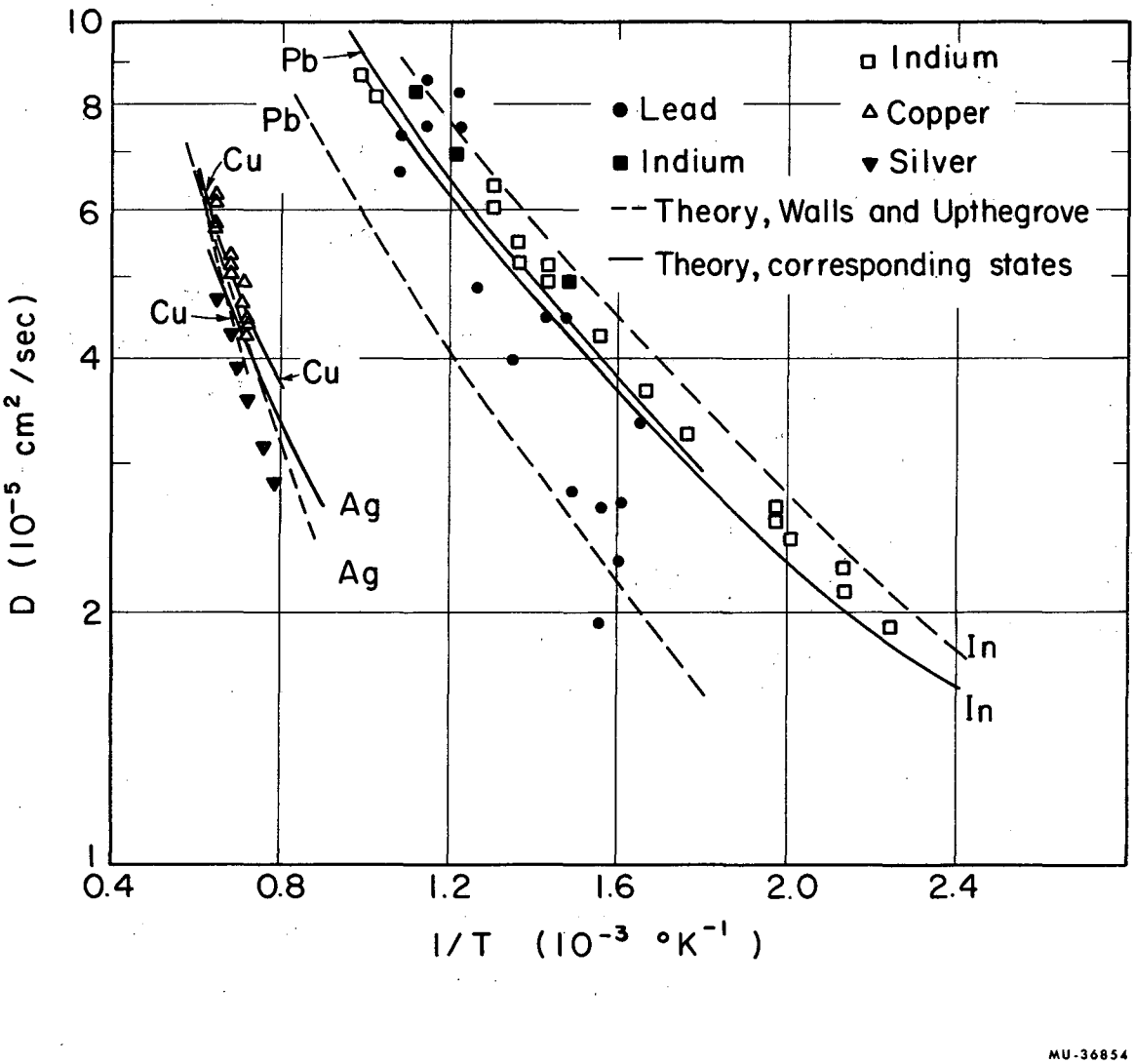
10
8
6
4
2
1
0.4
0.8
1.2
1.6
2.0
2.4
D (10^{-5} cm^2/sec)
1/T (10^{-3} °K^{-1})
Pb
Pb
Cu
Cu
Cu
Ag
Ag
In
In
Indium
Lead
Indium
Copper
Silver
Theory, Walls and Upthegrove
Theory, corresponding states
MU-36854

Fig. 10

Then † $$\tilde{D}_{BA}(\tilde{T}_B) = D_{BA}(T_B)\,\kappa_B^{-1} \qquad (42)$$

where $$\kappa_B = \frac{\epsilon_B^{*1/2}\, r_B^*}{m_B^{1/2}}$$

The parameters ϵ_B^* and r_B^* are functions of concentration and of the pure component properties ϵ_{BB}^*, r_{BB}^*, ϵ_{AA}^*, and r_{AA}^* and the interaction parameters ϵ_{AB}^* and r_{AB}^*. For simple substances where the intermolecular forces follow a Lennard-Jones 6-12 potential, it is possible to predict the interaction parameters r_{AB}^* and ϵ_{AB}^* from the pure-component parameters and to calculate ϵ_B^* and r_B^*. This may be done by means of the average potential model described by Prigogine.[56]

Similarly

$$\tilde{D}_{CA}(\tilde{T}_C) = D_{CA}(T_C)\kappa_C^{-1} \qquad (43)$$

where

$$\kappa_C = \frac{\epsilon_C^{*1/2}\, r_C^*}{m_C^{1/2}}$$

The same comments apply to ϵ_C^* and r_C^* as to ϵ_B^* and r_B^*.

If the two systems, B in A and C in A, obey the same law of corresponding states then, at the same reduced temperature

$$\tilde{T}_B = \tilde{T}_C = \tilde{T} \qquad (44)$$

$$\tilde{D}_{BA}(\tilde{T}_B) = \tilde{D}_{CA}(\tilde{T}_C) \qquad (45)$$

and from Eq. (44)

$$T_B = T_C\, \epsilon_B^*/\epsilon_C^* \qquad (46)$$

---

† For L.H.S. of Eq. (42) read: "Reduced diffusivity <u>at</u> reduced temperature T_B."

For R.H.S. read: "Diffusivity of B <u>at</u> temperature T_B."

It then follows that

$$D_{BA}\left(T_C \frac{\epsilon_B^*}{\epsilon_C^*}\right) = D_{CA}(T_C)\left(\frac{\epsilon_B^*}{\epsilon_C^*}\right)^{1/2}\left(\frac{r_B^*}{r_C^*}\right)\left(\frac{m_C}{m_B}\right)^{1/2} \qquad (47)$$

If one knows the diffusivity of C in the C-A system at temperature T_C i.e. $D_{CA}(T_C)$, and if one knows how to predict ϵ_B^*, ϵ_C^*, r_B^*, and r_C^*, one can then use Eq. (47) to calculate the diffusivity of B in the B-A system at temperature $T_C \frac{\epsilon_B^*}{\epsilon_C^*}$. This is the procedure outlined by Thomaes and Itterbeek.

It will now be shown how the theories of Thomaes and Itterbeek for mutual diffusion, outlined above, can be applied to the prediction of mutual diffusion coefficients in dilute liquid metal systems. In many molten metal systems on which diffusivity studies have been made, the self-diffusivity of the solvent has been measured. Instead of using an arbitrary "reference system" (such as C in A in the example just given), why not use the pure solvent itself as the reference system? This simplifies matters because the average parameters ϵ^* and r^* of the reference system are now the pure component parameters of the solvent. Only one pair of parameters, that for the system whose diffusivity we wish to predict need be estimated. For a dilute solution of B in A a further simplification is possible. If the solution is sufficiently dilute, collisions of B atoms with other B atoms almost never occur and only B-A interactions need be considered.

Thus for a dilute solution of B in A

$$\epsilon_B^* = \epsilon_{AB}^* \qquad (48)$$
$$r_B^* = r_{AB}^*$$

(All Prigogine's equations for ϵ_B^* and r_B^* reduce to Eq. (48) for $x_B \to 0$.)

Thus for a dilute solution of B in A, Eq. (47) can be rewritten

$$D_{BA}\left(T_A \frac{\epsilon^*_{AB}}{\epsilon^*_{AA}}\right) = D_A\left(T_A\right)\left(\frac{\epsilon^*_{AB}}{\epsilon^*_{AA}}\right)^{1/2}\left(\frac{r^*_{AB}}{r^*_{AA}}\right)\left(\frac{m_A}{m_B}\right)^{1/2} \qquad (49)$$

and it is understood that $D_A(T_A)$ is the self-diffusivity of the solvent at temperature T_A.

Once the self-diffusivity of the pure solvent is known, the only problem remaining before Eq. (49) can be used to predict mutual diffusion coefficients in dilute systems is the estimation of the interaction parameters ϵ^*_{AB} and r^*_{AB}. For simple substances where the attractive forces are dispersion forces, the usual geometric mean rule for the energy parameter and the average combining rule for the distance parameter apply

$$\epsilon^*_{AB} = \left(\epsilon^*_{AA} \cdot \epsilon^*_{BB}\right)^{1/2} \qquad (50)$$

and

$$r^*_{AB} = \frac{1}{2}\left(r^*_{AA} + r^*_{BB}\right) \qquad (51)$$

The use of these combining rules in liquid metal systems is questionable. Nevertheless, for lack of any better mixing rule, Eq. (51) will be used to estimate the distance parameter r^*_{AB} and thus the ratio r^*_{AB}/r^*_{AA} in Eq. (49).

The procedure which will be followed here is to apply Eqs. (49) and (51) to experimental diffusion data to "back-out" values of ϵ^*_{AB} using a trial and error approach. "Experimental" values of ϵ^*_{AB} determined in this way will then be compared with some methods for predicting ϵ^*_{AB} from thermodynamic data. First, rewrite Eq. (49)

$$D_A\left(T_A\right) = D_{BA}\left(T_A \frac{\epsilon^*_{AB}}{\epsilon^*_{AA}}\right)\left(\frac{m_B}{m_A}\right)^{1/2}\left(\frac{\epsilon^*_{AA}}{\epsilon^*_{AB}}\right)^{1/2}\left(\frac{r^*_{AA}}{r^*_{AB}}\right) \qquad (52)$$

D_{BA} is then the experimental value for the mutual diffusion coefficient at experimental temperature $T_A \frac{\epsilon^*_{AB}}{\epsilon^*_{AA}}$.

1. Assume a trial value of $\epsilon^*_{AB}/\epsilon^*_{AA}$.
2. Divide the experimental temperature by the assumed value of $\epsilon^*_{AB}/\epsilon^*_{AA}$ to find T_A.
3. From the experimental curve of D_A vs T_A, find $D_A(T_A)$.
4. Calculate $\left(\epsilon^*_{AA}/\epsilon^*_{AB}\right)^{1/2}$ using the value assumed in step 1 and then calculate the R.H.S. of Eq. (52) to find another value of $D_A(T_A)$.
5. Compare values of $D_A(T_A)$ determined in steps 3 and 4. When they match, the correct value of $\epsilon^*_{AA}/\epsilon^*_{AB}$ has been chosen.

This procedure will now be applied to mutual diffusion data for several systems. The measurements are by Niwa and Shimoji et al.[14] for tin, bismuth, antimony, and cadmium in lead, and antimony and bismuth in tin. Also data for the diffusion of lead in indium by Careri et al.[28] will be examined. Data for these systems have been taken at several temperatures, permitting an examination of the constancy of ϵ^*_{AB} with temperature. These systems also have the advantage that the electronegativity difference between solute and solvent is small and therefore they should be the type of system for which it is easiest to devise mixing rules. The self-diffusivity data are reported by Rothman and Hall[42] for lead, by Ma and Swalin[41] for tin, and by Careri et al.[28] for indium.

Table XVII outlines the trial and error procedure for determining experimental values for $\epsilon^*_{AB}/\epsilon^*_{AA}$.

Table XVIII summarizes all the trial and error determinations of $\epsilon^*_{AB}/\epsilon^*_{AA}$ for the seven systems. It can be seen that $\epsilon^*_{AB}/\epsilon^*_{AA}$ is independent of temperature in the experimental range.

Table XVII Trial and Error Method for $\epsilon^*_{AB}/\epsilon^*_{AA}$ for System Sb in Pb at 823°K

$T_A\left(\frac{\epsilon^*_{AB}}{\epsilon^*_{AA}}\right)$	$\left(\frac{\epsilon^*_{AB}}{\epsilon^*_{AA}}\right)$	T_A	$\frac{1}{T_A}$	$D_A(T_A)$	$D_{BA}\left(T_A\frac{\epsilon^*_{AB}}{\epsilon^*_{AA}}\right)$	$\left(\frac{m_B}{m_A}\right)^{1/2}$	$\left(\frac{\epsilon^*_{AA}}{\epsilon^*_{AB}}\right)^{1/2}$	$\left(\frac{r^*_{AA}}{r^*_{AB}}\right)$	$D_A(T_A)$ Eq. (52)
823	1.0	823	1.215	6.0	5.5	.767	1.0	1.04	4.40
823	1.147	718	1.393	4.0	5.5	.767	.934	1.04	4.11
823	1.130	727	1.376	4.15	5.5	.767	.941	1.04	4.14

$$\frac{\epsilon^*_{AB}}{\epsilon^*_{AA}} = 1.130$$

Table XVIII "Experimental" values $\epsilon^*_{AB}/\epsilon^*_{AA}$ from dilute solution diffusion data

T(°K)	Sn in Pb				
723	1.255				
783	1.213				
823	1.240				
873	1.215				
Avg.	1.231				
	Bi in Pb	Sb in Pb	Cd in Pb	Bi in Sn	Sb in Sn
723	.929	1.191	1.110	.993	.933
773	.916	1.175	1.092	.955	.953
823	.918	1.130	1.102	.928	.984
873	.925	1.142	1.126	.941	1.010
Avg	.922	1.160	1.108	.954	.970
	Pb in Sn				
661	.940				
760	.952				
Avg	.946				

3. Prediction of the Interaction Parameter ϵ^*_{AB}

As described previously, for simple molecules where the interaction forces are dispersion forces the geometric mean rule, Eq. (50) can be used to calculate the interaction parameter ϵ^*_{AB}. Such an approach cannot be used for liquid metals. Oriani[57] has shown that in metallic solutions (both solid and liquid), thermodynamic data (heats of mixing) lead to the conclusion that solute-solvent interactions are a function of composition and that solute-solute and solvent-solvent interactions in solution are not the same as in the pure solute or pure solvent and are also composition-dependent.

Despite these difficulties, several workers have attempted to extend the cell-model theories of Prigogine to the prediction of excess thermodynamic properties of metallic solutions. Should these theories be valid, it would be possible to start with thermodynamic data for liquid alloys and "back-out" the implied interaction parameters. Such thermodynamic data have been compiled by Hultgren, Orr, Anderson, and Kelley[58] for a large number of metallic systems.

Prigogine's theories postulate that the potential energy between two molecules is described by the Lennard-Jones 6-12 potential. Random mixing is also assumed. Then all thermodynamic excess functions can be described in terms of three parameters, θ, δ, and ρ:

$$\theta = \frac{1}{\epsilon^*_{AA}}\left(\epsilon^*_{AB} - \frac{1}{2}\,\epsilon^*_{AA} - \frac{1}{2}\,\epsilon^*_{BB}\right) \tag{53}$$

$$\delta = \left(\frac{\epsilon^*_{BB}}{\epsilon^*_{AA}}\right) - 1 \tag{54}$$

$$\rho = \left(\frac{r^*_{BB}}{r^*_{AA}}\right) - 1 \tag{55}$$

where ϵ^*_{AA}, ϵ^*_{BB}, and ϵ^*_{AB} are the bonding energies for the molecular combinations.

For the heat of mixing, Oriani[59] suggests using the equation

$$\Delta H = 1.435\ (-\theta + 4.50\ \rho^2)\ N_{Av}\ Z\ \epsilon^*_{AA}\ x_B\ x_A \qquad (56)$$

where Z is the coordination number (assumed to be 12) and x_i is the mole fraction of component i.

Shimoji[60] uses the Morse potential to describe intermolecular forces in metals instead of the 6-12 potential. His equation for the heat of mixing is

$$\Delta H = \left(-\theta + \frac{\rho^2}{2}\right) Z\ N_{Av}\ \epsilon^*_{AA}\ x_A\ x_B \qquad (57)$$

In Eqs. (53), (56), and (57), the pure-component bonding energies ϵ^*_{AA} and ϵ^*_{BB} are calculated from the heat of vaporization:

$$\text{Heat of Vaporization} = \frac{N_{Av} Z \epsilon^*}{2} \qquad (58)$$

The object of this thermodynamic analysis is the calculation of the interaction parameter ϵ^*_{AB} in dilute solutions. Since ϵ^*_{AB} may be a function of composition, partial molar heats of solution at infinite dilution will be considered. Equations (56) and (57) become

$$\text{(Oriani)}\ \overline{\Delta H}_B = 1.435\ N_{Av}\ Z\ \epsilon^*_{AA}\ (-\theta + 4.50\ \rho^2) \qquad (59)$$

$$x_B = 0$$

$$\text{(Shimoji)}\ \overline{\Delta H}_B = N_{Av}\ Z\ \epsilon^*_{AA}\ \left(-\theta + \frac{\rho^2}{2}\right) \qquad (60)$$

$$x_B = 0$$

Equations (58-60) and (53) can then be used to calculate $\frac{\epsilon^*_{AB}}{\epsilon^*_{AA}}$ from thermodynamic data. It turns out that partial molar heats of solution are very small relative to heats of vaporization. (The largest value of

$\overline{\Delta H}$ for the systems examined is 2.32 kcal for cadmium in lead at infinite dilution. The heat of vaporization of molten lead at its melting point is 45.1 kcal, that for cadmium is 24.8 kcal.) The most important contribution to the interaction parameter is made by the pure component parameters. In Eq. (59) the term $4.50\ \rho^2$ is significant and its inclusion usually improves the calculation.

Table XIX compares the average values of $\epsilon^*_{AB}/\epsilon^*_{AA}$ from diffusion data presented in Table XVIII with those calculated using Eq. (59) (column 3) and Eq. (60) (column 4). Column 5 lists values of $\epsilon^*_{AB}/\epsilon^*_{AA}$ calculated using Eq. (50) and Chapman's values of the pure component parameters.

Calculated values which are in poor agreement with the experimental values have been underlined. The calculation has also been attempted using Oriani's and Shimoji's equations but with Chapman's values of ϵ^*_{AA} and ϵ^*_{BB} in Eq. (53) instead of values determined from heat of vaporization data by Eq. (58). This calculation shows good agreement for the Cd in Pb system but poor agreement for the Sn in Pb, Sb in Sn and Pb in In systems. For the seven systems studied, the best agreement is obtained using Oriani's Eq. (59) and estimating pure-component bonding energies from heat of vaporization data.

4. Calculation of Mutual Diffusion Coefficients

Figures 11, 12, and 13 compare the experimental diffusivity data with values calculated using Eq. (49). The interaction distance parameters were calculated from Eq. (51) using Goldschmidt atomic diameters for the pure component values r^*_{AA} and r^*_{BB}. The interaction energy parameters are from column 3 of Table XIX. The agreement between theory and experiment is satisfactory in all cases except Cd in Pb. For the other three solutes

Table XIX Comparison of Experimental and Calculated Interaction Parameters ϵ^*_{AB}

System	$\epsilon^*_{AB}/\epsilon^*_{AA}$			
	Experimental	Calculated		
		(Oriani) Eq. (59)	(Shimoji) Eq. (60)	Eq. (50)
Sn in Pb	1.231	1.306	1.263	.974
Bi in Pb	.922	1.009	1.005	.872
Sb in Pb	1.160	1.157	1.131	1.158
Cd in Pb	1.108	.834	.758	1.087
Bi in Sn	.954	.921	.830	.898
Sb in Sn	.970	.902	.912	1.190
Pb in In	.946	.959	.902	1.030

in Pb, the theory predicts the correct relative size of the diffusion coefficient, i.e. $D_{Bi} > D_{Sb} > D_{Sn}$.

5. Procedure When Self-Diffusivity of the Solvent is Unknown

When the self-diffusivity of the solvent has not been measured, the general correlation of Fig. 7 can be used in place of a "reference system". The procedure will be illustrated for the system tin in bismuth for which Niwa and Shimoji give experimental values at four temperatures.

The ratio of the interaction parameters, $\epsilon^*_{AB}/\epsilon^*_{AA}$, is calculated using Eqs. (51) and (59) as described earlier. Since the generalized plot, Fig. 7, is based on the Chapman viscosity values of ϵ^*_{AA}, the interaction parameter ϵ^*_{AB} is calculated by multiplying the ratio $\epsilon^*_{AB}/\epsilon^*_{AA}$ by the viscosity value of ϵ^*_{AA}. These values and the mass of the tin atom are used to calculate the reducing factors for diffusion and temperature. For the Sn-Bi system $\epsilon^*_{AB}/k = 2900°K$, $r^*_{AB} = 3.41\text{Å}$, and the reducing factor $\kappa_B = \epsilon^*_{AB}\, r^*_{AB}/m_B^{1/2} = 154\times10^{-5}$. Values of $\tilde{D}$ are found from Fig. 7

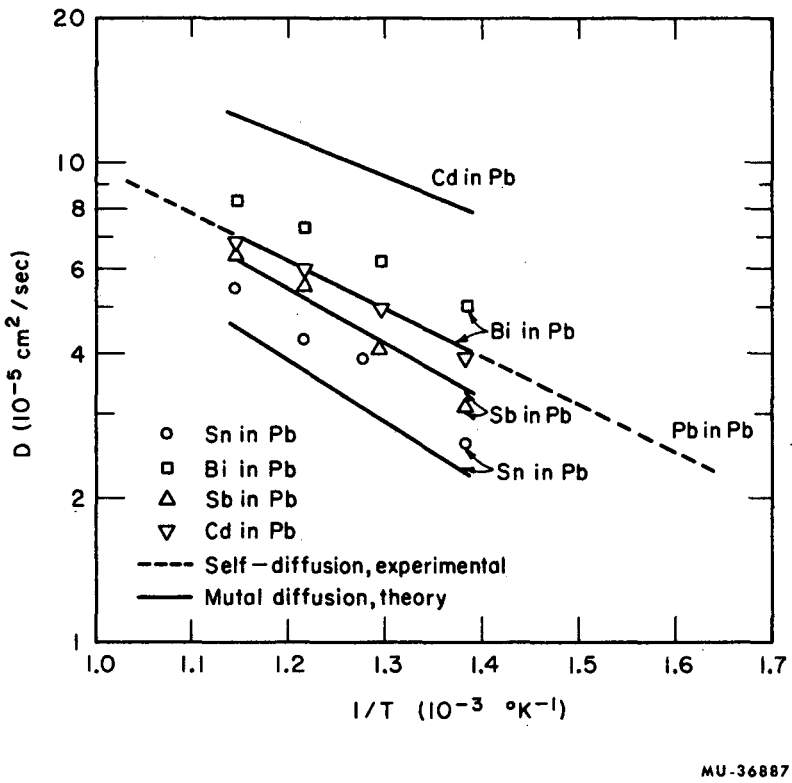
20
10
8
6
4
2
1
D (10⁻⁵ cm²/sec)
1.0
1.1
1.2
1.3
1.4
1.5
1.6
1.7
1/T (10⁻³ °K⁻¹)
Cd in Pb
Bi in Pb
Sb in Pb
Sn in Pb
Pb in Pb
Sn in Pb
Bi in Pb
Sb in Pb
Cd in Pb
Self-diffusion, experimental
Mutal diffusion, theory
MU-36887

Fig. 11

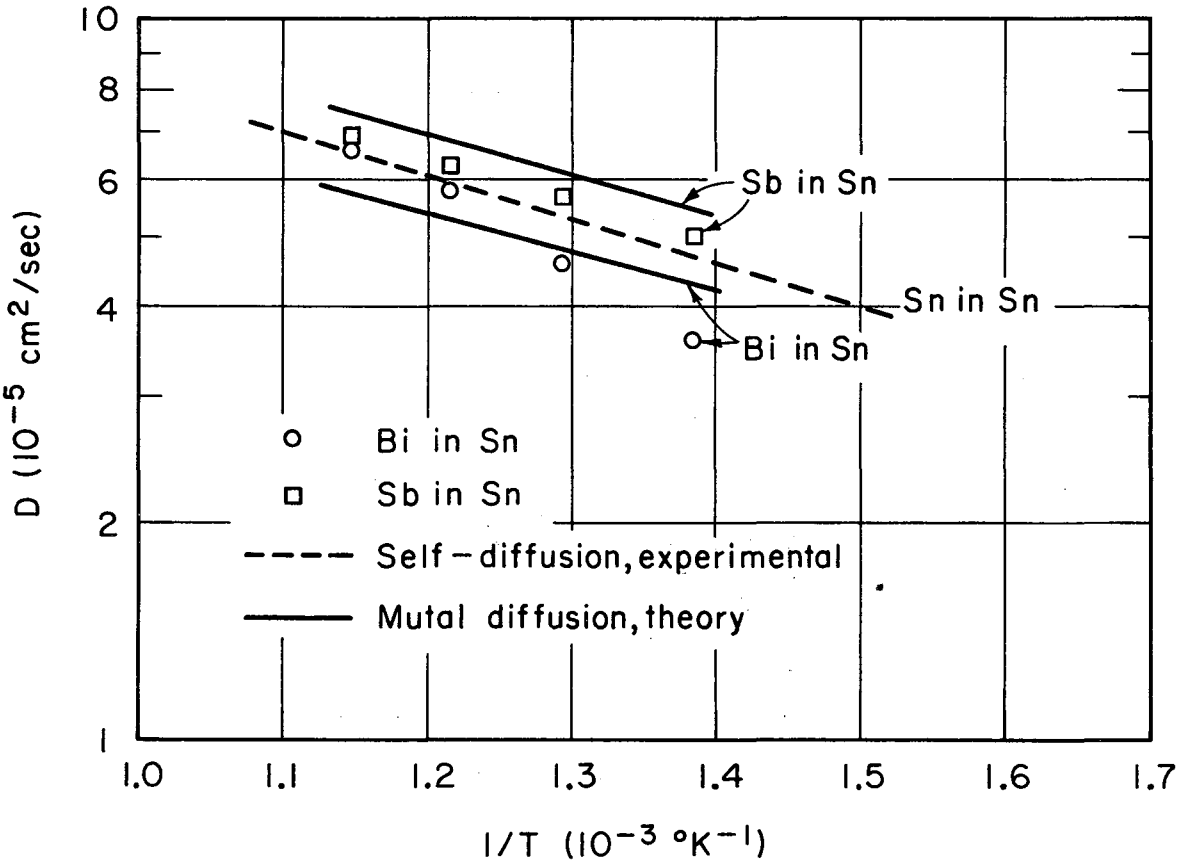
10
8
6
4
2
1
D (10⁻⁵ cm²/sec)
1.0
1.1
1.2
1.3
1.4
1.5
1.6
1.7
1/T (10⁻³ °K⁻¹)
Sb in Sn
Sn in Sn
Bi in Sn
Bi in Sn
Sb in Sn
Self-diffusion, experimental
Mutal diffusion, theory
MU-36888

Fig. 12

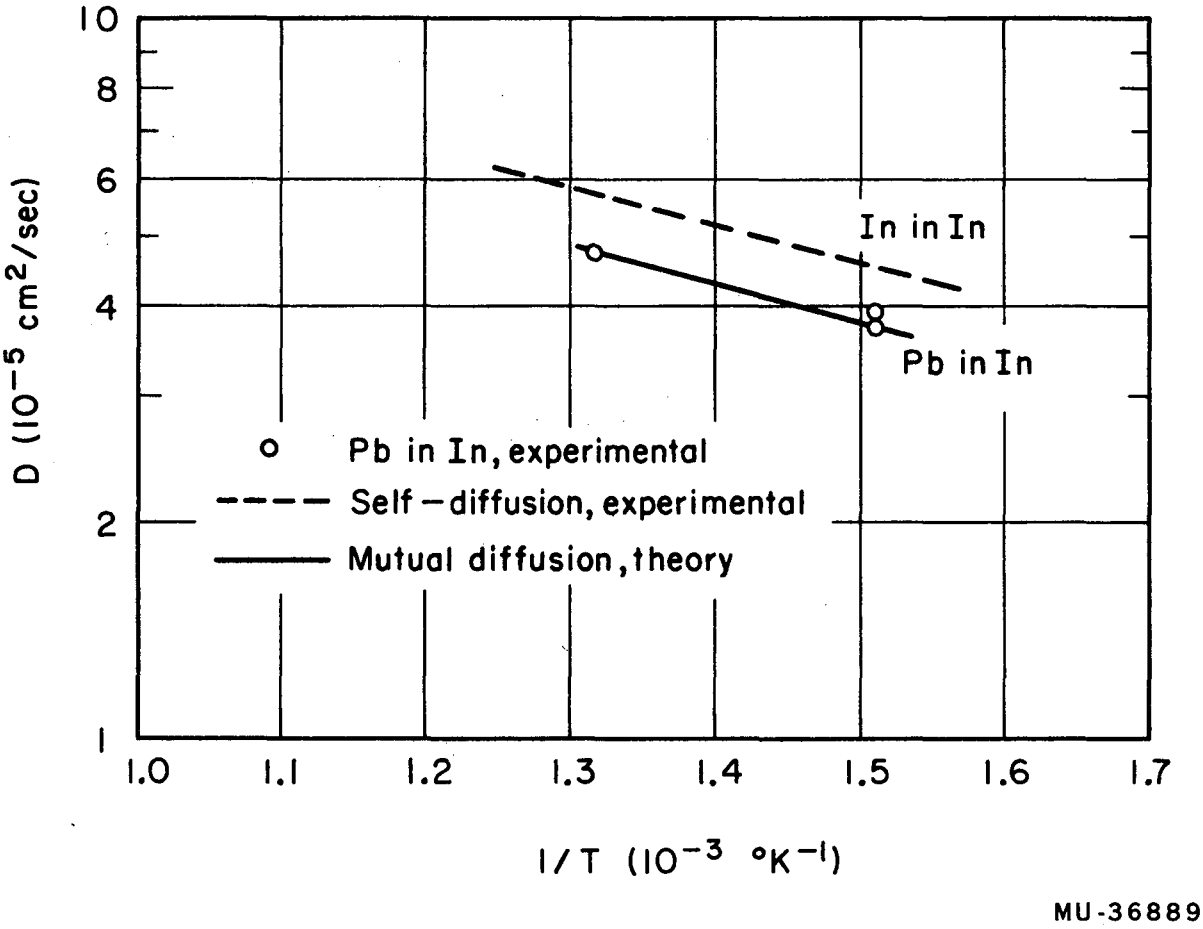
10
8
6
4
2
1
D (10⁻⁵ cm²/sec)
In in In
Pb in In
Pb in In, experimental
Self-diffusion, experimental
Mutual diffusion, theory
1.0
1.1
1.2
1.3
1.4
1.5
1.6
1.7
1/T (10⁻³ °K⁻¹)
MU-36889

Fig. 13

as a function of $\tilde{T}$. Finally, $D = \tilde{D} \cdot K$.

The generalized correlation can also be used to calculate mutual diffusion coefficients for the seven systems previously discussed. The calculated and experimental values are compared in Table XX.

The method which uses the generalized reduced diffusivity correlation is about as accurate as that which uses self-diffusivity data as the "reference-system". Use of the self-diffusivity reference system is more likely to give a better estimate of the temperature dependence of the mutual diffusion coefficient, but, on the basis of the seven systems compared here, there is little to choose between the two methods in terms of predicting absolute values of the diffusion coefficient.

6. Summary

It has been shown that a corresponding states approach can be used to correlate self-diffusivity in molten metals using only three parameters: an energy parameter ϵ^*, a distance parameter r^*, and the mass m. The distance parameter is the Goldschmidt atomic diameter and the energy parameter is the same as that derived from viscosity data. The theory may be extended to mutual diffusion in dilute solutions by appropriate choice of the interaction energy and distance parameters. The possibility of using thermodynamic data and correlations to calculate the interaction energy parameter has been discussed. The theory satisfactorily predicts values for the diffusion coefficient for most of the systems studied.

D. Comparison of Absolute Rate and Corresponding States Theories for Predicting Mutual Diffusion Coefficients in Dilute Metal Systems

The absolute rate (with the Olander modification) and the corresponding states theories can be compared as to ease of use and accuracy.

Table XX Calculation of Mutual Diffusion Coefficients in Dilute Liquid Metals Systems Using the Generalized Correlation of Fig. 7.

System	$\frac{\epsilon^*_{AB}}{k}$ (°K)	K_B (10^{-5})	T(°K)	$\tilde{T}$	$\tilde{D}$	$D_{cal'd}$ (10^{-5} cm^2/sec)	$D_{expt'l}$ (10^{-5} cm^2/sec)
Sn in Bi	2900	154	723	.249	.0264	4.1	5.5
			773	.266	.0302	4.6	6.5
			823	.284	.0342	5.3	7.3
			873	.301	.0382	5.9	8.2
Sn in Pb	3660	169	723	.197	.0164	2.8	2.6
			783	.214	.0194	3.3	3.9
			823	.275	.0215	3.6	4.3
			873	.239	.0244	4.1	5.5
Bi in Pb	2820	120	723	.256	.0280	3.3	5.0
			773	.274	.0320	3.8	6.2
			823	.292	.0361	4.3	7.3
			873	.310	.0405	4.9	8.3
Sb in Pb	3240	158	723	.223	.0211	3.3	3.1
			773	.238	.0241	3.8	4.1
			823	.254	.0275	4.3	5.5
			873	.269	.0309	4.9	6.4
Cd in Pb	2330	136	723	.310	.0405	5.5	3.9
			773	.332	.0460	6.3	5.0
			823	.353	.0515	7.0	6.0
			873	.375	.0571	7.8	6.8
Bi in Sn	2440	106	723	.296	.0370	3.9	3.6
			773	.317	.0422	4.5	4.6
			823	.337	.0474	5.0	5.8
			873	.358	.0528	5.6	6.6
Sb in Sn	2390	129	723	.302	.0385	5.0	5.0
			773	.323	.0437	5.6	5.7
			823	.344	.0492	6.4	6.3
			873	.365	.0546	7.0	6.9
Pb in In	2400	103	661	.276	.0325	3.3	3.85
			760	.317	.0422	4.3	4.75

The absolute rate theory requires only pure-component viscosity and density data, which are available for many liquid metals. For those metals (e.g. uranium) for which viscosity are not yet available, the viscosity correlations of Chapman[52] or Grosse[92] can be used.

The corresponding states method requires viscosity data for the solvent to determine the pure-component interaction parameter, ϵ^*_{AA}. In the absence of viscosity data, ϵ^*_{AA} may be estimated from the melting point.[52] If solvent self-diffusivity is used in the "reference-system" method (Eq. (49)) then self-diffusivity data are required; such data are available for only nine liquid metals. Both the "reference-system" method and the method using the generalized reduced diffusivity correlation require partial molal heat of mixing data which may not be available for the binary pair of interest. The absolute rate theory requires only pure-component data: no thermodynamic or other data for the binary pair of interest is required. It is thus the easier of the two methods to use and can be used with more systems.

The accuracy of the absolute rate and corresponding states theories is about the same. Of the eight systems compared here only the data for the Bi in Pb system lie completely outside of the ±25% confidence limits in the absolute rate correlation of Fig. 6. Each of the two corresponding states methods discussed predicts bad values for at least one system: the Cd in Pb system when the "reference-system" method is used and the Bi in Pb system when the generalized correlation method is used.

A comparison of the two methods of correlating mutual diffusivity data in dilute binary liquid metal systems must consider ease of use, amount of data required, and the number of systems successfully correlated. On all three counts, the absolute rate method is preferable to the corresponding

states method.

ADDENDUM

Chapman (UCRL-11930) gives the energy parameters for twenty-one metals. Energy parameters for the following three additional metals were calculated from viscosity data.

Metal	r^*(Å)	ϵ^*/k (°K)
Ga	3.06	1575
Bi	3.64	2135
Sb	3.22	3745

IV. KINETIC EXPERIMENTS

A. Apparatus

The kinetic experiments are carried out using as extraction column a graphite crucible with an overall length of 31 in., 1-1/4 in. outer diameter, and 9/16 in. inner diameter. The crucible is closed at the bottom by a machined graphite screw plug, which holds magnesium without any leakage. A 23-in. long reflux column also of graphite is placed directly above the extraction column. The reflux column condenses magnesium vapor and returns it to the extraction column, thus minimizing magnesium losses. Both extraction and reflux columns are placed in a stainless steel sheath to which is welded a 1/4-in. stainless steel inert gas line. The reflux column extends about 6 in. above the sheath. Figure 14 shows the arrangement by which argon enters the bottom of the sheath, flows over niobium wire (which scavenges oxygen) and up the annular space between the extraction column and the sheath. Four grooves cut in the top of the extraction column permit argon to enter it, flow over the molten magnesium surface and then up the reflux column. This arrangement not only keeps oxygen away from highly flammable molten magnesium, but it also prevents magnesium vapor from condensing inside the sheath and "welding" the extraction column to it. The argon flow is adjusted so that no MgO is seen rising from the reflux column. The argon flow rate is 2 cubic feet per hour.

Figure 15 is an "exploded" view showing the bottom of the graphite column, the inner liner (whose function will be described shortly) and the machined screw plug.

Fig. 16 shows the graphite crucible, reflux column, magnesium charge and dropping stick against a schematic of the furnace, γ-ray scintillation

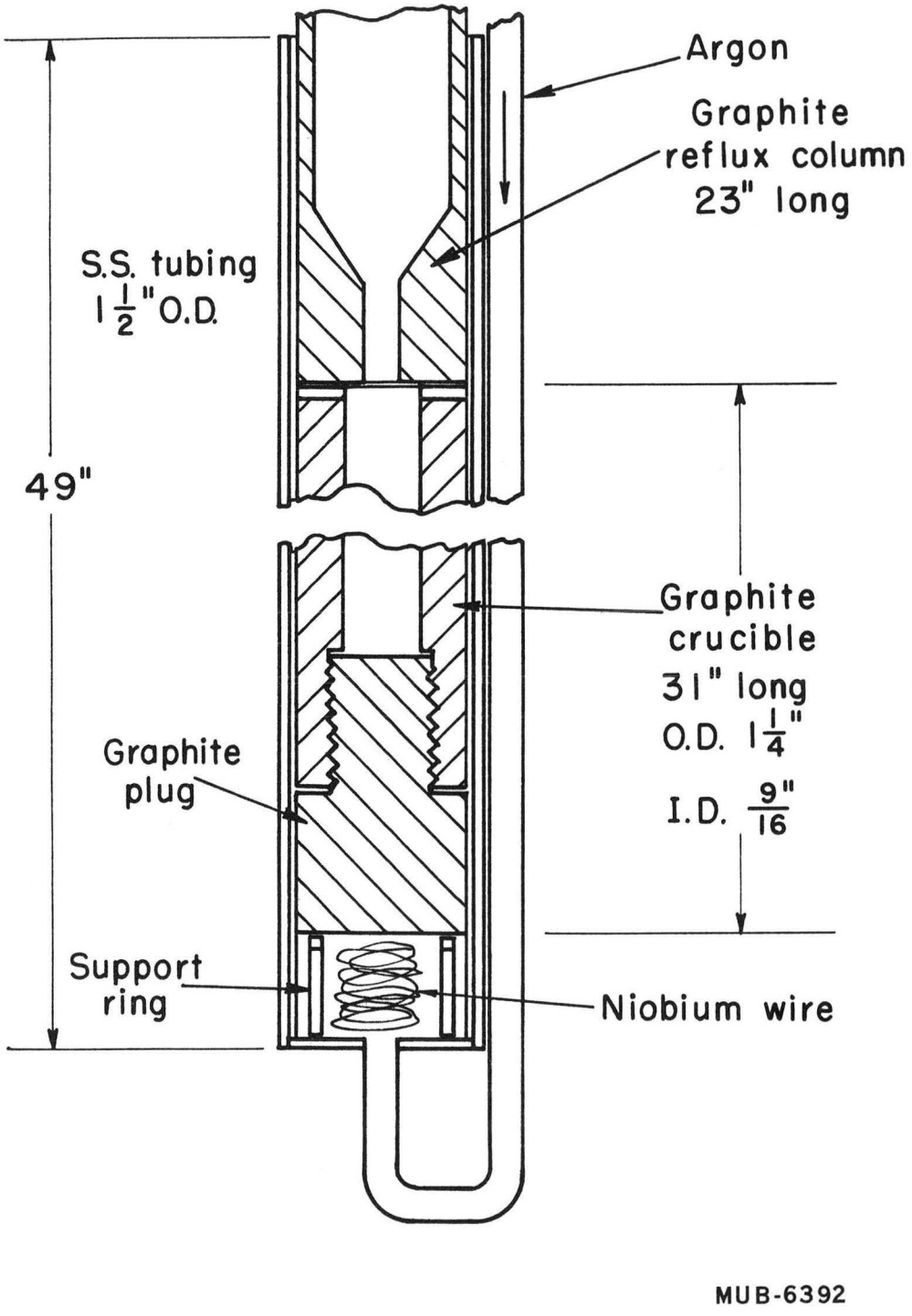
Argon
Graphite
reflux column
23" long
S.S. tubing
1 1/2" O.D.
49"
Graphite
crucible
31" long
O.D. 1 1/4"
I.D. 9/16"
Graphite
plug
Support
ring
Niobium wire
MUB-6392

Fig. 14

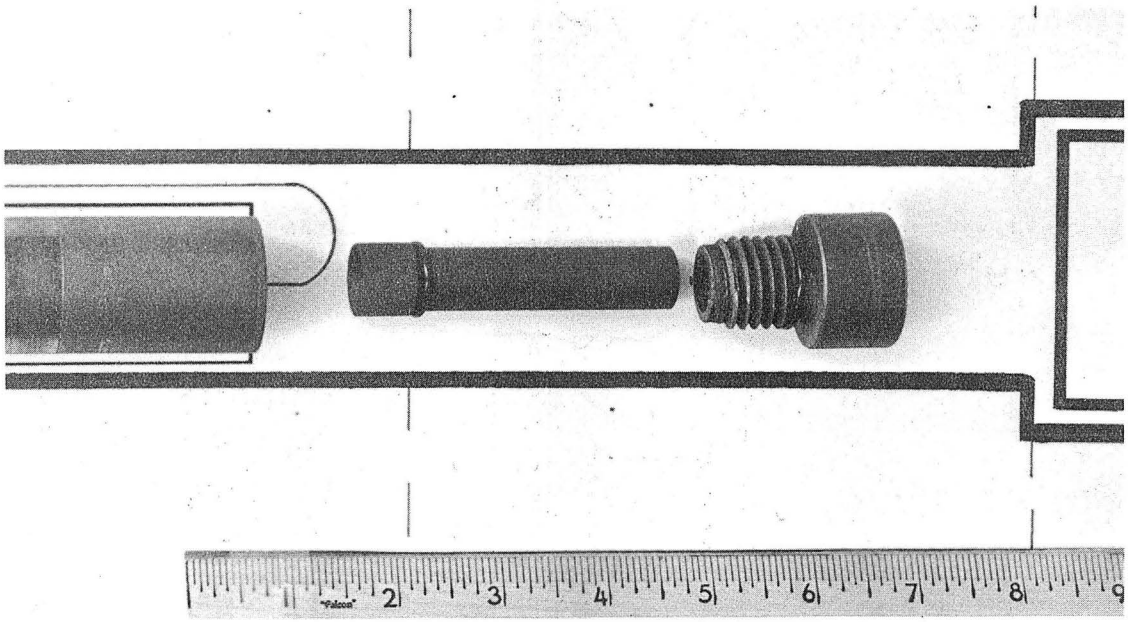

ZN-5468

Fig. 15

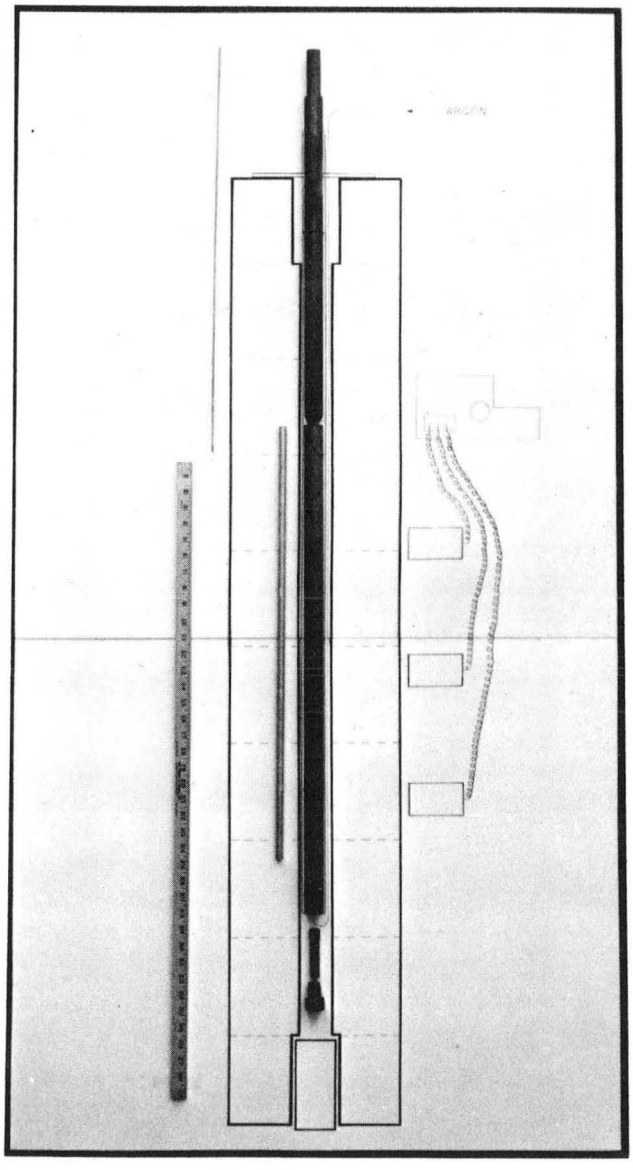

ZN-5470

Fig. 16

detectors and high speed recorder.

The sheath containing the extraction column is supported in a hinged vertical tube resistance furnace by means of an 8 in. diameter flange. Figure 17 shows the furnace open with the sheath in place. The top of the reflux column and the argon line can be seen near the top of the picture.

The vertical hinged tube resistance furnace was manufactured by the Hevi-Duty Electric Company of Watertown, Wisconsin. It consists of eight 6 in. heating zones and 5-1/2 in. insulating vestibules at the top and bottom (see Fig. 18). The top zone and the two bottom zones are manually controlled by variable transformers. Power to the other five heating zones is automatically adjusted by a saturable reactor (core) proportional controller. Each of the eight zones is rated at 1020 watts. The total furnace rating is 8.16 kw, 230/208 volts, single phase. Each zone is fitted with a chromel-alumel thermocouple. By means of a selector switch and a thermocouple read-out, the furnace temperature in each zone can be determinted. A control thermocouple is located in the zone which is fourth from the top.

A long stainless-steel sheathed chromel-alumel probe thermocouple was used to determine the temperature profile inside the column. It was found that temperatures inside the extraction column were about 40-50 degrees lower than the corresponding "furnace temperatures" which are taken on the outside of the stainless steel sheath. By adjusting the controller and the three manually controlled heating zones, a slight positive temperature gradient (from bottom to top) was obtained. The molten magnesium temperature, as determined by the probe, ranged from 980°C at the bottom of the extraction column to 1020°C at the top. The furnace

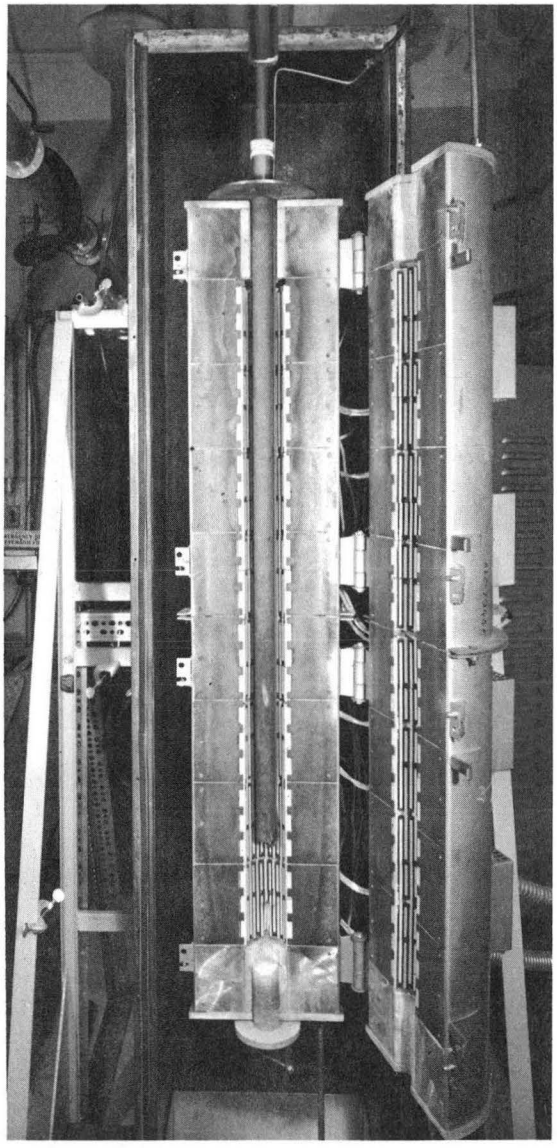

ZN-5467

Fig. 17

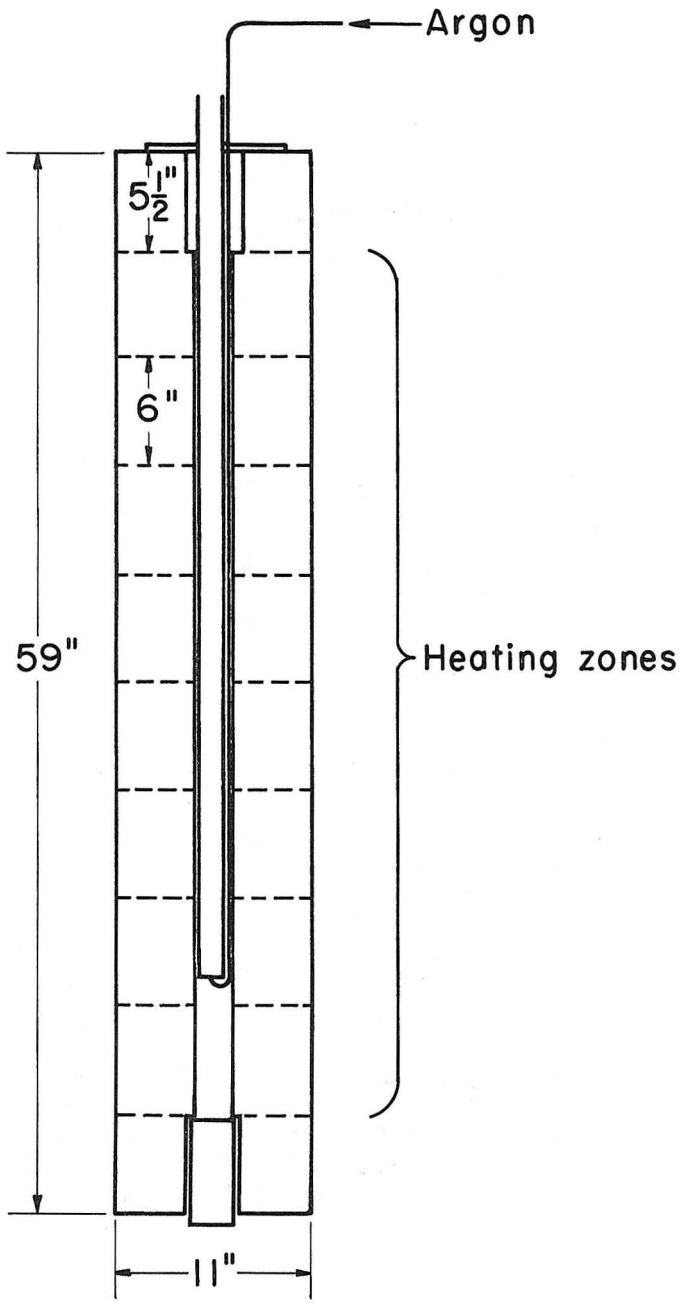

Fig. 18

temperatures corresponding to the desired column (probe) temperature profiles were recorded. Prior to each extraction run, the desired column profile was established by adjusting the furnace controls so that the zone-by-zone furnace temperature readings were the same as the recorded values. The positive temperature gradient was desired in order to minimize convection currents in the magnesium. The probe thermocouple was calibrated by melting silver (MP 960°C) in a quartz tube suspended inside the furnace.

The velocity of the U-Cr drop as it falls through the magnesium column is measured by three collimated scintillation detectors. The detectors are spaced 8 in. apart with the crystal faces 14 in. from the column axis. Each crystal is collimated behind 4 in. of lead with a 1/8 in. horizontal opening across the 2 in. width of the crystal face. The output of each detector is sent to a rate meter, a circuit which integrates the pulses generated as each gamma photon is detected. The rate meter output goes to a highly sensitive miniature galvanometer in a high speed recording oscillograph (Type 5-124 manufactured by the Consolidated Electrodynamics Corporation). A mirror in the galvanometer is deflected and reflects light from an illuminator lamp onto a moving strip of photographic paper. Paper speeds of 0.5 to 128 in. per second are possible. Three type 7-362 fluid damped galvanometers are used. They have an undamped natural frequency of 4150 cycles per second (cps) and a frequency range of 0 to 2500 cps. The oscillograph automatically inscribes timing lines of 1, 0.1, or 0.01 seconds on the photographic trace. Figure 19 shows the lead collimated scintillation detectors mounted on shelves in a 19 in. electronics rack. In the right foreground is the high speed recording oscillograph and its associated electronic equipment. The furnace control panel is visible at the left rear. Figure 16 shows the position of the detectors

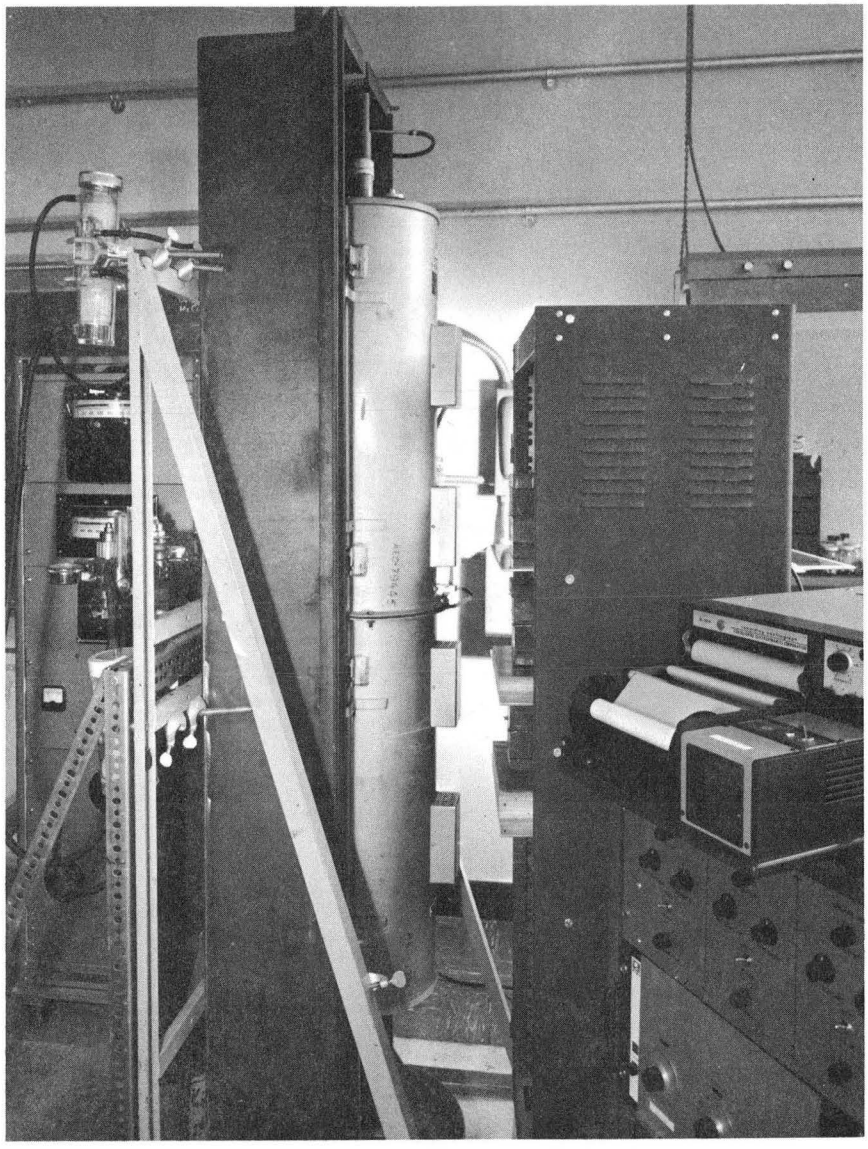

ZN-5469

Fig. 19

with respect to the column. Figure 20 shows a typical trace from the high speed recorder. Drop velocities were calculated between the top and middle and the middle and bottom detectors. Velocities in the second interval were about 15% higher than those measured in the top of the column and were taken as the terminal velocity.

B. Materials

The U-Cr eutectic alloy was purchased from the National Lead Company in the form of cylindrical pellets 1/4 in. in diameter and about 3/8 in. long. The alloy was made of depleted uranium containing about 0.2 w-% U^{235}. (Natural uranium contains 0.7 w-% U^{235}.) The supplier reported the melting point as 860°C. Analysis of alloy samples by the Lawrence Radiation Laboratory showed the chromium content to be 4.28 w-% (the eutectic alloy contains 5 w-% Cr). Spectrographic analysis showed no constituents other than Cr and U present in the samples.

Magnesium was obtained from the United Mineral and Chemical Corporation of New York in the form of 36 in.-long 1/2 in.-diameter sticks. A magnesium charge for a run weighed about 152 grams. Before placing a magnesium stick in the crucible it was cut to a length of 27-1/2 in. and the surfaces were carefully scraped or machined to remove the oxide coat.

C. Experimental Procedure

Two ingots of U-Cr alloy, one weighing 67 grams, the other 22 grams, were cast in graphite crucibles under vacuum in an induction furnace. Pellets were cut from these ingots using small hack-saws in an argon filled dry box. As nearly as possible, the pellets were cut in the shape of cubes. Pellet weights varied from 0.1 to 0.6 grams. A small hole was drilled through the center of each pellet using a high speed electric

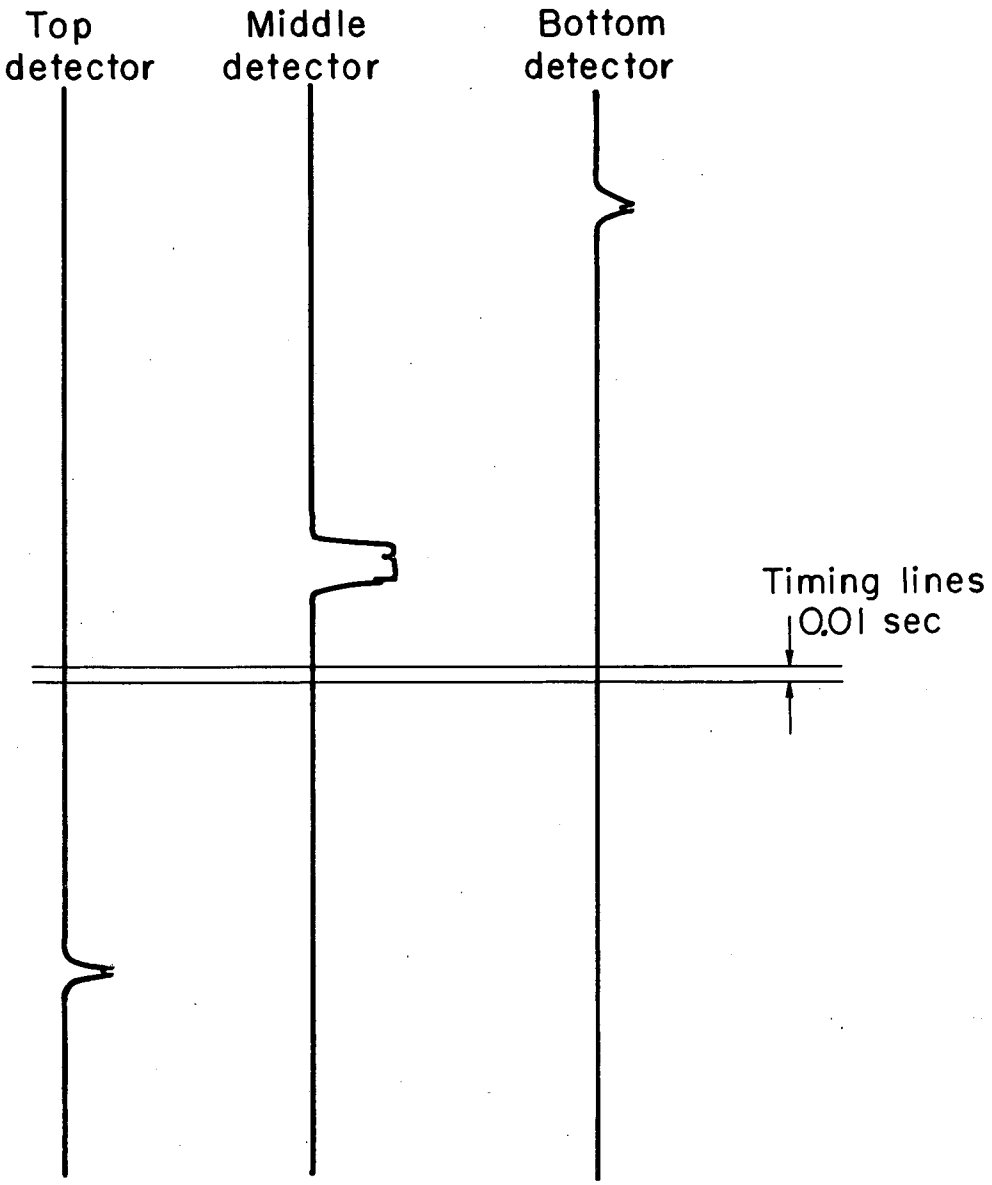
Top
detector
Middle
detector
Bottom
detector
Timing lines
0.01 sec
MUB-6394

Fig. 20

drill. Number 61 (.039-in.) high-speed wire drills were used. After weighing, the pellets were individually sealed in argon-filled quartz capsules by the Health Chemistry Division of UCLRL. The pellets were then sent to the LPTR for irradiation. Irradiation was for 48 hours at thermal neutron fluxes of 10^{12} to 10^{13} neutrons/cm^2-sec. The La^{140} activity of the pellet before the experiment was measured on the multichannel analyzer.

The pellet was prepared for introduction into the extraction column by suspending it from a 5 mil tungsten wire loop at the end of a 36 in. long 1/8 in. diameter stainless steel rod. After the furnace had been brought to temperature, but before introducing the irradiated pellet, a small unirradiated U-Cr pellet was dropped through the column to shake loose any bubbles that might have formed in the molten magnesium. The rod was lowered through the reflux column, through a 1/4 in. constriction at the bottom of the reflux column (see Fig. 14), and into the extraction column. The rod was lowered until the pellet was just below the molten magnesium surface. Within a few seconds, the pellet melted off the tungsten loop and fell through the column, its passage being detected by three collimated scintillation counters placed along the column. In this way, it was certain that the pellet entered the column as a liquid drop.

The technique of forming molten metal drops on wire loops was first tried on tin (MP 232°C) and lead (MP 328°C). Small pellets of the metals (~ 3-4 mm in diameter) were suspended in the molten KCl-LiCl eutectic (MP 350°C) in a pyrex test-tube. Since fused salts are transparent, the drop process could be directly observed. As soon as a drop melted it fell from the wire straight to the bottom of the test-tube without breaking-up. Figure 21 shows a U-Cr pellet suspended from a tungsten loop. Figure 22 shows a loop from which a pellet has been dropped, after it has been withdrawn from the magnesium column.

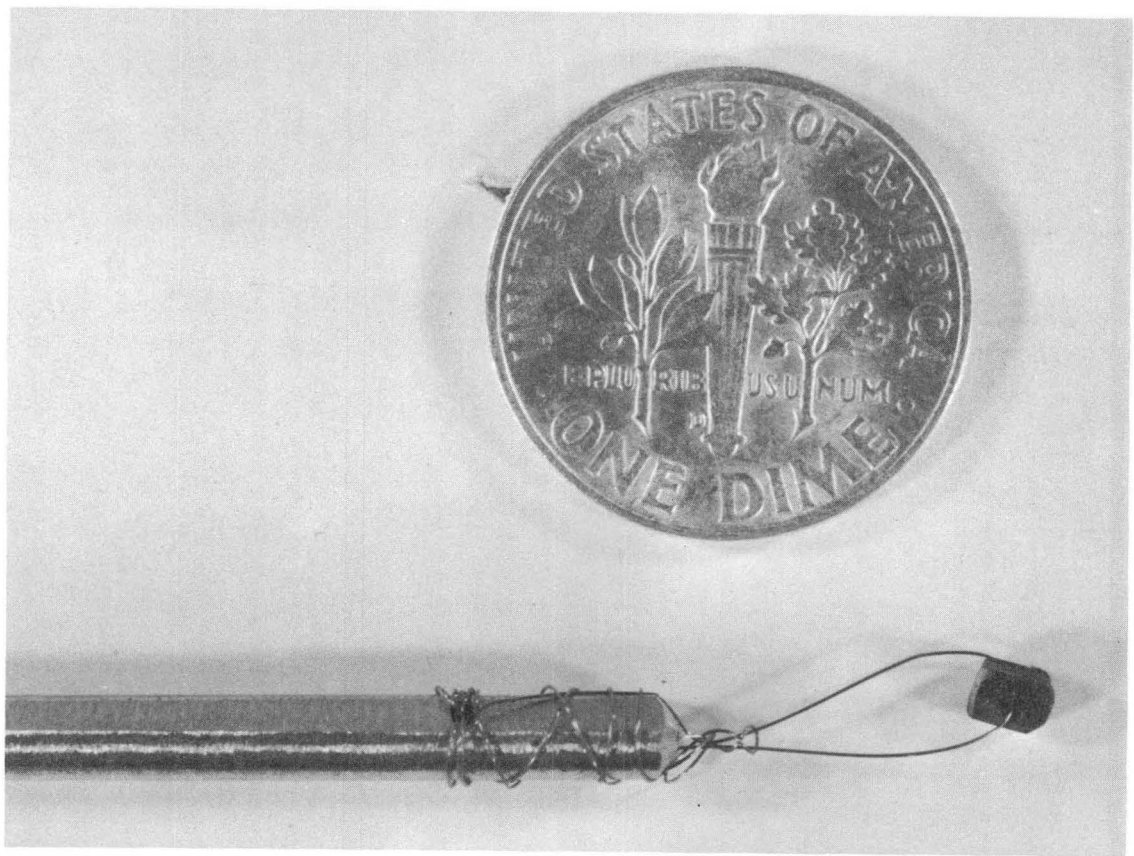

ZN-5473

Fig. 21

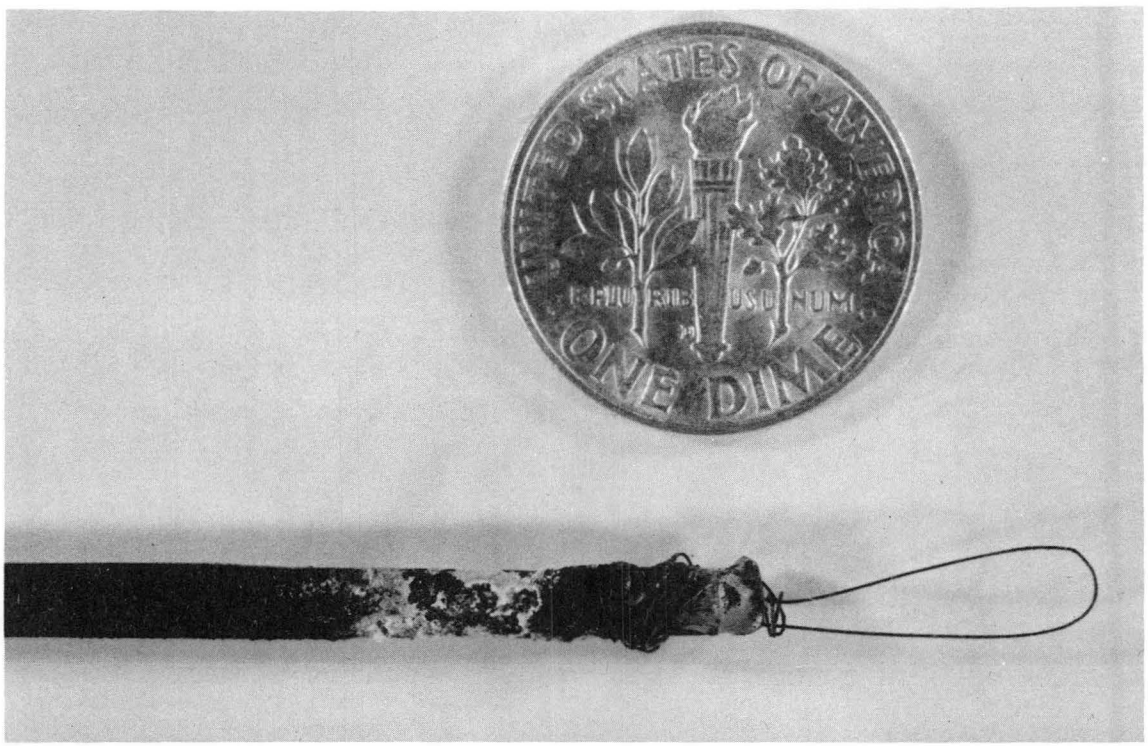

ZN-5474

Fig. 22

The irradiated pellet melted off the tungsten loop, fell through the molten magnesium and into a puddle of molten $BaCl_2$ about 1 in. deep contained in a graphite inner liner at the bottom of the column just above the screw plug. (The inner liner is shown in Fig. 15.) As soon as the scintillation detectors recorded the fall of the U-Cr drop, the furnace was immediately turned off in order to freeze the $BaCl_2$, whose melting point, 960°C, is only 20°C below the temperature of the bottom of the column. (Molten $BaCl_2$ is twice as dense as Mg at 1000°C. It is chemically stable with respect to uranium, magnesium, and lanthanum.) The U-Cr pellet at the bottom of the crucible was thus physically separated from the molten magnesium which takes longer to freeze (MP 650°C). In this way, continued extraction after the pellet had reached the bottom of the column was prevented.

The operation of the experiment required two people. One person lowered the U-Cr pellet into the column. The second person, a safety observer from the Health Chemistry Division, carefully watched the high speed photographic recording oscillograph which traced the output of the three collimated scintillation counters.

As soon as the oscillograph recorded the passage of the U-Cr drop, the furnace was turned off. The dropping rod, coated with condensed hot magnesium was slowly withdrawn from the reflux column under a direct argon stream. Even with an argon stream playing directly on the top of the reflux column, the dropping stick had to be removed very slowly to prevent the magnesium from burning. This operation took about half a minute. The freezing process at the bottom of the column was accelerated by removing the ceramic plug in the bottom vestibule and directing a stream of cold air up into the furnace for several minutes with an electric blower.

The entire furnace arrangement was allowed to cool for approximately 45 minutes to 1 hour until the furnace readings indicated that the entire magnesium column was frozen. The hinged furnace was opened and the stainless steel sheath removed with the aid of asbestos gloves. The sheath was placed on a bench covered with transite and asbestos paper and the reflux column removed. By tipping the sheath slightly, the graphite crucible was easily made to slide out. Cooling the graphite crucible to the point where it could be handled took another 30 minutes. The machined screw plug was then removed. The crucible was placed in a drill press in a supporting wooden block and with the aid of 1/2 in. diameter steel bars of various lengths the magnesium column and inner liner was slowly "pressed-out" of the crucible. In this way it was possible to save the crucible for future runs. (This technique is not infallible; a number of crucibles were broken in the process.) The recovered magnesium stick was placed in an argon filled dry box and the inner liner containing the U-Cr pellet, buried in frozen $BaCl_2$, sawed-off. The magnesium stick, inner liner, and crucible were placed in polyethylene bags and then examined with the multichannel analyzer for La^{140}. The activity of the Mg ingot was followed for several weeks after the experiment in order to determine the parameter F as described in Section I-D.

Lanthanum-140 activity in the inner liner (corrected for the additional gamma self-absorption due to the unirradiated pellet dropped through the column) plus La^{140} activity in the Mg ingot accounted for about 95% of the original activity. The apparent loss of activity may be due to gamma absorption by the frozen $BaCl_2$ and to departure from spherical shape of the frozen U-Cr. Lanthanum-140 activity in the graphite crucible was negligible. The fraction of La^{140} extracted was based on the measured activity in the Mg ingot.

V. PHYSICAL PROPERTIES OF THE U-Cr, Mg SYSTEM WITH La AND Ba SOLUTES

In order to compare the data with existing correlations based upon aqueous-organic systems, a number of physical properties of the U-Cr, Mg system are required.

Density - The density of magnesium has been measured by McGonigal, Kirshenbaum and Grosse.[82] The value at 1000°C is 1.50 g/cc. The density of molten uranium from its melting point (1406°K) to 2000°K has been measured by Grosse, Cahill, and Kirshenbaum.[83] The density of uranium is represented by the equation ρ g/cc = 19.356-10.328 • 10^{-4} T°K ±.078% which gives a value of 18.04 g/cc at 1000°C. The density of molten U-Cr has not been measured and so must be estimated. An ingot of U-Cr was cast in a graphite crucible in an induction furnace, machined to a right-circular cylinder by the UCLRL machine shop facilities and its density determined by weighing the known volume. The room-temperature density of the U-Cr eutectic was determined to be 17.5 g/cc. The density of uranium at 1000°C, 18.04 g/cc is 5.2% less than its room temperature density of 19.06 g/cc. The percentage density loss of the U-Cr eutectic was assumed to be the same as that for U, and so the density of the molten eutectic at 1000°C is estimated to be 16.6 g/cc.

Viscosity - The viscosity of magnesium has been measured by Culpin[24] and Gebhardt.[15] Gebhardt's data cover a wider range of temperature (from 650°C to 900°C) than Culpin's (652-725°C). Also Culpin's data lead to positive values for the entropy of activation for viscosity, whereas all other metals show negative values. Extrapolating Gebhardt's data to 1000°C gives a value of .0055 poise for the viscosity of Mg at 1000°C. No measurements are available for the viscosity of uranium or U-Cr alloys,

and this number must be estimated. The viscosity of the U-Cr eutectic at 1000°C is assumed equal to that of super-cooled uranium and the latter is estimated using the correlation of Chapman[52] for the viscosity of molten metals. Chapman's correlation predicts a viscosity for uranium of 3.98 cp at its melting point (1132°C) and 4.88 cp at 1000°C. A method of estimating viscosity of molten metals due to Grosse[92] gives 5.88 cp at the melting point and 7.78 cp at 1000°C for the viscosity of uranium.

Surface Tension and Interfacial Tension - The value of surface tension for magnesium has been reported at 650, 700, and 800°C. The values are 559, 542, and 508 dynes per cm respectively.[84] A linear extrapolation to 1000°C gives an estimated value of 440 dynes per cm.

Cahill and Kirshenbaum[85] measured the surface tension of liquid uranium from its melting point to 1850°K by the maximum bubble pressure method. Their data are represented by the equation $\sigma_U = 1747-0.14T(°K)\pm40$ dynes/cm. At the melting point $\sigma_U = 1550$ dynes/cm. This value agrees with a value determined by Spriet[86] who measured the surface tension of uranium by the drop weight method and found $\sigma_U = 1500$ dynes/cm. Extrapolating the data of Cahill and Kirshenbaum to 1000°C, the calculated value is $\sigma_U = 1570$ dynes/cm.

Grosse[87] has reviewed the available data on surface tension for a number of molten metals. He reports a value of 1590±50 dynes/cm for the surface tension of liquid chromium at its melting point, 2176°K, determined by Eremenko and Neiditch. In the same paper, Grosse discusses a calculation for estimating the temperature coefficient of surface tension. The calculation assumes that surface tension decreases linearly with temperature until it disappears at the critical temperature. (Other papers by Grosse[88] discuss measurements and estimates of critical temperatures for metals.)

Following Grosse's procedures, the critical temperature of chromium is estimated to be 10,000°K and the temperature coefficient of surface tension for chromium $\frac{d\sigma}{dT}$, is estimated to be -.203 dynes/cm-°K. Thus the estimated value for σ_{Cr} at 1000°C is 1771 dynes/cm.

There is no generally accepted theory for determining the concentration dependence of the surface tension of alloys from pure-component values. Some systems show a monotonic curve, others have a minimum or a maximum. For the purposes of this calculation, it was assumed that the surface tension of uranium-chromium alloys varies linearly with the mole fractions of the two components. Thus $\sigma_{U\text{-}Cr}$ is estimated to be 1609 dynes/cm at 1000°C.

The interfacial tension between the molten U-Cr eutectic and magnesium has been estimated using Antonov's rule ($\sigma_i = \sigma_{U\text{-}Cr} - \sigma_{Mg}$) which gives a value of 1169 dynes/cm. Girifalco and Good[89] have proposed a rule for interfacial tension ($\sigma_i = \sigma_A + \sigma_B - 2\,\Phi\sqrt{\sigma_A\,\sigma_B}$) where Φ is empirically found to depend on the type of system. For water-organic systems, $\Phi \sim 1$, for non-metallic liquid-mercury systems, $\Phi \sim .55 - .75$, and for water-mercury, $\Phi = .32$. Using a value of $\Phi = 1$, σ_i is calculated to be 369 dynes/cm.

Table XXI summarizes the physical property values required for estimating drop velocity in the uranium-chromium eutectic-magnesium system.

Diffusivities - There are no measured values for the diffusivity of La in U or in U-Cr alloys. Smith,[94] however, has measured the diffusivity of cerium in uranium over the temperature range 1170°-1480°C. The temperature dependence of the diffusion constant is represented by the equation $D = 4.5 \times 10^{-3} \exp[-11{,}000/RT]$. This relation is valid over the range

Table XXI. Measured and Estimated Properties of the Molten Magnesium Uranium-Chromium Eutectic System at 1000°C

Property	Value	Reference
Density of Mg, ρ_e	1.50 g/cc	82
Density of U	18.04 g/cc	83
Density of U-Cr eutectic	16.6	estimated*
Density Difference, $\Delta\rho$	15.1 g/cc	
Viscosity of Mg, μ_e	0.0055 poise	15
Surface Tension of Mg, σ_{Mg}	440 dynes/cm	84
Surface Tension of U, σ_U	1570 dynes/cm	85
Surface Tension of Cr, σ_{Cr}	1771 dynes/cm	87
Surface Tension of U-Cr, σ_{U-Cr}	1609 dynes/cm	estimated
Interface Tension, σ_i	1169 dynes/cm	estimated by Antonov's Rule

* Density of the U-Cr eutectic at 25°C is 17.5 g/cc, measured in the course of this work.

1170°-1350°C. Smith believes that his observed values at higher temperatures were too large, due to convection currents. Extending the relationship to super-cooled uranium gives a value of $D = 5.85 \times 10^{-5}$ cm^2/sec at 1000°C.

The various diffusivities of interest have been estimated by the absolute rate method (Olander modification) developed in Section III, and the results are shown in Table XXII.

Table XXII Diffusivities in U-Cr and Mg at 1000°C

Solute	Solvent	Diffusivity (10^{-5} cm^2/sec)
La	U-Cr*	2.69
Ba	U-Cr*	2.77
Ce	U-Cr*	2.78
La	Mg	14.5
Ba	Mg	14.9

* U-Cr assumed to be pure uranium. Viscosity estimated by Chapman's method.[52]

The viscosity and density of molten La and Ce have been reported in various Mound Laboratory Reports.[104] From this data, the free energies of activation of the solute rare earths, ΔF^*_{SS} were estimated for use in predicting diffusivities. The estimate of ΔF^*_{SS} for Ba is based on an estimate of Ba viscosity by Chapman's method. (Chapman's correlation predicts values of viscosity at 1000°C for La and Ce which are too high by 14% and 19% respectively.)

VI DROP VELOCITIES

A. Experimental Results

A total of 13 kinetic experiments were conducted. The measured terminal velocities for the 11 satisfactory attempts are tabulated in Table XXIII. The trace for run no. 12 showed a double blip at the bottom detector and it was assumed that this drop split up. The pellets used in runs no. 12 and 13 evidently broke during the melting process since in each case a large fragment of the drop was later found near the top of the column against the crucible wall. Data for runs 12 and 13, the two largest pellets, were rejected. The drop velocities recorded in Table XXIII are independent of pellet size with the exception of run no. 6 which showed a lower velocity than the others. This drop, the smallest pellet used, may have hit the column wall while falling.

B. Comparison With the Hu-Kintner Correlation

A number of investigators have studied drop velocity in aqueous-organic systems.[79-81] From these investigations it is possible to draw some qualitative conclusions: Initially, as drop diameter increases, so does terminal velocity. Eventually a "peak point" is reached at which the terminal velocity has its maximum value and above which velocity either decreases very slowly or remains constant as drop diameter increases. Peak diameter and peak velocity are characteristic of the particular system. The smaller the peak diameter, the higher the peak velocity. At diameters larger than that corresponding to the peak point, the drop oscillates as it falls. Interfacial tension and the viscosity of the continuous phase have a damping effect on oscillation. Higher interfacial tension increases velocity, i.e., the higher the interfacial tension, the larger the diameter

Table XXIII Summary of Drop Velocity Data

Run No.	Weight w,gms	Diameter d, cm	Terminal Velocity U_T, cm/sec	Reynolds Number Re	Drag Coefficient C_D
6	.082	.211	46.2	2660	1.30
14	.089	.218	67.6	4010	.63
7	.204	.286	76.6	5960	.64
15	.231	.299	72.5	5900	.75
1	.252	.307	71.3	5970	.79
2	.327	.335	64.5	5890	1.06
4	.376	.351	62.5	5980	1.18
9	.382	.353	67.7	6520	1.01
10	.441	.370	72.5	7300	.92
17	.593	.410	72.5	8100	1.02
11	.603	.411	67.7	7590	1.18

at which a drop continues to behave like a solid sphere. The correlation was developed by Hu and Kintner[79] for organic drops falling through water at room temperature utilizes the following dimensionless groups.

$$\text{the drag coefficient, } C_D = \frac{4}{3}\frac{\Delta\rho}{\rho_e}\frac{dg}{U_T^2}$$

$$\text{the Weber Number, } We = \frac{U_T^2 \rho_e d}{\sigma_i g}$$

$$\text{the Reynolds Number, } Re = \frac{d\, U_T\, \rho_e}{\mu}$$

$$\text{the physical property group, } P = \frac{\rho_e}{\Delta\rho} \cdot \frac{\rho_e \sigma_i^3}{g\mu^4}$$

The Reynold's number and drag coefficients for each of the 11 runs are listed in Table XXIII.

This correlation shows two regions with a distinct break at a value of Reynolds number where peak velocity occurs. The two regions can be represented by the following equations:

$$Y = \frac{4}{3} X^{1.275} \text{ for } 2 < Y \leq 70 \qquad (61)$$

$$Y = (0.045)\, X^{2.37} \text{ for } Y \geq 70 \qquad (62)$$

where

$$Y = C_D\, We\, P^{0.15}$$

and

$$X = Re/P^{0.15+0.75}$$

Hu and Kintner found that these equations give errors usually below 10% for the systems they studied. Figure 23 compares the data with the generalized Hu and Kintner correlation. The data have been treated using the two values of interfacial tension σ_i = 1169 dynes/cm, and σ_i = 369

dynes/cm. The larger value for interfacial tension gives a better fit to the generalized curve. Figure 24 compares the drop velocity data with the curve predicted by the generalized correlation. The average of the observed values is about 13% higher than that predicted by the correlation. The system studied here extends the correlation to values of the physical properties which far exceed those studied by Hu and Kintner. For the U-Cr, Mg system the density difference is 15.1 g/cc. The largest value of $\Delta\rho$ used in the generalized correlation was ~1.95 g/cc. Interfacial tension in the U-Cr, Mg system (1610 dynes/cm) far exceeds values typical of immiscible aqueous-organic systems. The largest value of σ_i in the original correlation is 44 dynes/cm. Due primarily to the large density difference, the terminal velocities observed in the present system (~65-75 cm/sec) are greater than the largest observed by Hu and Kintner (~26 cm/sec.).

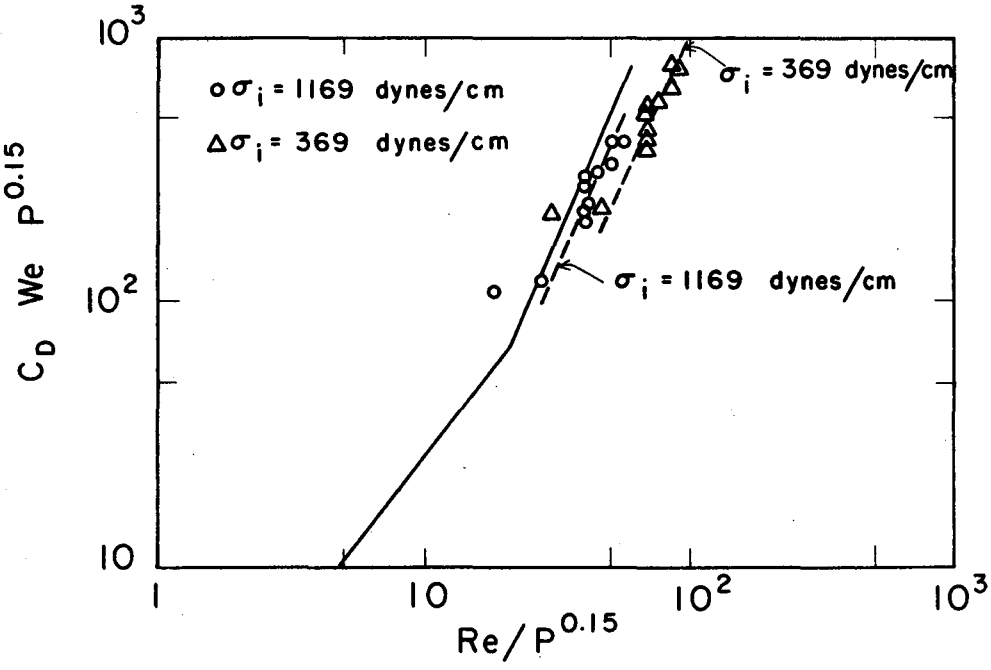
10^3
10^2
10
1
10
10^2
10^3
C_D We $P^{0.15}$
$Re/P^{0.15}$
o σ_i = 1169 dynes/cm
Δ σ_i = 369 dynes/cm
σ_i = 369 dynes/cm
σ_i = 1169 dynes/cm
MU-36989

Fig. 23

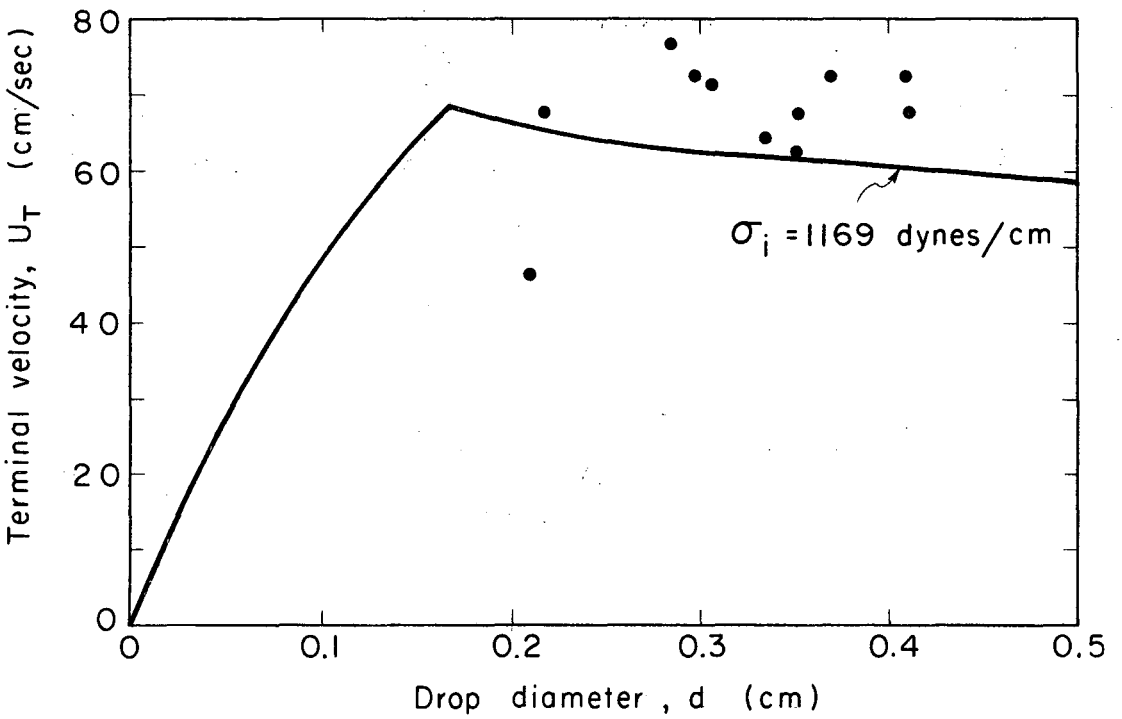
Terminal velocity, U_T (cm/sec)
80
60
40
20
0
0
0.1
0.2
0.3
0.4
0.5
Drop diameter , d (cm)
σ_i =1169 dynes/cm
MU-36990

Fig. 24

VII SOLUTE EXTRACTION

A. Experimental Results

The fraction of La extracted, f_{La}, was determined by the before and after measurements of La^{140} activity in pellet and Mg ingot with the appropriate self-absorption (for the pellet) and geometrical (for the ingot) corrections as described in Appendices A, B, and C. The ratio of the extracted fractions of La to Ba, F, was determined by a plot of Eq. (2) as illustrated in Fig. 25. (An abscissa value of 0.01 in this plot corresponds to a time of 12.8 days after extraction.) The fraction of Ba^{140} extracted was determined by Eq. (4) using known values of f_{La} and F.

In order to determine the height of liquid and the time it took a pellet to fall through the column, the Mg ingots were weighed and the weight converted to liquid column length using the cross-sectional area of the graphite crucible and the density of Mg at 1000°C. Average velocities, determined between the first and third detectors, were used in the calculation.

Table XXIV shows data for runs 6 through 11 and 14 through 17. Runs 1 through 5 were devoted to developing the experimental technique. In some of these runs, no puddle of $BaCl_2$ salt was used at the bottom of the column. Examination of the frozen Mg ingot after extraction by counting collimated two-inch lengths showed large end-effects when the pellet remained in contact with molten Mg during the cooling period. The presence of the salt-Mg interface in later runs prevented these large end effects. Extraction data for the first five runs were rejected, although velocity data for these runs were reported in Table XXIII. All data for runs 12 and 13 were rejected for reasons discussed earlier.

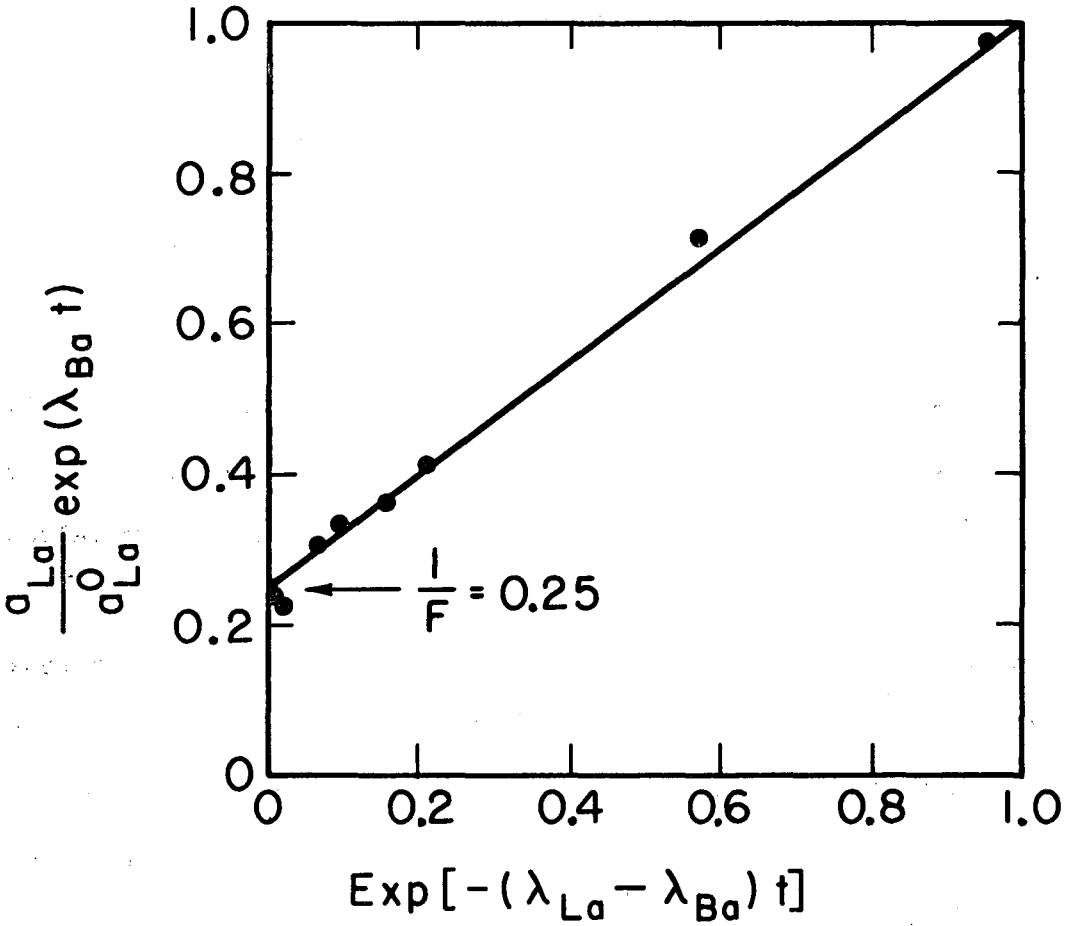
1.0
0.8
0.6
0.4
0.2
0
0
0.2
0.4
0.6
0.8
1.0
$\frac{a_{La}}{a^{o}_{La}} \exp(\lambda_{Ba} t)$
$\frac{1}{F} = 0.25$
$\mathrm{Exp}[-(\lambda_{La} - \lambda_{Ba})\, t]$
MUB-6390

Fig. 25

Table XXIV Summary of Experimental Results

Run No.	Drop Diam. d, cm	Mg Ingot Weight gms.	Length of Molten Mg Column at 1000°C cm	Average Drop Velocity U, cm/sec	Time of Fall t, sec	Fraction of La removed f_{La}	F	Fraction of Ba removed f_{Ba}
6	.211	142.2	59.1	43.0	1.374	.145	6.66	.0218
14†	.218	149.0	62.0	62.5	.992	.148	14.3	.0104
7	.286	143.9	59.8	68.8	.870	.104	7.15	.0145
15†	.299	148.5	61.8	70.1	.880	.0386	9.1	.0042
8	.324	144.2	60.0	60.2	.996	.0485	5.25	.0092
9	.353	149.9	62.3	62.5	.996	.0112	7.15	.0016
16†	.367	147.0	61.1	[65]*	.902	.0495	14.3	.0035
10	.370	148.8	61.8	67.7	.911	.0613	4.0	.0153
17†	.410	147.0	61.1	67.2	.910	.0763	6.0	.0127
11	.411	149.7	62.2	63.5	.980	.0434	11.1	.0039

* Falling drop was not detected. Velocity estimated.

† Pellets coated with Mg prior to irradiation.

The fraction of La^{140} extracted seems low. Also, the considerable scatter in the data and the fact that analysis of the results indicates the presence of a large external resistance all suggest the possibility of oxide film on the U-Cr surface which would block mass transfer at the eutectic-magnesium interface. Uranium is extremely reactive, but so is magnesium. MgO is thermodynamically more stable than UO_2, and it might be expected that any UO_2 present on the pellet surface would be reduced as the pellet falls through the column. It is not certain, however, that this reaction could completely clean the U-Cr in the approximately one second of contact time. To minimize the possibility of UO_2 formation on the pellet surface, four of the U-Cr pellets (runs 14 through 17) were given a protective magnesium coating prior to irradiation. This was accomplished as follows: Approximately five grams of magnesium were melted in a graphite crucible under argon in a clamshell resistance heater. The crucible had a 1/2-in. inner diameter and was about 5-in. deep. In the crucible bottom a small 1/8-in. diameter hole was drilled about 3/4-in. deep. The magnesium charge was carefully machined to fit all these dimensions to prevent entrapment of air between the magnesium and the crucible walls or in the small hole at the bottom. When the magnesium was molten, a freshly cut weighed pellet of U-Cr was dropped into the crucible and pushed down into the bottom of the 1/8-in. diameter hole. (A tantalum rod was used as the "pusher".) The pellet was allowed to soak in molten Mg at 750°C for about 15 minutes. After cooling, the crucible was broken and the cast Mg ingot removed. The tip of the 1/8-in. diameter section containing the U-Cr pellet, was sawed-off. The .039-in. hole, later used for introducing the pellet in the extraction column, was then drilled through the magnesium coat and the pellet. In

run number 17, the hole was drilled and stuffed with graphite before the magnesium soak. After coating the pellet with magnesium, the graphite stuffing was drilled-out. Pellets 14 through 17 were then sealed in argon-filled quartz capsules and irradiated as before.

Table XXIV shows no significant difference between runs made using magnesium coated (14-17) or uncoated pellets. It was therefore concluded that observed low values for fraction extracted are either a real property of the system and are not due to surface contamination, or that the operation of soaking the U-Cr pellets in liquid Mg did not succeed in completely removing the oxide coat.

B. Data Analysis by the Series Resistance Concept

The overall mass transfer coefficient, K, can be related to the fraction extracted by:[90]

$$f = 1-e^{-K(\frac{6}{d})t} \approx K\,(\frac{6}{d})\,t \qquad (63)$$

If f is very small, the first two terms of a series expansion of the exponential approximates the entire series and the fraction extracted can be expressed by the last term of Eq. (63). Since

$$f_{Ba} = f_{La}/F \qquad (4)$$

$$K_{Ba} \approx \frac{f_{La}}{f_{Ba}}\,(\frac{d}{6})\,\frac{1}{t}\,. \qquad (64)$$

If the approximation of Eq. (63) is valid for both La and Ba,

$$\frac{K_{La}}{K_{Ba}} = \frac{f_{La}}{f_{Ba}} = F \qquad (65)$$

The exponential form of Eq. (63) has been used to determine the

overall mass transfer coefficient for lanthanum based upon the U-Cr phase, K_{La}, and Eq. (64), has been used for the coefficient for barium, K_{Ba}. The results are tabulated in Table XXV. The average value of K_{La}, neglecting run no. 9, is .00417±30% cm/sec.

In the two-film theory of mass transfer, K, the overall coefficient is related to k_i and k_e, the internal and external film mass transfer coefficients, by Eq. (65)

$$\frac{1}{K} = \frac{1}{k_i} + \frac{1}{mk_e} \qquad (65)$$

where m is the distribution coefficient of the solute.

In the following it is assumed that k_i and k_e are the same for both La and Ba. This is equivalent to assuming equal diffusivities in each phase for the two isotopes.

In Table XXII of Section V, estimates of the diffusivities of La and Ba in U-Cr and in Mg at 1000°C are presented. The estimates show that the diffusivity of La and Ba are approximately equal in each phase. The estimate for Ce in U-Cr is considerably lower than the value based on an extrapolation of Smith's[94] measurements for Ce in U. Nevertheless, it seems reasonable to believe that whatever the absolute error in estimating the diffusivity of rare earths in uranium is, the same error is involved in estimating the diffusivity of Ba in uranium. The largest source of error in the estimates for Ce, La, and Ba in U-Cr is probably the estimate of the viscosity of the U-Cr eutectic.

Assuming that the film coefficients are the same for the two solutes it is possible to write Eq. (65) for each solute and to solve the two equations simultaneously:

$$\frac{1}{K_{La}} = \frac{1}{k_i} + \frac{1}{m_{La} k_e} \qquad (66)$$

$$\frac{1}{K_{Ba}} = \frac{1}{k_i} + \frac{1}{m_{Ba} k_e}$$

A pair of Eqs. (66) is written for each run and solved for $\frac{1}{k_i}$ and $\frac{1}{k_e}$. The distribution coefficients used were $m_{La} = .16$ and $m_{Ba} = .0035$. Values of k_i and k_e calculated by Eq. (66) are listed in Table XXV.

Neglecting run no. 9, the average value of k_e is .183±49% cm/sec. The average value of k_i is .00514±30% cm/sec.

Katz, Hill, and Speirs[73] of the Brookhaven National Laboratory measured the rate of extraction of samarium from drops of Bi-Mg-Sm alloy by a fused-salt extractant at 500°C using the falling liquid drop technique. Their data show the scatter typical of such systems but they were able to achieve considerable extraction: up to 80% of the Sm extracted in 1 second contact time. Some of their data (the higher experimental values of fraction extracted at contact times up to about 0.5 seconds) are in agreement with values predicted by Eq. (63) where the overall mass transfer coefficient, K, has been calculated by Eq. (65), with the film coefficients calculated using a model given by Handlos and Baron[90] for the drop coefficient, k_i, and a model given by Higbie[91] for the continuous phase (or external) coefficient, k_e.

The Handlos and Baron model assumes that solute transfer within the drop is due to drop circulation. The expression for the internal film coefficient is

$$k_i = \frac{0.00375U}{1+\mu_d/\mu_e} \qquad (67)$$

where U is the drop velocity, μ_d and μ_e are the viscosities of the drop

Table XXV. Experimental Mass Transfer Coefficients

Run No.	Drop Diam.	Surface to Volume Ratio	Contact Time	Fraction of La^{140} Extracted	Fraction of Ba^{140} Extracted	Overall Mass Transfer Coeff. for La^{140}	Overall Mass Transfer Coeff. for Ba^{140}	Internal Film Mass Transfer Coeff.	External Film Mass Transfer Coeff.
	d, cm	a_S, cm^{-1}	t, sec	f_{La}	f_{Ba}	K_{La} $\frac{cm}{sec}$	K_{Ba} $\frac{cm}{sec}$	k_i $\frac{cm}{sec}$	k_e $\frac{cm}{sec}$
6	.211	28.4	1.374	.145	.0218	.00401	.000556	.00466	.180
14	.218	27.5	.992	.148	.0104	.00585	.000379	.00861	.113
7	.286	21.0	.870	.104	.0145	.00600	.000795	.00700	.256
15	.299	20.1	.880	.0386	.0042	.00223	.000240	.00272	.075
8	.324	18.5	.996	.0485	.0092	.00269	.000500	.00298	.172
9	.353	17.0	.996	.0112	.0016	.00066	.000092	.00076	.030
16	.367	16.4	.902	.0495	.0035	.00344	.000235	.00492	.071
10	.370	16.2	.911	.0613	.0153	.00430	.001025	.00462	.377
17	.410	14.6	.910	.0763	.0127	.00595	.000995	.00673	.318
11	.411	14.6	.980	.0434	.0039	.00310	.000273	.00401	.084

and continuous phases, respectively. The Handlos and Baron expression is interesting in that diffusion within the drop does not enter the calculation. There is some doubt that the expression is applicable at very short contact times.

The expected high viscosity of uranium and interfacial tension of the U-Cr-Mg system leads one to speculate that the falling drop is not circulating but is stagnant. In this case, solute transfer within the drop depends on diffusivity alone. An expression due to Newman[93] for stagnant spherical drops assuming no resistance to transfer in the external phase is

$$k_i = -\frac{d}{6t}\,\ell n\left[\frac{6}{\pi^2}\sum_{n=1}^{\infty}\frac{1}{n^2}\exp\left(-n^2\pi^2\tau\right)\right] \qquad (68)$$

where τ (dimensionless time) $= \frac{4D_i t}{d^2}$. For $\tau < .1$, an alternate expression is:

$$k_i = -\frac{d}{6t}\,\ell n\left[1 - \frac{6}{\sqrt{\pi}}\tau^{1/2} + 3\tau\right] \qquad (69)$$

The Higbie model for external coefficients assumes unsteady-state diffusion through a film of the continuous phase fluid which is continuously replaced by a new film each time the drop moves a distance equal to its own diameter. The Higbie expression is

$$k_e = 2\left(\frac{D_e U}{\pi d}\right)^{1/2} \qquad (70)$$

In this expression, D_e is the diffusivity of the solute in the continuous phase.

Theoretical film coefficients have been calculated by the three methods just discussed and are compared with the experimental values in Table XXVI. The Handlos and Baron model predicts values of k_i which

Table XXVI Comparison of Experimental and Theoretical Mass Transfer Coefficients

Run No.	Internal Coefficients k_i (10^{-3} cm/sec)					External Coefficients k_e (10^{-1} cm/sec)			
	Expt'l.	Theoretical				Expt'l	Theoretical		
		(a)	(b)	(c)	(d)		(e)	(f)	(g)
6	4.7	16.4	10.7	7.8	5.2	1.8	1.9		
14	8.6	23.8	15.5	9.2	6.1	1.1	2.3		
7	7.0	26.2	17.6	9.7	6.5	2.6	2.1		
15	2.7	26.7	17.4	9.6	6.5	.8	2.1		
8	3.0	22.9	14.9	9.0	6.0	1.7	1.8	1.7	1.3
9	.7	23.6	15.5	9.4	6.0	.3	1.8		
16	4.9	24.7	16.1	9.4	6.3	.7	1.8		
10	4.6	25.8	16.8	9.4	6.2	3.8	1.8		
17	6.7	25.6	16.7	9.4	6.2	3.2	1.7		
11	4.0	24.2	15.7	8.9	6.0	.8	1.7		

(a) Handlos and Baron, $\mu_{U\text{-}Cr}$ = 4.88 cp. Eq. (67). Ref. 90.

(b) Handlos and Baron, $\mu_{U\text{-}Cr}$ = 7.78 cp. Eq. (67). Ref. 90.

(c) Newman, $D_i = 5.85 \times 10^{-5}$ cm^2/sec. Eq. (69). Ref. 93.

(d) Newman, $D_i = 2.69 \times 10^{-5}$ cm^2/sec. Eq. (69). Ref. 93.

(e) Higbie, $D_e = 14.5 \times 10^{-5}$ cm^2/sec. Eq. (70). Ref. 91.

(f) Garner, $D_e = 14.5 \times 10^{-5}$ cm^2/sec. Eq. (71). Ref. 108.

(g) Griffith, $D_e = 14.5 \times 10^{-5}$ cm^2/sec. Eq. (74). Ref. 110.

are 3 to 5 times too high depending on which value of U-Cr viscosity is used. The stagnant drop (diffusion) model, using a value of internal diffusivity extrapolated from Smith's measurements, predicts values of k_i which are about twice as large as the experimental values. A value of D_i calculated from the absolute rate theory correlation of Section III predicts values of k_i which are in good agreement with the experimental values. The Higbie model predicts values for the external coefficient, k_e, which agree with the mean of the experimental values.

The external coefficient has also been estimated by Garner's[108] correlation

$$Sh = -126 + 1.8\ Re^{1/2}\ Sc^{0.42} \tag{71}$$

where the Sherwood Number, $Sh = \frac{dk_e}{D_e}$ (72)

and the Schmidt Number, $Sc = \frac{\mu_e}{\rho_e D_e}$ (73)

The Schmidt number for the system La in Mg is estimated to be 25. The calculated value of k_e is close to that predicted by Higbie's expression.

Griffith's[110] formula for a rapidly moving surface,

$$Sh = 2 + 1.13\ Pe^{1/2}\ k_v^{1/2} \tag{74}$$

where the Peclet Number, $Pe = ReSc$ (75)

and k_v is the ratio of the actual interfacial speed to the potential flow interfacial speed, gives a value of k_e somewhat lower than either the Higbie or the Garner expressions.

Table XXVII shows the relative importance of the internal and external resistances for each solute.

Table XXVII Relative Importance of Internal and External Resistances

	La	Ba
Average internal film transfer coefficient, k_i cm/sec	.00514	.00514
Average external film transfer coefficient, k_e cm/sec	.183	.183
Distribution coefficient, m	.161	.0035
Internal resistance = $\frac{1}{k_i}$ sec/cm	195	195
External resistance = $\frac{1}{mk_e}$ sec/cm	34	1560
Total resistance = $\frac{1}{K} = \frac{1}{k_i} + \frac{1}{mk_e}$ sec/cm	229	1755
Average overall mass transfer coefficient, K cm/sec	.00417	.000555
Total resistance = $\frac{1}{K}$ sec/cm	240	1800
Percentage internal resistance	85%	11%
Percentage external resistance	15%	89%

C. Data Analysis by Stagnant Diffusion with External Resistance

The measured fractions of lanthanum extracted are very small. It was shown earlier that measured internal film coefficients are even smaller than those predicted by a stagnant drop model where molecular diffusion is the only mechanism of mass transfer if a value of $D_i = 5.85 \times 10^{-5}$ cm^2/sec^1 based on Smith's measurements is accepted. (See Table XXVI.)

Since the distribution coefficients for rare earths between uranium and magnesium are small, then there may be a considerable external resistance, and the theories of internal mass transfer based upon no external resistance are not valid.

It is of interest to analyze the data based upon a model of diffusion through a stagnant drop with external resistance.

The diffusion equation for a sphere is

$$\frac{\partial c}{\partial t} = D_i \left(\frac{\partial^2 c}{\partial r^2} + \frac{2}{r} \frac{\partial c}{\partial r} \right) \tag{76}$$

the boundary conditions are:

$$c(r,0) = 1$$

$$c(0,t) = \text{finite}$$

$$- D_i \left(\frac{\partial c}{\partial r} \right)_a = mk_e \, c(a,t) \tag{77}$$

where a is the drop radius. The mathematical solution for this model is given by Crank[97] after the solution by Newman:[98]

$$f = 1 - \sum_{n=1}^{\infty} \frac{6b^2 \, e^{-\beta_n^2 \tau}}{\beta_n^2 [\beta_n^2 + b(b-1)]} \tag{78}$$

where $$b = \frac{amk_e}{D_i} \tag{79}$$

The β_n's are the roots of

$$\beta_n \cos \beta_n + b-1 = 0 \tag{80}$$

and τ is the dimensionless time:

$$\tau = \frac{D_i t}{a^2} \tag{81}$$

Both Crank and Newman give f for values of τ up to 10. Experimental values of τ here are of the order of 10^{-3}. A short-time approximation to the problem, as derived in Appendix E gives:

$$f = \frac{6}{\sqrt{\pi}} \left(\frac{b}{b-1}\right)^2 \sqrt{\tau} - 3\left(\frac{b}{b-1}\right) \tau - 3\left(\frac{b}{b-1}\right)^2 \left(\frac{1-g}{b-1}\right) \tag{82}$$

where $$g = e^{(b-1)^2 \tau} \operatorname{erfc} [(b-1)\sqrt{\tau}] .$$

(Values of g are tabulated by Carslaw and Jaeger.[99])

For no external resistance (i.e. very large distribution coefficient or external film coefficient) $b \to \infty$, and it can be seen that

$$\lim_{b \to \infty} f = \frac{6}{\sqrt{\pi}} \sqrt{\tau} - 3\tau \tag{83}$$

which is the short-time approximation for stagnant spherical drops with no external resistance, Eq. (69).

Values of f calculated by Eq. (82) have been plotted in Fig. 26. Both b and τ depend on drop diameter, d, and the diffusion coefficient, D_i, inside the drop.

Entering Fig. 26 with experimental values of f_{La} and τ it is possible to determine b. From b and the measured value of the distribution coefficient, m_{La}, the value of the external film coefficient, k_e, has been calculated. The results are given in Table XXVII. Omitting the

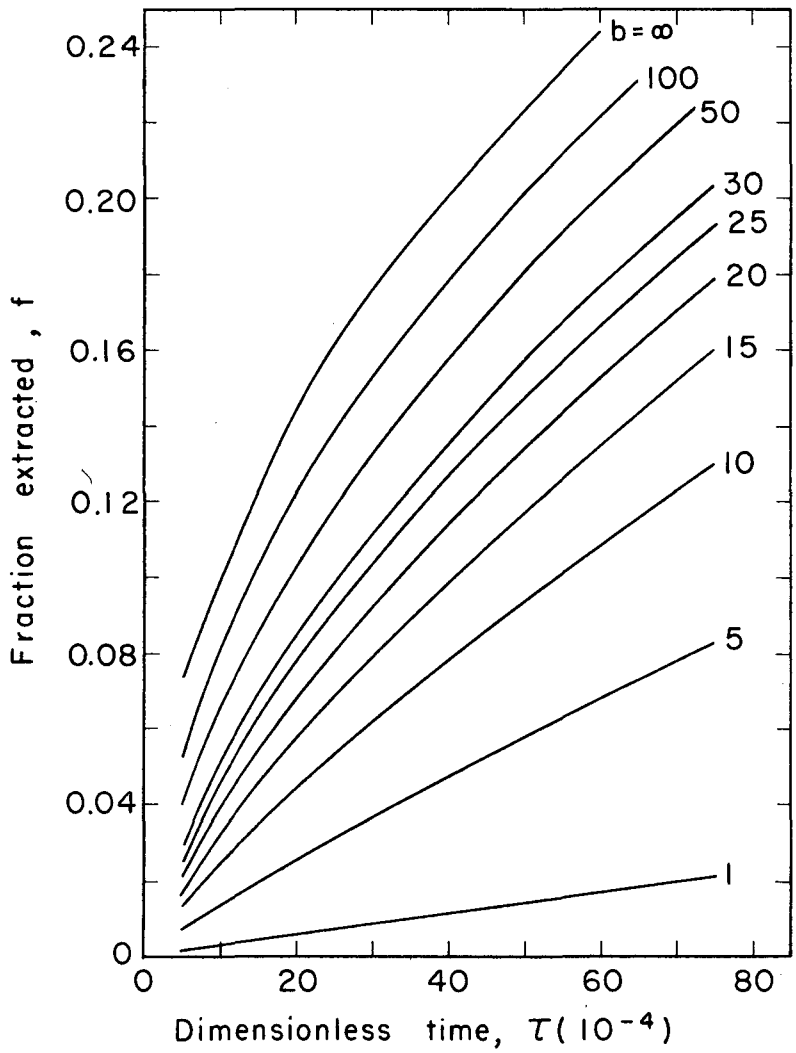
b = ∞
100
50
30
25
20
15
10
5
1
0.24
0.20
0.16
0.12
0.08
0.04
0
0
20
40
60
80
Fraction extracted, f
Dimensionless time, τ(10⁻⁴)
MU-37034

Fig. 26

Table XXVII Analysis for Stagnant Drop with External Resistance

Run no.	Drop diam. d, cm	Time of fall t, sec	Dimensionless time $\tau(10^{-4})$	Fraction extracted f_{La}	b	External film coefficient: Expt'l k_e cm/sec	External film coefficient: Theor.* k_e cm/sec
6	.211	1.374	72.2	.145	13	.045	.19
14	.218	.992	48.8	.148	26	.088	.23
7	.286	.870	24.9	.104	34	.086	.21
15	.299	.880	23.1	.0386	7	.017	.21
8	.324	.996	22.2	.0485	10	.023	.18
9	.353	.996	18.7	.0112	2	.004	.18
16	.367	.902	15.7	.0495	16	.032	.18
10	.370	.911	15.6	.0613	23	.045	.18
17	.410	.910	12.7	.0763	50	.088	.17
11	.411	.980	13.6	.0434	15.5	.026	.17

$$k_e = \frac{2D_i b}{md}, \quad D_i = 5.85\times10^{-5} \text{ cm}^2/\text{sec}$$

$$m_{La} = .161$$

* Higbie, Ref. 91. (See Eq. (70)). $D_e = 14.5\times10^{-5}$ cm^2/sec.

results of run no. 9, the average value of the external coefficient, k_e, is .050±50% cm/sec. This value for k_e is less than the experimental value determined by the two-film (series resistance) analysis (.183±49% cm/sec). It is only one-fourth as large as the average predicted by the Higbie equation.

One possible explanation for the low value of k_e is that there was some surface contamination present on the pellets despite the efforts taken to avoid this. Surface contamination would reduce mass transfer and lead to a low apparent value of the external film coefficient. But such a conclusion depends upon an accurate value for D_i. For a given value of f_{La}, b (and thus k_e) is very sensitive to small changes in D_i. This is especially true at low values of τ. If a value of $D_i = 2.69 \times 10^{-5}$ cm^2/sec is used in the analysis of Fig. 26, the average calculated value of k_e is larger then that predicted by the Higbie equation.

VIII CONCLUSIONS

The rate of transfer of La^{140} and Ba^{140} from the U-Cr eutectic to Mg at 1000°C has been measured by the falling liquid drop technique with the following results:

1. The average value of the overall mass-transfer coefficient for La based on the U-Cr phase, is .00417±30% cm/sec. The average value of the overall mass transfer coefficient for Ba based on the U-Cr phase is .000555±46% cm/sec.

2. The solute extraction data has been treated by the series resistance concept and by a model of diffusion through a stagnant drop with external resistance. The series resistance concept shows that the transfer of La is governed primarily by internal resistance, and that the transfer of Ba is governed primarily by external resistance. The analysis by diffusion through a stagnant drop with external resistance indicates the possibility of residual interface contamination (presumably due to formation of uranium oxide), but this conclusion depends on an accurate knowledge of the internal diffusion coefficient.

3. Drop velocities in the system are about 70 cm/sec for drops of 2-4 mm diameter in size. This value is about 13% higher than predicted by a correlation due to Hu and Kintner for aqueous-organic systems.

The equilibrium distribution of La^{140} and Ba^{140} between the U-Cr eutectic and Mg at 1000°C has been measured with the following results:

4. The distribution coefficient for La^{140} on a concentration basis is 0.16 at 1000°C, that for Ba^{140} is about .0035 at 1000°C. ΔH for La^{140} is 25.6 kcal.

5. Diffusion coefficients in liquid metal systems have been correlated by absolute rate and corresponding states theories.

Appendix A. Determination of Relative Gamma-Ray Abundance

The equipment used to measure gamma radiation consisted of a scintillation detector and a multichannel analyzer with 400 channels.

Samples were counted for a fixed period of time (depending on source strength) at a measured distance from the face of the detector crystal.

The multichannel analyzer sorts out, counts, and assigns pulses to memory channels according to their energy level. This technique is called gamma-ray measurement by pulse height analysis.

The analyzer was calibrated using known sources which emit gamma-rays of known energy. The calibration sources used and the energy of their characteristic photons were,

Nuclide	Energy of γ-photon, Mev
Na^{22}	.511
Cs^{137}	.662
Mn^{54}	.84
Co^{60}	1.17 1.33
La^{140}	1.6

For convenience, the analyzer was adjusted so that the 1.6 Mev peak from La^{140} fell in channel number 160. Thus each channel stored pulses in an energy increment of .01 Mev. The calibration was linear over the range .0 to 1.60 Mev.

When counting a mixture of nuclide sources, the γ-ray spectrum is a composite curve consisting of peaks which represent the various nuclides present. Since the 1.6 Mev La^{140} was at the high-energy end of the spectrum,

the problem of peak distortion due to Compton scattered photons originating at higher energies was minimal. That is, the total absorption peak of the highest γ-ray energy in the mixture should have its base line at zero and therefore all ordinate values on the peak should be directly proportional to emission rate or abundance. Nevertheless, a technique developed by D. F. Covell[105] of the United States Naval Radiological Defense Laboratory for the quantitative determination of radionuclide abundance in a mixture of radionuclides was used to determine the area under the La^{140} gamma-peak.

Covell's analysis is simply a geometrical technique for eliminating the "pedestal" on which a photo-peak stands. Only the approximately gaussian-shaped region of the peak is used to compute its area.

Covell's formula for the area N under the peak is

$$N = a_0 + \sum_{1}^{n} a_i + \sum_{1}^{n} b_i - (n+1/2)(a_n + b_n) \qquad \text{(A-1)}$$

where

a_0 is the number of counts in the peak channel,

a_i is the number of counts in the ith channel on the low amplitude side of the peak,

b_i is the number of counts in the ith channel on the high amplitude side of the peak,

n is the number of channels on either side of the peak channel used in the computation

a_n and b_n are the counts in the nth channel on either side of the peak channel (the last channel used in the computation).

Since all measurements in this study were relative measurements, a fixed value of n = 10 was used in all computations. Since the analyzer calibration was linear, a fixed value of n represents a fixed and constant energy differential.

At the end of each measurement (counting period), the numbers stored in the analyzer memory were transferred to IBM tape, thence to IBM cards on a tape of card converter. Formula (A-1) was computed on a Direct Couple System consisting of an IBM 7040 and an IBM 7094.

Appendix B. Correction for Self-Absorption in Spheres

Abundance of La^{140} in cubically shaped-irradiated U-Cr pellets was determined before extraction. It was necessary to correct the measured value for self-absorption of γ-rays in the pellet. It will be assumed that the shape of a cube approximates that of a sphere. The formulas for computing self-attenuation of γ-rays in various geometries are given in Chapter 5 of Radiation Shielding by Price, Horton and Spinney.[106]

For a spherical sample of radius R, of source strength per unit volume S and negligible self-attenuation, the current j at distance d is

$$j_{unatten} = \frac{\frac{4}{3}\pi R^3 S}{4\pi d^2} = \frac{1}{3}\frac{R^3}{d^2} S \text{ for } d \geq R \qquad \text{(B-1)}$$

The current at a distance d from an attenuating sphere is

$$j = \frac{SR^2}{4\mu d^2}\left[1 - \frac{1}{2R^2\mu^2} + e^{-2R\mu}\left(\frac{1}{R\mu} + \frac{1}{2\mu^2R^2}\right)\right] \text{ for } d \geq R \qquad \text{(B-2)}$$

where μ is the linear attenuation coefficient. It is desired to find the probability of escape f_e from an absorbing sphere of radius R where f_e is defined by Eq. (B-3):

$$f_e = \frac{j}{j_{unatten.}} \qquad \text{(B-3)}$$

then dividing Eq. (B-2) by Eq. (B-1) and letting $\mu R = x$

$$f_e = \frac{j}{j_{unatten}} = \frac{3}{4}\,\frac{1 - \frac{1}{2x^2} + \frac{1}{x}e^{-2x}\left(1 + \frac{1}{2x}\right)}{x} \qquad \text{(B-4)}$$

Since all U-Cr pellets used in this study were very small (2-4 mm), formula (B-4) can be simplified for the case $x \to 0$. This can be done by writing

the exponential in (B-4) as a series and then truncating the series.

$$e^{-2x}\left(1+\frac{1}{2x}\right) = \frac{1}{2x} - x + \frac{4}{3}x^2 - x^3 + \frac{8}{15}x^4 + \ldots. \qquad \text{(B-5)}$$

$$f_e = \frac{3}{4x}\left[\frac{4}{3}x - x^2 + \frac{8}{15}x^3 + \ldots\right] = 1 - \frac{3}{4}x + \frac{2}{5}x^2 + \ldots \qquad \text{(B-6)}$$

$$\lim_{x \to 0} f_e = 1 - \frac{3}{4}x + \frac{2}{5}x^2 \qquad \text{(B-7)}$$

Total mass attenuation coefficients $\left(\frac{\mu}{\rho}, \frac{cm^2}{g}\right)$ are listed in the National Bureau of Standards Circular 583, April 1957. The value for uranium at 1.6 Mev is .053 cm^2/g. A similar value was assumed for chromium. From the density of uranium and chromium, the linear γ-ray attenuation coefficients are calculated to be .995 cm^{-1} for uranium and .36 for chromium. The estimated value for the alloy is $\mu_{U\text{-}Cr} = .963\ cm^{-1}$.

From the room temperature density of the U-Cr eutectic (17.5 g/cc) and the value of $\mu_{U\text{-}Cr}$ just calculated, the parameter $\mu R = x_{U\text{-}Cr}$ can be calculated as a function of pellet weight, $W_{U\text{-}Cr}$.

$$X_{U\text{-}Cr} = .230\ W_{U\text{-}Cr}^{1/3} \qquad \text{(B-8)}$$

Finally the probability of escape, f_e is plotted as a function of pellet weight using Eqs. (B-7) and (B-8).

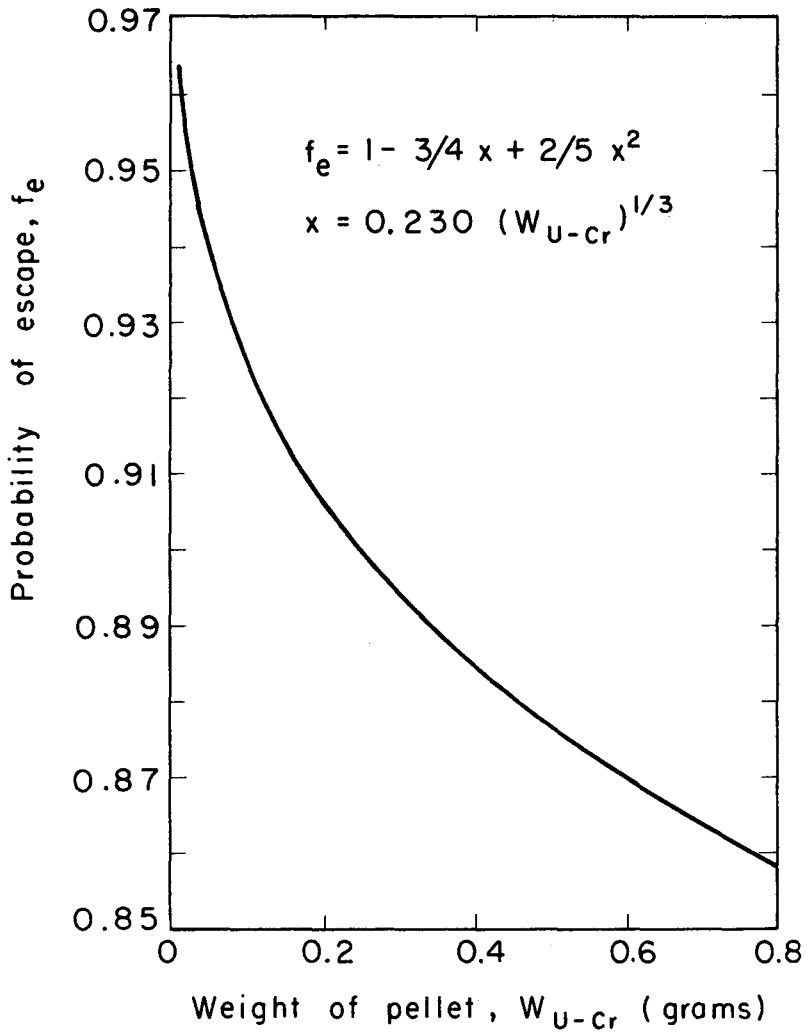
0.97
0.95
0.93
0.91
0.89
0.87
0.85
0
0.2
0.4
0.6
0.8
$f_e = 1 - 3/4\ x + 2/5\ x^2$
$x = 0.230\ (W_{U-Cr})^{1/3}$
Probability of escape, f_e
Weight of pellet, W_{U-Cr} (grams)

MU-36988

Appendix C Correction for an Unshielded Line Source

The Mg ingots measured after the extraction experiments can be considered unshielded line sources.

Price, Horton, and Spinney[106] (p. 225) give for the current j at a distance d from a line source of strength S per unit unit length.

$$j = \frac{S}{4\pi d} (\sin \Psi_1 + \sin \Psi_2) \qquad (C\text{-}1)$$

where Ψ_1 and Ψ_2 are the half-angles subtended by the line source at the point of detection.

If the arrangement is symmetrical so that $\Psi_1 = \Psi_2$

$$j = \frac{S}{4\pi d} (2 \sin \Psi_1) \qquad (C\text{-}2)$$

The total source strength S' is given by Eq. (C-3)

$$S' = SL \qquad (C\text{-}3)$$

where L is the length of the line source. Then

$$S' = j \frac{4\pi dL}{2 \sin \Psi_1} = j \frac{4\pi d^2}{2 \sin \Psi_1} \left(\frac{L}{d}\right) \qquad (C\text{-}4)$$

This can be converted to an equivalent point source by dividing by $4 \pi d^2$. It is seen that the required geometrical correction is

$$\left(\frac{L}{d}\right) \frac{1}{2 \sin \Psi_1} \quad . \qquad (C\text{-}5)$$

For a 20 in. line source 25 in. from the detector, the geometrical correction factor given by formula (C-5) is 1.08.

The total mass attenuation coefficient $\frac{\mu}{\rho}$ of Mg for a 1.6 Mev γ-ray, is .05 cm^2/g.

Multiplying by the density of magnesium gives a linear attenuation coefficient μ of .087. For a 1.43 cm diameter rod, μD = .125.

Figure 5.4.1 on page 228 of Price, Horton, and Spinney[106] shows that the self-attenuation correction for a cylinder is negligible at a value of $\mu D = .125$.

Appendix D Decay of Daughter Activity in a Two-Member Chain Which Approaches Secular Equilibrium

$$Ba^{140} \xrightarrow[\lambda_{Ba}]{} La^{140} \xrightarrow[\lambda_{Ba}]{} Ce^{140} \tag{D-1}$$

The differential equations for the scheme given by Eq. (D-1) are

$$\frac{dN_1}{dt} = -\lambda_1 N_1 \tag{D-2}$$

$$\frac{dN_2}{dt} = \lambda_1 N_1 - \lambda_2 N_2 \tag{D-3}$$

The general solution to this set of equations is well known and is given by Eqs. (D-4) and (D-5).

$$N_1 = N_1^0 e^{-\lambda_1 t} \tag{D-4}$$

$$N_2 = \frac{\lambda_1}{\lambda_2 - \lambda_1} N_1^0 \left(e^{-\lambda_1 t} - e^{-\lambda_2 t} \right) + N_2^0 e^{-\lambda_2 t} \tag{D-5}$$

If $N_2^0 = 0$, $\lambda_2 > \lambda_1$, and if t is sufficiently large, then $e^{-\lambda_2 t} < e^{-\lambda_1 t}$ and Eq. (D-5) becomes

$$N_2 = \frac{\lambda_1}{\lambda_2 - \lambda_1} N_1^0 e^{-\lambda_1 t} \tag{D-6}$$

Substitution of Eq. (D-4) in Eq. (D-6) gives at "secular equilibrium"

$$N_2 = \frac{\lambda_1}{\lambda_2 - \lambda_1} N_1 \tag{D-7}$$

If $\lambda_2 \gg \lambda_1$, then

$$N_2 \lambda_2 = \lambda_1 N_1 \tag{D-8}$$

or

$$a_2 = a_1 \tag{D-9}$$

and the activities of parent and daughter are equal. Equations (D-8) and (D-9) describe a situation known as "secular equilibrium". This

situation arises when the daughter isotope is less stable than the parent.

Equations (D-6) and (D-7) apply to the Ba → La → Ce decay chain. (The decay constant for Ba, λ_1 is smaller than that for La, λ_2; but it is not so small that it can be neglected.) Equation (D-6) shows that at secular equilibrium, La^{140} will decay with an apparent half-life equal to the Ba^{140} half-life. If t = 12.8 days, $e^{-\lambda_2 t}$ is one-hundredth of $e^{-\lambda_1 t}$. Therefore 12.8 days may be considered to be the required cooling time for close approach to secular equilibrium if the initial La^{140} abundance is zero.

Consider the case where N_2^0 has some finite value.

$$\text{Let} \quad N_2^0 = N_1^0 \frac{\lambda_1}{\lambda_2 - \lambda_1} F. \tag{D-10}$$

F, therefore, has been arbitrarily defined as a factor representing the degree of departure from secular equilibrium.

Substitution of Eq. (D-10) in the general Eq. (D-5) gives

$$N_2 = \frac{\lambda_1}{\lambda_2 - \lambda_1} N_1^0 \left[e^{-\lambda_1 t} + (F-1) e^{-\lambda_2 t} \right] . \tag{D-11}$$

Divide Eq. (D-11) by Eq. (D-10)

$$\frac{N_2}{N_2^0} = \frac{a_2}{a_2^0} = \frac{e^{-\lambda_1 t}}{F} + \left(1 - \frac{1}{F}\right) e^{-\lambda_2 t} \tag{D-12}$$

Examination of Eq. (D-12) shows that a plot of $(a_2/a_2^0)e^{\lambda_1 t}$ vs $e^{-(\lambda_2 - \lambda_1)t}$ should be a straight line with an intercept of 1/F. By means of such a plot and Eq. (D-10) the ratio of La^{140} to Ba^{140} present at zero time in any sample may be determined.

In the kinetic experiments, the fraction of La extracted from the U-Cr drop by the Mg is determined by the ratio of La^{140} activity in the

Mg ingot immediately after extraction to the La^{140} activity in the U-Cr pellet just before extraction. If La^{140} activity in the Mg ingot is followed over a period of time and plotted as indicated by Eq. (D-12), then the ratio of La to Ba in the Mg immediately after extraction can be determined from the value of F thus determined and the defining equation (D-10). From the measured fraction of La extracted, f_{La}, and the value of F for the magnesium phase, the fraction of Ba extracted, f_{Ba}, can also be determined if the La to Ba abundance ratio in the original U-Cr pellet is known. The exact relationship for the case where the original pellet is at "secular equilibrium" will be shown.

At secular equilibrium in the U-Cr pellet the La to Ba ratio is given by Eq. (D-7)

$$\left(\frac{N_{La}}{N_{Ba}}\right)_{U\text{-}Cr} = \frac{\lambda_{Ba}}{\lambda_{La}-\lambda_{Ba}} \qquad \text{(D-13)}$$

Suppose that while the pellet falls, fractions f_{La} and f_{Ba} of La and Ba respectively are extracted into the Mg phase. Then

$$\left(\frac{N^{O}_{La}}{N^{O}_{Ba}}\right)_{Mg} = \frac{f_{La}}{f_{Ba}}\left(\frac{N_{La}}{N_{Ba}}\right)_{U\text{-}Cr} = \frac{f_{La}}{f_{Ba}}\frac{\lambda_{Ba}}{\lambda_{La}-\lambda_{Ba}} \qquad \text{(D-14)}$$

Rearranging:

$$\frac{f_{La}}{f_{Ba}} = \left(\frac{N^{O}_{La}}{N^{O}_{Ba}}\right)_{Mg}\frac{\lambda_{La}-\lambda_{Ba}}{\lambda_{Ba}} = F^{Mg}. \qquad \text{(D-15)}$$

Therefore, if the original pellet is at secular equilibrium before extraction, the ratio of the fractions of La and Ba extracted equals F for the Mg ingot.

How long must a pellet be cooled to allow the attainment of "secular equilibrium"? For batch decay ($N^{O}_{La} = 0$) the calculation is very simple

and shows that 12.8 days is a sufficient cooling period. For a sample of irradiated uranium, the problem is complicated by the fact that some decay occurs during the irradiation period. The solution to the problem is well known and is given by Benedict and Pigford.[107]

The abundance of the first and second nuclides in a decay-chain as a function of irradiation time T, cooling time t, and some arbitrary production rate P are given by Eqs. (D-16) and (D-17) respectively.

$$N_1(T,t) = \frac{P}{\lambda_1}\left(1 - e^{-\lambda_1 T}\right) e^{-\lambda_1 T} \qquad \text{(D-16)}$$

$$N_2(T,t) = \lambda_1 P \left[\frac{\left(1-e^{-\lambda_1 T}\right)e^{-\lambda_1 t}}{\lambda_1(\lambda_2-\lambda_1)} + \frac{\left(1-e^{-\lambda_2 T}\right)e^{-\lambda_2 t}}{\lambda_2(\lambda_1-\lambda_2)}\right] \qquad \text{(D-17)}$$

For the purposes of this study only the ratio of the two nuclides as a function of irradiation and cooling times is needed in order to calculate the cooling time required to approach the ratio at "secular equilibrium".

Dividing Eq. (D-17) by Eq. (D-16) and simplifying

$$\frac{N_2(T,t)}{N_1(T,t)} = \frac{\lambda_1}{\lambda_2-\lambda_1}\left[1 - B(T)e^{-(\lambda_2-\lambda_1)t}\right] \qquad \text{(D-18)}$$

where

$$B(T) = \frac{\lambda_1}{\lambda_2}\left[\frac{1-e^{-\lambda_2 T}}{1-e^{-\lambda_1 T}}\right] \qquad \text{(D-19)}$$

B(T) is a function only or irradiation time. For T = 48 hours, B(T) = 0.719 for the $Ba^{140} \rightarrow La^{140}$ system. Examination of Eq. (D-18) shows that secular equilibrium is reached when $B(T)e^{-(\lambda_2-\lambda_1)t} = 0$, and that a nuclide abundance ratio only 1% from secular equilibrium is given by

Eq. (D-20)

$$B(T)\, e^{-(\lambda_2-\lambda_1)t} = 0.01 \qquad \text{(D-20)}$$

for B(T) = .719 (T = 48 hours) Eq. (D-20) is solved to find t = 285 hours = 11.9 days. Thus a sample of uranium which has been irradiated for 2 days must be cooled for 11.9 days to allow the La to Ba ratio to approach within 1% of the ratio at secular equilibrium.

All irradiated samples were cooled for about two weeks to allow the γ-ray intensity to decrease to the point where direct handling was convenient. All samples had, therefore, reached secular equilibrium before extraction.

Appendix E Diffusion from Stagnant Drop with External Resistance - Short-Time Approximation

The following is an outline of Olander's derivation of the short-time approximation to the solution of the problem of diffusion through a stagnant drop with external resistance (Eq. (82)):

Let $c(r,t)$ = fraction of original concentration

i.e. $c(r,0) = 1$ (initial concentration equals 1)

Assume that the external coefficient is constant despite the changing surface concentration. Assume a stagnant drop.

The diffusion equation in spherical coordinates is

$$\frac{\partial c}{\partial t} = D\left(\frac{\partial^2 c}{\partial r^2} + \frac{2}{r}\frac{\partial c}{\partial r}\right) \tag{E-1}$$

The initial condition is $c(r,0) = 1$ (E-2)

The boundary conditions are $c(0,t) =$ finite (E-3)

$$-D\left(\frac{\partial c}{\partial r}\right)_a = mk_e c(a,t) \tag{E-4}$$

a = drop radius

[if $mk_e \to \infty$, boundary condition (E-4) becomes

$$c(a,t) = 0. \ ]$$

Let

$$\eta = r/a \tag{E-5}$$

$$\tau = \frac{Dt}{a^2} = 4\frac{Dt}{d^2} \tag{E-6}$$

$$b = \frac{mk_e a}{D} \tag{E-7}$$

then (E-1) becomes:

$$\frac{\partial c}{\partial \tau} = \frac{\partial^2 c}{\partial \eta^2} + \frac{2}{\eta}\frac{\partial c}{\partial \eta} \tag{E-8}$$

with initial conditions $c(\eta,0) = 1$ (E-9)

and boundary conditions $c(0,\tau) = \text{finite}$ (E-10)

and $$\left(\frac{\partial c}{\partial \eta}\right)_1 + bc\,(1,\tau) = 0 \tag{E-11}$$

Take Laplace transform (p = transform variable, $q = \sqrt{p}$)

$$\frac{d^2\tilde{c}}{d\eta^2} + \frac{2}{\eta}\,\frac{d\tilde{c}}{d\eta} = p\tilde{c} - 1 \tag{E-12}$$

or

$$\frac{d^2}{d\eta^2}\left(\eta\tilde{c}\right) - q^2\left(\eta\tilde{c}\right) = -\eta \tag{E-13}$$

with boundary conditions $\tilde{c}(0) = \text{finite}$ (E-14)

and

$$\left(\frac{d\tilde{c}}{d\eta}\right)_1 + b\tilde{c}(1) = 0 \tag{E-15}$$

The general solution of (E-13) is given by Carslaw and Jaeger[99] (p. 348) and is,

$$\eta\tilde{c} = A \sinh q\eta + B \cosh q\eta + \frac{\eta}{p} \tag{E-16}$$

But, to satisfy (E-14), $B = 0$

$$\tilde{c}(\eta) = \frac{1}{p} + \frac{A \sinh q\eta}{\eta} \tag{E-17}$$

$$\frac{d\tilde{c}}{d\eta} = A\left\{\frac{q\eta \cosh q\eta - \sinh q\eta}{\eta^2}\right\} \tag{E-18}$$

Substituting (E-17) and (E-18) into (E-15) with $\eta = 1$

$$A = -\frac{b/p}{(b-1)\sinh q + q\cosh q} \tag{E-19}$$

(E-17) becomes

$$\tilde{c}(\eta) = \frac{1}{p} - \left[\frac{b/p}{(b-1)\sinh q + q\cosh q}\right]\frac{\sinh q\eta}{\eta} \qquad \text{(E-20)}$$

$$c_{AV} = \frac{1}{\frac{4}{3}\pi a^3}\int_0^a 4\pi r^2 c(r,\tau)dr = 3\int_0^1 \eta^2\, c(\eta,\tau)\, d\eta \qquad \text{(E-21)}$$

Take the Laplace transform of (E-21):

$$\tilde{c}_{AV} = 3\int_0^1 \eta^2\, \tilde{c}(\eta)\, d\eta \qquad \text{(E-22)}$$

Insert (E-20) into (E-21) and integrate

$$\tilde{c}_{AV} = \frac{1}{p} - \frac{3}{p}\left[\frac{b/p}{(b-1)\sinh q + q\cosh q}\right](q\cosh q - \sinh q) \qquad \text{(E-23)}$$

or

$$\tilde{c}_{AV} = \frac{1}{p} - \frac{3b}{p^2}\left[\frac{q(1+\epsilon) - 1}{q(1+\epsilon) + h}\right] \quad \text{where} \quad \begin{cases} 1+\epsilon = \dfrac{\cosh q}{\sinh q} \\ q = \sqrt{p} \\ h = b-1 \end{cases} \qquad \text{(E-24)}$$

Short time (small τ) corresponds to large values of q (or p). Express hyperbolic functions as exponentials and use expansion in terms of powers of e^{-q}.

$$\epsilon = \frac{\cosh q}{\sinh q} - 1 = \frac{e^q + e^{-q}}{e^q - e^{-q}} - 1 = \frac{1+e^{-2q}}{1-e^{-2q}} - 1$$

$$= 2(e^{-2q} + e^{-4q} + \ldots) \qquad \text{(E-25)}$$

If q is sufficiently large to neglect all exponential terms, then $\epsilon = 0$ and

$$\tilde{c}_{AV} = \frac{1}{p} - \frac{3b}{p^2}\left(\frac{q-1}{q+h}\right), \text{ or since } p^2 = q^4$$

$$\tilde{c}_{AV} = \frac{1}{p} - 3b \left[\frac{1}{q^3(q+h)} - \frac{1}{q^4(q+h)} \right]$$

since $\frac{1}{q^4(q+h)} = \frac{1}{h}\left[\frac{1}{q^4} - \frac{1}{q^3(q+h)}\right]$,

$$\tilde{c}_{AV} = \frac{1}{p} - 3b \left[\frac{1}{q^3(q+h)} - \frac{1}{hq^4} + \frac{1}{hq^3(q+h)} \right]$$

$$\tilde{c}_{AV} = \frac{1}{p} - 3b \left[\frac{h+1}{hq^3(q+h)} - \frac{1}{hq^4} \right]$$

since $h = b-1$

$$\tilde{c}_{AV} = \frac{1}{p} - 3\left(\frac{b}{b-1}\right)\left[\frac{b}{q^3(q+h)} - \frac{1}{q^4} \right] \qquad \text{(E-26)}$$

The terms in brackets may be inverted term-by-term using the Bateman Tables, Vol. I., p. 233.

The inverse of $\frac{1}{q^4}$ is τ.

The inverse of $\frac{h^2}{q^3(q+h)}$ is $\left[\frac{2}{\sqrt{\pi}} h \sqrt{\tau} - (1-g) \right]$

where $g = e^{(b-1)^2\tau} \operatorname{erfc}\left[(b-1)\sqrt{\tau}\right]$

and values of g as a function of $e^{x^2} \operatorname{erfc} x$ are given by Carslaw and Jaeger on p. 488.

$$b = \frac{b}{h^2} h^2 = \frac{b}{(b-1)^2} h^2$$

Therefore, the inverse of $\frac{b}{q^3(q+h)}$ is $\frac{b}{(b-1)^2}\left[\frac{2}{\sqrt{\pi}} h \sqrt{\tau} - (1-g) \right]$

$$\text{or} \quad \frac{b}{b-1}\,\frac{2}{\sqrt{\pi}} - \frac{b}{b-1}\,\frac{1-g}{b-1}$$

Substituting the inverted terms in (E-26):

$$c_{AV} = 1-3\left[\left(\frac{b}{b-1}\right)^2 \frac{2}{\sqrt{\pi}}\,\sqrt{\tau} - 3\left(\frac{b}{b-1}\right)\tau - \left(\frac{b}{b-1}\right)^2\left(\frac{1-g}{b-1}\right)\right]$$

The fraction extracted f, is defined as

$$f = 1 - c_{AV}$$

Therefore,

$$f = \frac{6}{\sqrt{\pi}}\left(\frac{b}{b-1}\right)^2 \sqrt{\tau} - 3\left(\frac{b}{b-1}\right)\tau - 3\left(\frac{b}{b-1}\right)^2\left(\frac{1-g}{b-1}\right), \qquad \text{(E-27)}$$

which is Eq. (82) in the text.

$$\lim_{b \to \infty} f = \frac{6}{\sqrt{\tau}} - 3\,\tau$$

$$\lim_{(b-1)\sqrt{\tau} \to 0} f = 3b\left[\tau - \frac{4}{3\sqrt{\pi}}\, b\, \tau^{3/2}\right] .$$

Appendix F Estimation of Distribution Coefficients

In very dilute solutions, all solutes may be expected to follow Henry's law: the activity of solute 1 in phase A is proportional to its mole fraction in that phase

$$a_1^A = k_1^A x_1^A \tag{F-1}$$

where k_1^A is the Henry's law constant of substance 1 in phase A. In dilute solutions, the constant of proportionality may be considered independent of composition. The constant may be identified with the activity coefficient, γ.

$$a_1^A = \gamma_1^A x_1^A \tag{F-2}$$

If solute 1 is distributed between two phases, A and B, at equilibrium its activity is the same in both phases:

$$a_1^A = a_1^B \tag{F-3}$$

or

$$\gamma_1^A x_1^A = \gamma_1^B x_1^B \tag{F-4}$$

It is desired to estimate the distribution coefficient on a mole fraction basis K^x. K^x is defined as the ratio of the mole fractions of the solute in the two phases at equilibrium and is defined by Eq. (F-5).

$$K_1^x = \frac{x_1^B}{x_1^A} \tag{F-5}$$

From Eq. (F-4) it follows that

$$K_1^x = \frac{\gamma_1^A}{\gamma_1^B} \tag{F-6}$$

Thus, in dilute solutions, the distribution coefficient on a mole fraction

basis is simply the ratio of the activity coefficients, and the activity coefficients can be considered independent of concentration.

In the following, the activity coefficients of rare earth solutes in uranium and the uranium-chromium alloy will be estimated from the solubility data of Haefling and Daane[95] and Voigt.[66] Activity coefficients of these solutes in magnesium will be estimated by means of the Hildebrand regular solution theory.

Activity Coefficients in U and U-Cr

If two pure liquids which are essentially immiscible are equilibrated then the activity of each liquid in its rich phase may be considered unity. Its activity in the phase in which it is dilute is also unity by Eq. (F-3), and its activity coefficient in that phase is simply the reciprocal of its mole fraction.

$$\gamma_B^A = \frac{1}{x_B^A} \quad (\text{if } x_B^B \sim 1) \qquad \text{(F-7)}$$

Haefling and Daane[95] have reported solubilities of Ce and La (as well as some other rare earths) in U over a temperature range of 1150°C to 1225°C. These solubilities have been converted to mole fractions and the activity coefficients calculated by Eq. (F-7). In regular solution theory $\ell n\ \gamma \propto 1/T$. Therefore these measured values of γ have been extrapolated to 900°C by plotting γ vs $1/T$ on semi-log paper to determine the activity coefficients in super-cooled uranium. The results are given in Tables F-I and F-II.

Voigt[66] reported the solubility of Ce in the U-Cr eutectic at 970°C to be 1.5 w-% which is equivalent to 0.0215 a-%. The activity coefficient, $\gamma_{Ce}^{U\text{-}Cr}$, at 970°C by Eq. (F-7) is 46.5. The activity coefficient for Ce in pure U at 970°C was estimated to be 90. (See Table F-I.) Thus the

Table F-I Activity coefficients of cerium in uranium

T(°C)	T(°K)	$\frac{1}{T}(10^{-3}°K^{-1})$	Solubility w-% Ce	Solubility a-% Ce	Activity coefficient of cerium in uranium γ_{Ce}^{U}
1250	1523	.656	1.5*	.0252	39.7
1150	1423	.702	1.16*	.0196	51.1
1100	1373	.728			59 ‡
1000	1273	.785			81 ‡
900	1173	.852			117 ‡

* Haefling and Daane, Ref. 95

‡ Extrapolated values

Table F-II Activity coefficients of lanthanum in uranium

T(°C)	T(°K)	$\frac{1}{T}(10^{-3}°K^{-1})$	Solubility w-% La	Solubility a-% La	Activity coefficient lanthanum in uranium γ_{La}^{U}
1225	1498	.668	0.84*	.0143	69.8
1150	1423	.702	0.77*	.0131	76.0
1100	1373	.728			81 ‡
1000	1273	.785			94 ‡
900	1173	.852			112 ‡

* Haefling and Daane, Ref. 95

‡ Extrapolated values

activity coefficients of Ce in U-Cr are estimated to be 51.6% as large as those of Ce in pure U.

Table F-III Activity Coefficient of Cerium in Uranium-Chromium Eutectic

T(°C)	T(°K)	$\frac{1}{T}(10^{-3}°K^{-1})$	Solubility w-% Ce	Solubility a-% Ce	Activity Coef. of Ce in U-Cr γ_{La}^{U-Cr}
970	1243	.804	1.5*	.0215	46.5

*Voigt, Ref. 66

Activity coefficients for La in the U-Cr eutectic are assumed to be 51.6% of those for La in U. This is equivalent to assuming that the addition of chromium to uranium increases the solubility of the two rare earths by the same fraction over their solubility in pure uranium but does not change the temperature coefficient of solubility which is assumed to be the same as in pure uranium.

The extrapolated and estimated values of activity coefficients for Ce in U, La in U, and La in U-Cr are summarized in Table F-IV.

Activity Coefficients in Mg

Activity coefficients of La and Ce in Mg have been estimated using the regular solution theories of Hildebrand.[109]

The activity coefficient is given by Eq. (F-8)

$$\ln \gamma_2 = \frac{a_{12} V_2}{RT} \phi_1^2 \qquad \text{(F-8)}$$

Table F-IV Summary of extrapolated and estimated activity coefficients for Ce in U, La in U, and La in U-Cr

T(°C)	T(°K)	$\frac{1}{T}(10^{-3}°K^{-1})$	Activity Coefficients		
			Ce in U γ_{Ce}^{U}	La in U γ_{La}^{U}	La in U-Cr $\gamma_{La}^{U\text{-}Cr}$
1250	1523	.650	39.7		
1225	1498	.668		69.8	36§
1150	1423	.702	51.1	76.0	39§
1100	1373	.728	59‡	81‡	42§
1000	1273	.785	81‡	94‡	48§
900	1173	.852	117‡	112‡	58§

‡ Extrapolated

§ Estimated

where V_2 is the molar volume of the solute, ϕ_1 is the volume fraction of the solvent and a_{12} is a parameter expressing the deviation from ideal-solution behavior. (The parameter a_{12} is always positive in regular solutions; there are some cases for liquid metals where it is negative.) The parameter a_{12} is estimated from pure component thermodynamic data as follows:

$$a_{12} = |\delta_1 - \delta_2|^2 \qquad (F\text{-}9)$$

where δ is the Hildebrand solubility parameter.

$$\delta = \left(\frac{\Delta E^V}{V}\right)^{1/2} = \left[\frac{\Delta H^V - RT}{V}\right]^{1/2} \qquad (F\text{-}10)$$

where ΔE^V and ΔH^V are the energy and heat of vaporization for the pure components.

Pitzer and Brewer[112] have shown how regular solution theory may be applied to liquid metals to predict mutual solubilities in immiscible systems.

As a first approximation, one can assume that if the mutual solubility is small, the activities of the metals are not appreciably reduced from unity. Then the solubilities are given by the reciprocal of the activity coefficients as in Eq. (F-7). Activity coefficients are calculated by Eq. (F-8).

Silver and chromium form one such immiscible pair. From the data given by Pitzer and Brewer, the solubility parameter for silver is $75.1 \left(\frac{\text{cals}}{\text{cc}}\right)^{1/2}$, that for chromium is 108.5, and the parameter a_{12}, given by Eq. (F-9) is 1115 cals/cc. The activity coefficient for chromium in silver (assuming that the volume fraction of silver is unity) is 10.8 giving 9.25 a-% Cr and 90.75 a-% Ag for the composition of the silver-rich phase. The calculated activity coefficient for very dilute silver in chromium is 29.2 giving 3.4 a-% Ag and 96.6 a-% Cr for the composition of the chromium rich phase. The reported saturated compositions are 3.4 a-% and 85 a-% Ag.

In a series of successive trials, the compositions calculated in a previous trial may be used to calculate volume fractions, activity coefficients, and activities in the following trial. For the Ag-Cr system, three trials give for the calculated saturated composition 4.6 a-% and 86.6 a-% Ag.

The solubility parameters for Ce, La, and Mg at 1000°C have been calculated using heat of vaporization data from Stull and Sinke.[112] They are listed in Table F-V. Density values for the rare earths are taken from Mound Lab Report MLM-1118.[104]

Table F-V Solubility parameters at 1000°C

Metal	Density ρ, g/cc	Heat of vaporization ΔH^V cal/g-mole	RT cal/g-mole	Energy of vaporization ΔE^V	Molar volume V cc/c-mole	Solubility parameters $\delta\left(\text{cals/cc}\right)^{1/2}$
Mg	1.50	~ 31,200	2500	28,700	16.2	42.0
Ce	6.64	~ 75,000	2500	72,500	21.1	58.5
La	5.94	96,200	2500	93,700	23.4	63.3

The values of the parameter a_{12} are given by Eq. (F-8) and are 272 cals/cc for Ce-Mg and 454 cals/cc for La-Mg.

Values of the activity coefficients for Ce in Mg and La in Mg in very dilute solutions are given by Eq. (F-7) with $\phi = 1$. These values are listed in Table F-VI.

Table F-VI Activity Coefficients for Cerium and Lanthanum in Magnesium

T(°C)	T(°K)	$\frac{1}{T}(10^{-3}°K^{-1})$	Activity Coefficients	
			Ce in Mg γ_{Ce}^{Mg}	La in Mg γ_{La}^{Mg}
1150	1423	.702	7.6	43.5
1100	1373	.728	8.2	50
1000	1273	.785	9.7	67
900	1173	.852	11.8	94

$$|\delta_{Ce}-\delta_{Mg}|^2 = 272 \frac{cals}{cc}$$

$$|\delta_{La}-\delta_{Mg}|^2 = 454 \frac{cals}{cc}$$

The distribution coefficients on a mole fraction basis, K^x, may now be calculated for the three systems using Eq. (F-6) and the values of activity coefficients given in Tables F-IV and F-VI. Calculated distribution coefficients are given in Table F-VII.

Table F-VII Calculated Distribution Coefficients

T(°C)	T(°K)	$\frac{1}{T}\left(10^{-3}\,°K^{-1}\right)$	System: Ce between U and Mg $K^x = \frac{\gamma_{Ce}^{U}}{\gamma_{Ce}^{Mg}}$	System: La between U and Mg $K^x = \frac{\gamma_{La}^{U}}{\gamma_{La}^{Mg}}$	System: La between U-Cr and Mg $K^x = \frac{\gamma_{La}^{U\text{-}Cr}}{\gamma_{La}^{Mg}}$
1150	1423	.702	$\frac{51.1}{7.2} = 7.1$	$\frac{76.0}{43.5} = 1.75$	$\frac{39}{43.5} = .90$
1100	1373	.728	$\frac{59}{8.2} = 7.2$	$\frac{81}{50} = 1.62$	$\frac{42}{50} = .84$
1000	1273	.785	$\frac{81}{9.7} = 8.4$	$\frac{94}{67} = 1.40$	$\frac{48}{67} = .72$
900	1173	.852	$\frac{117}{11.8} = 9.9$	$\frac{112}{94} = 1.19$	$\frac{58}{94} = .62$

ACKNOWLEDGEMENTS

This work was supported in part by the United States Atomic Energy Commission through the Lawrence Radiation Laboratory.

I would like to acknowledge and express my appreciation for the generous, patient, and invaluable guidance of Professor Donald R. Olander, of the Nuclear Engineering Department of the University of California, Berkeley, who directed this work.

I am indebted to Mrs. Pat Cookson for her quick and accurate help in the preparation of the rough and final drafts of this thesis.

I wish to thank Mohan Rajan whose survey of the literature on drop velocity and drop extraction was of great help.

NOMENCLATURE

a	radius of drop or molecule, cm
a	activity (radioactivity), events per unit time
a	chemical activity
a_{12}	$\lvert\delta_1 - \delta_2\rvert^2$ cals/cc
a_S	drop surface to volume ratio, cm^{-1}
b	ratio of atomic diameter to interatomic distance
b	parameter $= \frac{a\ m\ k_e}{D_i}$
C_D	drag coefficient $= \frac{4}{3}\ \frac{\Delta\rho}{\rho_e}\ \frac{dg}{U_T^2}$
d	drop diameter, cm
D	diffusion coefficient, cm^2/sec
ΔE	energy change, cal/mole
ΔF^*	free energy of activation, cal/mole
f	fraction of the total free energy of activation due to the bond breaking or kinetic component
F	factor representing departure of lanthanum to barium abundance ratio at an arbitrary zero time from the ratio at secular equilibrium (Eq. (3))
f	fraction of solute extracted
ΔH	enthalpy change, cal/mole
ΔH^*	enthalpy of activation, cal/mole
K	overall mass transfer coefficient based on drop phase, cm/sec
K^x	distribution coefficient, mole fraction basis
k	film transfer coefficient, cm/sec
k_v	ratio of actual interfacial speed to the potential flow interfacial speed.
M	molecular weight, gms/mole

m	atomic mass, gms
m	distribution coefficient, concentration basis
N	number of atoms
P	physical property group $= \frac{\rho_e}{\Delta\rho} \cdot \frac{\rho_e \sigma_i^3}{g \mu^4}$
Pe	Peclet number = Re Sc
r^*	distance coordinate of the intermolecular potential function minimum
r^*_{ii}	distance coordinate of the intermolecular potential function minimum between like molecules
r^*_{ij}	distance coordinate of the intermolecular potential function minimum between unlike molecules
r^*_i	average composition dependent interaction constant
Re	Reynold's number $= \frac{dU\rho_e}{\mu}$
ΔS^*	entropy of activation, cals/mol-deg
Sc	Schmidt number $= \frac{\mu_e}{\rho_e D_e}$
Sh	Sherwood number $= \frac{dk_e}{D_e}$
T	absolute temperature, °K
t	time (cooling time, contact time, etc.)
$t_{1/2}$	radioactive half-life (units of time)
U	drop velocity, cm/sec
U_T	drop terminal velocity, cm/sec
V	molar volume, cc/mole
We	Weber number $= \frac{U^2 \rho_e d}{\sigma_i g}$
Y	$\left(\frac{D\mu}{T}\right)\left(\frac{\xi}{k}\right)\left(\frac{V}{N_{AV}}\right)^{1/3}$
x_i	mole fraction of component i
z	coordination number

GREEK LETTERS

γ activity coefficient

γ liquid configuration constant = 4/3

δ parameter Eq. (29)

δ molecular parameter, Eq. (54)

δ solubility parameter, $\left(\frac{\text{cals}}{\text{cc}}\right)^{1/2}$

ϵ^* energy coordinate of the intermolecular potential function minimum

ϵ^*_{ii} energy coordinate of the intermolecular potential function minimum between like molecules

ϵ^*_{ij} energy coordinate of the intermolecular potential function minimum between unlike molecules

ϵ^*_i average, composition dependent interaction constant

θ molecular parameter, Eq. (53)

κ reducing factor for diffusion, cm^2/sec, Eq. (35)

λ radioactive decay constant (sec^{-1})

μ viscosity (poise)

ξ parameter in diffusion correlation

ρ molecular parameter, Eq. (55)

ρ density, gm/cc

$\Delta\rho$ density difference between drop and continuous phase, g/cc

σ lattice parameter, number of closest neighbors

σ surface tension, dynes/cm

σ_i interfacial tension, dynes/cm

τ lattice parameter, number of closest neighbors in one layer

τ dimensionless time = $\frac{4D_i t}{d^2}$

ϕ volume fraction

SUBSCRIPTS

AA	interaction between solvent molecules
AS	interaction between solvent and solute molecules
Ba	barium
D	mutual diffusion in a binary system
d	drop phase
e	external (extractant) phase
i	internal (drop) phase
La	lanthanum
μ	viscosity or self-diffusion in pure solution
1	precursor isotope in radioactive decay chain
2	daughter isotope in radioactive decay chain

SUPERSCRIPTS

0	zero time
~	reduced variable
v	vaporization

CONSTANTS

g	gravitational constant = 980.665 cm/sec^2
h	Planck's constant = 6.6252×10^{-27} erg-sec
N_{Av}	Avogadro's number = 6.0232×10^{23} $mole^{-1}$
R	gas constant = 1.98726 cal/deg-mole

MISCELLANEOUS

a-%	atomic percent
w-%	weight percent
D.F.	decontamination factor

REFERENCES

1. Roberts-Austen, W. C., Phil. Trans. Roy. Soc. Ser A. 187, 400 (1896).
2. Turman, N. H., and W. C. Cooper, J. Am. Chem. Soc., 72, 5667 (1950).
3. Cooper, W. C., and N. H. Turman, J. Am. Chem. Soc., 14, 6183 (1952).
4. Stackelberg, M., and V. Toome, Z. Elecktrô., 58, 726 (1954).
5. Olander, D. R., J.A.I.Ch.E., 9, 207 (1963).
6. Glasstone, S., K. J. Laidler, and H. Eyring, The Theory of Rate Processes, (McGraw-Hill Publishing Co., New York, 1941).
7. Ree, F. H., T. Ree, and H. Eyring, Ind. Eng. Chem., 50, 1036 (1958).
8. Thomaes, G., and J. Van Itterbeek, J. Mol. Phys. 2, 372 (1959).
9. Li, J. C., and P. Chang, J. Chem. Phys., 23, 518 (1955).
10. Walls, H. A., and W. R. Upthegrove, Acta Met., 12, 461 (1964).
11. Glasstone, S., K. J. Laidler, and H. Eyring, The Theory of Rate Processes, (McGraw-Hill Publishing Company, New York, 1941) p. 515.
12. Pauling, L., Nature of the Chemical Bond, (Cornell University Press, Ithaca, New York, 1960) p. 514.
13. The Physical Chemistry of Metallic Solutions and Intermetallic Compounds, Symposium held at the National Physical Laboratory, Teddington, Middlesex, England (1960)p. 54.
14. Niwa, K., M. Shimoji, S. Kado, Y. Watanabe, and T. Yokokawa, Trans. AIME, 209, 96 (1957).
15. Gebhardt, E., M. Becker, H. Sebastian, Z. Metallk. 46, 669-672 (1955).
16. Gebhardt, E., K. Kostlin, Z. Metallk. 48, 601 (1957).
17. Gebhardt, E., and K. Kostlin, Z. Metallk. 48, 636-641 (1957).
18. Bienas, A., and F. Sauerwald, Z. anorg. Chem. 161, 51 (1957).
19. Gebhardt, E., and G. Wörwag, Z. Metallk 42, 358 (1951).

20. Gebhardt, E., M. Becker and E. Trägner, Z. Metallk, 46, 90 (1955).

21. Liquid-Metals Handbook, U.S. Bureau of Naval Research, p. 40.

22. Leak, V. G., and R. A. Swalin, Trans. AIME, 230, 426 (1964).

23. Swalin, R. A., and V. G. Leak, Acta Met., 13, 471 (1965).

24. Culpin, M. F., Proc. Phys. Soc. Lond. B70, 1069 (1957).

25. Diffusion, W. Jost (Academic Press, Inc., New York, 1960) p. 479.

26. Gebhardt, E., M. Becker, and S. Dormer, Z. Metallk. 44, 510 (1953).

27. Gebhardt, E., M. Becker, and H. Sebastian, Z. Metallk. 46, 669-672 (1955).

28. Careri, G., A. Paoletti, and M. Vincentini, Il Nuovo Cimento 10, 1088 (1958).

29. Morgan, D. W., and J. Kitchener, Trans. Faraday Soc., 50, 51 (1954).

30. Physical Chemistry, Moelwyn-Hughes, (Pergamon Press, 2nd. edition, 1961) p. 715.

31. Metals Reference Book, C. J. Smithells, Vol. II (Butterworths, Washington, D.C. 1962) p. 600.

32. "Structure and Properties of Liquid Metals", A. M. Samarin, AEC-tr-4879, p. 129.

33. Turner, R. C., and C. A. Winkler, Can. J. Chem. 29, 469 (1951).

34. Weischedel, F., Z. Physik 85, 29 (1933).

35. Gebhardt, E., and K. Detering, Z. Metallk. 50, 379 (1959).

36. Cahill, J. A., and A. V. Grosse, J. Phys. Chem. 69, 518 (1965).

37. Meyer, R. E., and N. H. Nachtrieb, J. Chem. Phys., 23, 1851 (1955).

38. Meyer, R. E., J. Phys. Chem., 65, 567 (1961).

39. Mirshamsi, M., reported by Walls and Upthegrove, Ref. (10).

40. Swalin, R. A., Acta Met., 7, 736 (1959).

41. Ma, C. H., and R. A. Swalin, J. Chem. Phys., 36, 3014 (1962).

42. Rothman, S. T., and L. D. Hall, J. Metals 8, 199 (1956).

43. Lodding, V. A., Z. fur Naturforschung, 11A, 200 (1956).

44. Henderson, J., and L. Yang, Trans. AIME, 221, 72 (1961).

45. Yang, L., S. Kado, and G. Derge, Trans. AIME, 212, 628 (1958).

46. Petit, J., and N. H. Nachtrieb, J. Chem. Phys., 24, 1027 (1956).

47. Lange, W., W. Pippel and F. Bendel, Z. Physik Chem., 212, 238 (1959).

48. Hammett, L. P., Introduction to the Study of Physical Chemistry, (McGraw-Hill Book Company, New York, 1952) p. 409.

49. Thomaes, G., and J. Van Itterbeek, J. Mol. Phys., 2, 372 (1959).

50. Helfand, E., and S. A. Rice, J. Chem. Phys., 32, 1642 (1960).

51. Naghizadeh, J., and S. A. Rice, J. Chem. Phys., 36, 2710 (1962).

52. Chapman, T. W., "The Viscosity of Liquid Metals", University of California, Lawrence Radiation Laboratory Report 11930, February 1965.

53. Kirkwood, J. G., J. Chem. Phys., 14, 180 (1946).

54. Born, M., and H. S. Green, A General Kinetic Theory of Liquids, (University Press, Cambridge, 1949).

55. Ling, R. C., J. Chem. Phys. 25, 609 (1956).

56. Prigogine, I., The Molecular Theory of Solutions, (North-Holland Publishing Company, Amsterdam, 1957) p. 185.

57. Oriani, R. A., "Thermodynamics and Models of Metallic Solutions", in The Physical Chemistry of Metallic Solutions and Intermetallic Compounds, Vol. I, (Chemical Publishing Company, Inc., 1960) p. 152.

58. Hultgren, R., R. L. Orr, P. D. Anderson, and K. K. Kelley, Selected Values of Thermodynamic Properties of Metals and Alloys, (John Wiley and Sons, Inc., New York, 1963).

59. Oriani, R. A., Acta Met., 4, 15 (1956).

60. Shimoji, M., and K. Niwa, Acta Met., 5, 496 (1957).

61. Motta, E. E., Proc. Intl. Conf. on Peaceful Uses of Atomic Energy, Geneva, 9, 596 (1955).

62. Voigt, A. F., et al., Jl. AICHE, 2, 169 (1956).

63. Baker, R. D., and J. A. Leary, Proc. Intl. Conf. on Peaceful Uses of Atomic Energy, Geneva, 17, 356 (1958).

64. Howe, J. P., Proc. Intl. Conf. on Peaceful Uses of Atomic Energy, Geneva, 9, 179 (1955).

65. Fisher, R. W., and C. B. Fullhart, Proc. Intl Conf. on Peaceful Uses of Atomic Energy, Geneva, 7, 216 (1958).

66. Voigt, A. F., Proc. Intl Conf. on Peaceful Uses of Atomic Energy, Geneva, 9, 591 (1955).

67. Barney, R. A., and F. J. Keneshea, Jr., "Pyrochemical Separations Methods: II. The Distribution of Plutonium and Fission Products Between Uranium and Magnesium", NAA-SR-1324.

68. Chiotti, P., and A. F. Voigt, Proc. Intl. Conf. on Peaceful Uses of Atomic Energy, Geneva, 17, 369 (1958).

69. Chiotti, P., and H. E. Shoemaker, Ind. and Eng. Chem., 50, 137 (1958).

70. McKenzie, D. E., Can. J. Chem. 34, 749 (1956).

71. Martin, F. S., I. L. Jenkins and N. J. Keen, Proc. Intl. Conf. on Peaceful Uses of Atomic Energy, Geneva, 17, 352 (1958).

72. Leary, J. A., et al., Proc. Intl. Conf. on Peaceful Uses of Atomic Energy, Geneva, 17, 376 (1958).

73. Katz, H. M., F. B. Hill, and J. L. Speirs, Trans. AIME, 218, 770 (1960).

74. Hammond, R. P., and J. R. Humphreys, Jr., Nuc. Sci. and Eng. 18, 421 (1964).

75. Bidwell, R. M., Nuc. Sci. and Eng., 18, 426, 435 (1964).

76. Daane, A. H., and A. S. Wilson, J. Metals, 7, 1219 (1955).

77. Chiotti, P., G. A. Tracy and H. A. Wilhelm, Trans. AIME, 206, 562 (1956).

78. "Chemical Engineering Division Summary Report for January, February and March, 1957 - Argonne National Laboratories, ANL-5730.

79. Hu, S., and R. C. Kintner, AIChE Journal, 1, 42 (1955).

80. Johnson, A. I., and L. Braida, Can. J. Chem. Eng., 35, 165 (1957).

81. Klee, A. J., and R. E. Treybal, AIChE Journal 2, 444 (1956).

82. McGonigal, P. J., A. D. Kirshenbaum, and A. V. Grosse, J. Phys. Chem., 66, 737 (1962).

83. Grosse, A. V., J. A. Cahill, and A. D. Kirshenbaum, J. Am. Chem. Soc., 83, 4665 (1961).

84. Metal Progress, 58, 252, 258-259, 261 (1950).

85. Cahill, J. A., and A. D. Kirshenbaum, J. Inorg. Nucl. Chem. 27, 73 (1965).

86. Spriet, B., Mem. Sci. Rev. Met., 60, 531 (1963).

87. Grosse, A., J. Inorg. and Nucl. Chem., 26, 1349 (1964).

88. Grosse, A., J. Inorg. Nucl . Chem., 22, 23 (1962); Ibid., 24, 147 (1962).

89. Girifalco, L. A., and R. J. Good, J. Phys. Chem., 61, 904 (1957).

90. Handlos, A. E. and T. Baron, AIChE Journal, 3, 129 (1957).

91. Higbie, R., Trans. AIChE., 31, 365 (1935).

92. Grosse, A. V., J. Inorg. and Nucl. Chem. 23, 33 (1961); Ibid., 317 (1962).

93. Newman, A. B., Trans. AIChE., 27, 203 (1931).

94. Smith, T., J. Electrochem. Soc., 106, 1046 (1959).

95. Haefling, J., and A. Daane, Trans. AIME, 215, 336 (1959).

96. Culpin, M. F. Proc. Phys. Soc. (London), 70B, 1079 (1957).

97. Crank, J. The Mathematics of Diffusion, (Oxford at the Clarendon Press, 1956), p. 91.

98. Newman, A. B., Trans. Am. Inst. of Chem. Eng., 27, 203 (1931).

99. Carslaw, H. S., and Jaeger, J. C. Conduction of Heat in Solids, 2nd. Edition, (Oxford at the Clarendon Press, 1959), p. 485.

100. Levenson, M. et al., Proc. Intl. Conf. on Peaceful Uses of Atomic Energy, Geneva, 17,414 (1958).

101. Bidwell, R. M., Nuc. Sci. and Eng. 18, 435 (1964).

102. Rough, F. A., and A. A. Bauer, "Constitution of Uranium and Thorium Alloys", BMI-1300.

103. Ames Laboratory, U. S. Atomic Energy Commission, Iowa State University, Ames, Iowa. Newsletter for Division of Reactor Development, Reactor Materials, and Low Decontamination Separations (March 1961).

104. Mound Laboratory Reports, MLM-1113, MLM-1118, MLM-1135, MLM-1137.

105. Covell, D. V., "Determination of Gamma-Ray Abundance Directly from the Total Absorption Peak", Research and Development Technical Report USNRDL-TR-288, 4 December 1958.

106. Price, B. T., C. C. Horton, and K. T. Spinney, "Radiation Shielding", (Pergamon Press, 1957).

107. Benedict, M., and Pigford, T. H., Nuclear Chemical Engineering, (McGraw-Hill Book Co., Inc., 1957) p. 29.

108. Garner, F. H., and A. H. P. Skelland, Ind. Eng. Chem., 46, 1255 (1954).

109. Hildebrand, J. H., and R. L. Scott, The Solubility of Non-Electrolytes (Reinhold, 1950).

110. Griffith, R. M., Chem. Eng. Sci, 12, 198 (1960).

111. Stull, D. R., and G. C. Sinke, Thermodynamic Properties of the Elements, (American Chemical Society, 1956).

112. Lewis, G. N., and M. Randall, revised by K. S. Pitzer and L. Brewer, Thermodynamics, 2nd Edition (McGraw-Hill Book Co., 1961) p. 297 problem 21-5.

FIGURE CAPTIONS

Fig. 1 Section showing interface between U-Cr and Mg phases.

Fig. 2 γ-ray spectrum of a sample of the uranium-chromium eutectic which has been neutron irradiated for 2 days and cooled for 24 days. (Spectrum taken with a Harshaw Type 8S8 scintillation detector consisting of a 2"x2" thallium activated sodium iodide crystal and a type 6655A photomultiplier tube. Photomultiplier output recorded by a Packard Instrument 400-channel analyzer.)

Fig. 3 Arrangement for freezing uranium-chromium eutectic and magnesium following equilibration.

Fig. 4 Decay plot of La^{140} activity in Mg and U-Cr phases for equilibrium run no. 21.

Fig. 5 Comparison of measured distribution coefficients for La with the data of Barney and Keneshea and with the predictions of regular solution theory.

Fig. 6 Correlation of mutual diffusion data in binary molten metal systems by Olander's method.

Fig. 7 Corresponding states plot for self-diffusion in molten metals. Mercury (Ref. 38), Sodium (Ref. 37), Indium (Ref. 28), Tin (Ref. 28), Silver (Ref. 22), Gallium (Ref. 46), Lead (Ref. 42), Copper (Ref. 44), Zinc (Ref. 47).

Fig. 8 Comparison of corresponding states theory with theory of Walls and Upthegrove for self-diffusion of molten mercury, Sodium (Ref. 37), Cadmium (Ref. 10).

Fig. 9 Comparison of corresponding states theory with theory of Walls and Upthegrove for self-diffusion of molten tin, gallium, and zinc. Tin closed circles (Ref. 28), Tin open circles (Ref. 41), Gallium (Ref. 46), Zinc (Ref. 47).

Fig. 10 Comparison of corresponding states theory with theory of Walls and Upthegrove for self-diffusion in molten lead, indium, copper, and silver. Lead (Ref. 42), Indium closed squares (Ref. 28), Indium open swaures (Ref. 43), Copper (Ref. 44), Silver (Ref. 22).

Fig. 11 Comparison of corresponding states theory with mutual diffusion data. Data for Bi, Cd, Sb, and Sn in Pb (Ref. 14). Self-diffusion data for Pb (Ref. 42).

Fig. 12 Comparison of corresponding states theory with mutual diffusion data. Data for Sb and Bi in Sn (Ref. 14), self-diffusion data for Sn (Ref. 28).